JAERI-M
91-200

CONTROL ROD EFFECTS ON REACTION RATE DISTRIBUTIONS IN TIGHT PITCHED PuO_2-UO_2 FUEL ASSEMBLY

November 1991

Choong-Sup GIL*, Keisuke OKUMURA and Yukio ISHIGURO

日本原子力研究所
Japan Atomic Energy Research Institute

JAERI-Mレポートは，日本原子力研究所が不定期に公刊している研究報告書です。
入手の問合わせは，日本原子力研究所技術情報部情報資料課（〒319-11茨城県那珂郡東海村）あて，お申しこしください。なお，このほかに財団法人原子力弘済会資料センター（〒319-11 茨城県那珂郡東海村日本原子力研究所内）で複写による実費頒布をおこなっております。

JAERI-M reports are issued irregularly.
Inquiries about availability of the reports should be addressed to Information Division, Department of Technical Information, Japan Atomic Energy Research Institute, Tokai-mura, Naka-gun, Ibaraki-ken 319-11, Japan.

編集兼発行　日本原子力研究所
印　　刷　㈱原子力資料サービス

JAERI-M 91-200

Control Rod Effects on Reaction Rate Distributions in Tight Pitched PuO_2-UO_2 Fuel Assembly

Choong-Sup GIL*, Keisuke OKUMURA and Yukio ISHIGURO

Department of Reactor Engineering
Tokai Research Establishment
Japan Atomic Energy Research Institute
Tokai-mura, Naka-gun, Ibaraki-ken

(Received October 21, 1991)

Investigations were made for the heterogeneity effects caused by insertion or withdrawal of a B_4C control rod on fine structure of reaction rates distributions in a tight pitched PuO_2-UO_2 fuel assembly. Analysis was carried out by using the VIM and SRAC codes with the libraries based on JENDL-2 for the hexagonal fuel assembly basically corresponding to the PROTEUS-LWHCR experimental core.

The reaction rates are affected more remarkably by the withdrawal of the control rod rather than its insertion. The changes of the reaction rates were decomposed into three terms of spectrum shifts, the changes of effective cross sections with fine groups, and their higher order components. From the analysis, it is concluded that most changes of reaction rates are caused by spectral shifts. The SRAC code with fine group constants can predict the distribution of reaction rates and their ratios with the accuracy of about 5% except for the values related to Pu-242 capture rate, as compared with the VIM results. To increase the accuracy, it is necessary to generate the effective cross sections of the fuel near control rods with consideration of the heterogeneities in the fuel assembly.

---

* Korea Atomic Energy Research Institute (in the course of the STA Scientist Exchange Program sponsored by the Science and Technology Agency of Japan)

Keywords: High Conversion Light Water Reactor, Tight Pitch Lattice, HCLWR, PROTEUS, VIM, SRAC, JENDL-2, Hexagonal Fuel Assembly

稠密格子PuO_2－UO_2燃料集合体内における反応率分布の制御棒効果

日本原子力研究所東海研究所原子炉工学部
吉　　忠燮*・奥村　啓介・石黒　幸雄

（１９９１年10月21日受理）

稠密格子の燃料集合体において，B_4C制御棒の挿入・引き抜きによる各種反応率分布の詳細なエネルギー構造に対する非均質効果を検討した。解析は，ＰＲＯＴＥＵＳ－ＬＷＨＣＲ実験炉心に対応する六角燃料集合体に対して，ＪＥＮＤＬＥ－２ライブラリーとＶＩＭ及びＳＲＡＣコードを使用して行った。

反応率は，制御棒の挿入よりはむしろ，その引抜きにより顕著な影響を受ける。制御棒の挿入・引き抜きにより生ずる反応率の変化をスペクトルシフト，詳細群実効断面積の変化，及びそれらの高次項へと分解して解析した。その結果，反応率の変化は主としてスペクトルシフトによるものとの結論を得た。詳細群定数を用いたＳＲＡＣによる計算は，Ｐｕ－242に関する量を除けば，反応率及び反応率比を，ＶＩＭの計算値に較べて５％の精度で予測することが可能である。さらに精度を向上させるためには，特に共鳴エネルギー領域において，燃料集合体内の非均質性を考慮して，制御棒近傍の燃料に対する実効断面積を作成する必要がある。

東海研究所：〒319－11 茨城県那珂郡東海村白方字白根２－４
＊　韓国原子力研究所（科学技術庁のＳＴＡ交流制度研究員）

Contents

1. Introduction 1
2. Geometrical Model and Calculation 2
2.1 Geometrical Model 2
2.2 VIM Calculation 3
2.3 SRAC Calculation 4
3. Results and Discussions 5
3.1 Macroscopic Heterogeneity Effects 5
3.2 Microscopic Heterogeneity Effects 7
4. Conclusions 9
Acknowledgements 9
References 10
Appendix Supplementary figures 49

目　　次

1. まえがき 1
2. 幾何形状モデルと計算 2
2.1 幾何形状モデル 2
2.2 ＶＩＭによる計算 3
2.3 ＳＲＡＣによる計算 4
3. 計算結果と議論 5
3.1 巨視的な非均質効果 5
3.2 微視的な非均質効果 7
4. 結　　論 9
謝　　辞 9
参考文献 10
付　　録　補 足 図 49

1. Introduction

The high conversion light water reactor(HCLWR) concept has received considerable attention over several years, for the potential of better fuel utilization relative to conventional LWRs. The basic idea of HCLWRs is to increase the conversion ratio by hardening the neutron spectrum with an undermoderated tight pitched lattice. After the first indication of the potential of HCLWRs by Edlund in 1975[1], feasibility studies have been made in many institutes but unacceptable differences have been observed in prediction of main physics parameters[2)-4)]. In the 30th meeting of the Nuclear Energy Agency Committee of Reactor Physics(NEACRP) in 1987, it was concluded to be necessary to clarify the physical problems included in data and method for HCLWRs[4].

The prediction accuracy of neutron physics parameters by calculation needs to be examined by comparison with appropriate experimental data. A series of relevant integral experiments had been carried out in the PROTEUS zero power facility at Switzerland during 1981-1990, which is well known as the PROTEUS-LWHCR Phase Ⅰ, Ⅱ Program. The results have been compared with those of calculations using various methods and data[5),6)].

The late experiments[7),8)] had been performed for the core in which Pu/U mixed oxide(MOX) fuel rods with 7.5% $Pu^{fis.}$ were arranged in the hexagonal lattice with a pitch of 10.7mm. The moderator-to-fuel volumetric ratio was 0.48. In the experiments, distributions of principal neutron balance components such as nuclide-wise reaction rates and their ratios were measured in the hexagonal lattices with an absorber rod or a water tube in the center and compared with the calculated values. However, some innegligible discrepancies were observed between them[7),8)]. It is necessary to investigate more detailed structure of distributions of neutron balance components in the tight pitched fuel assembly with the heterogeneities, because the reactivity control in HCLWRs is based on the use of cluster type control rods by which considerable uncertainties are caused in reactor physics design.

In this report, to get the information on the perturbation of neutron balance components due to control rods, calculations are carried out for the tight pitched hexagonal fuel assemblies where a central MOX fuel rod is substituted for a B_4C rod or a water tube. This calculational model is based on the HCLWRs experiment performed in the PROTEUS experimental facilities. The calculations are carried out by using a continuous energy Monte Carlo code VIM[9)], and the JAERI thermal reactor neutronics design code SRAC[10)] with the libraries based on JENDL-2 data file.

Unfortunately, the detailed experimental results are not available, so analyses are performed by regarding the results of the VIM calculation as references of neutron balance components. Here, the fission reactions of Pu-239(F_9), U-235(F_5), U-238(F_8), Pu-241(F_1), and the capture reactions of U-238(C_8), Pu-240(C_0), Pu-242(C_2), Pu-239(C_9), and their ratios on per-atom basis are considered. The fine structure of reaction rate differences between infinite unit pin cell and the fuel rods adjacent to the B_4C rod or water hole of the assemblies under study are represented in figures and tables. The dependence of reaction rates and power form factors on the number of condensed energy groups employed for the assembly calculations with SRAC is also investigated in comparison with the VIM results.

2. Geometrical model and calculation

2.1 Geometrical model

Figure 1 shows the one-sixth geometrical model of hexagonal fuel assembly and unit pin cell model employed in this calculation. The hexagonal fuel assembly consists of 397 MOX fuel rods with 7.5% fissile plutonium enrichment and has a rod-to-rod pitch of 10.7mm. The diameter of the fuel rod is 9.57mm, and the thickness of the cladding made of stainless steel is 0.55mm. The principal lattice parameters are based on the lattice of the PROTEUS experimental program II[7),8)]. The considered fuel assembly includes water gap in outer boundary, which is not included in the finite test lattice of the PROTEUS experiment, but which is necessary for the infinite lattice calculations with a perfect reflective boundary condition.

The calculations with the SRAC and VIM codes are performed for the following cases :

1) infinite unit pin cell (see the geometrical model at the bottom of Fig.1),
2) assembly with only MOX fuel rods (the material of the region-1 in Fig.1 is MOX fuel, that is to say, "undisturbed" case),
3) assembly with a B_4C rod (the material of the region-1 in Fig.1 is B_4C absorber, that is to say, control rod inserted case),
4) assembly with a water tube (the material of the region-1 in Fig.1 is water, that is to say, control rod withdrawn case).

Table 1 shows the compositions of the fuel, cladding, moderator, and control rod of B_4C absorber with 93% enriched B-10, which are assumed in the present calculations. The plutonium isotopic composition of the fuel

Unfortunately, the detailed experimental results are not available, so analyses are performed by regarding the results of the VIM calculation as references of neutron balance components. Here, the fission reactions of Pu-239(F_9), U-235(F_5), U-238(F_8), Pu-241(F_1), and the capture reactions of U-238(C_8), Pu-240(C_0), Pu-242(C_2), Pu-239(C_9), and their ratios on per-atom basis are considered. The fine structure of reaction rate differences between infinite unit pin cell and the fuel rods adjacent to the B_4C rod or water hole of the assemblies under study are represented in figures and tables. The dependence of reaction rates and power form factors on the number of condensed energy groups employed for the assembly calculations with SRAC is also investigated in comparison with the VIM results.

2. Geometrical model and calculation

2.1 Geometrical model

Figure 1 shows the one-sixth geometrical model of hexagonal fuel assembly and unit pin cell model employed in this calculation. The hexagonal fuel assembly consists of 397 MOX fuel rods with 7.5% fissile plutonium enrichment and has a rod-to-rod pitch of 10.7mm. The diameter of the fuel rod is 9.57mm, and the thickness of the cladding made of stainless steel is 0.55mm. The principal lattice parameters are based on the lattice of the PROTEUS experimental program II[7),8)]. The considered fuel assembly includes water gap in outer boundary, which is not included in the finite test lattice of the PROTEUS experiment, but which is necessary for the infinite lattice calculations with a perfect reflective boundary condition.

The calculations with the SRAC and VIM codes are performed for the following cases :

1) infinite unit pin cell (see the geometrical model at the bottom of Fig.1),
2) assembly with only MOX fuel rods (the material of the region-1 in Fig.1 is MOX fuel, that is to say, "undisturbed" case),
3) assembly with a B_4C rod (the material of the region-1 in Fig.1 is B_4C absorber, that is to say, control rod inserted case),
4) assembly with a water tube (the material of the region-1 in Fig.1 is water, that is to say, control rod withdrawn case).

Table 1 shows the compositions of the fuel, cladding, moderator, and control rod of B_4C absorber with 93% enriched B-10, which are assumed in the present calculations. The plutonium isotopic composition of the fuel

employed in the PROTEUS experiment was approximately 1% Pu-238, 64% Pu-239, 23% Pu-240, 8% Pu-241, and 4% Pu-242. The library of isotope Pu-238 for the present study was not available, so the composition for the fuel was changed as 64.6% Pu-239, 23.2% Pu-240, 8.1% Pu-241, and 4.1% Pu-242.

The reaction rate ratios in this report are defined on per-atom basis, for example,

$$C_8/F_9 = \sigma_c^{28} / \sigma_f^{49},$$

where σ_c^{28} and σ_f^{49} are one-group effective microscopic cross sections for capture of U-238 and for fission of Pu-239, respectively. The definition of the the conversion ratio(C.R.) in this report is as follows :

$$C.R. = \Sigma_c^{fer.} / \Sigma_a^{fis.},$$

where $\Sigma_c^{fer.}$ and $\Sigma_a^{fis.}$ stand for one-group capture cross section of U-238 and Pu-240 and for absorption cross section of U-235, Pu-239 and Pu-241, respectively.

2.2 VIM calculation

The VIM code is a continuous energy Monte Carlo code designed primarily for fast reactor calculations, but also has a thermal neutron capability. The cross section definition in VIM is by composition independent microscopic data sets. Resonance and smooth cross sections are specified pointwise with linear interpolation to provide continuous energy cross section description; unresolved resonances are described by the probability table method. The reaction rate types, fission, elastic scattering, inelastic scattering, and (n,2n) reactions are specifically defined, while "capture" is defined as the remaining possible outcome of neutron collision. All output quantities are provided with standard deviation estimates at the completion of a run.

Figure 2 shows the flow diagram of generating library data for the VIM code in JAERI[11]. Most of material libraries were generated on the basis of JENDL-2, while for some nuclides which were not evaluated in JENDL-2, the material libraries were generated on the basis of ENDF/B-Ⅳ. Table 2 shows the data of materials employed in this calculations. All of the libraries were processed so that the accuracy of linearized pointwise

cross sections was within 0.1% at any energy point. The chemical binding effect was considered for H_2O moderator with the $S(\alpha,\beta,T)$ data in ENDF/B－Ⅲ. In the VIM code, neutron flux is normalized so that total neutron source is unity, while in the SRAC code normalized so that total absorption rate is unity. For the convenience of comparison, the reaction rates edited by the VIM code were renormalized to the total absorption rates. A perfect reflective boundary condition was employed for a series of calculations.

2.3 SRAC calculation

The SRAC code has been developed at JAERI as a thermal reactor standard neutronics design code system and is characterized by application of the collision probability method on the cell calculations over the whole neutron energy. A comprehensive set of collision probability routines(PIJ) for 13 types of geometries yields wide application of the SRAC code to almost all types of thermal reactors. Recent modifications of data and methods extend its applicability to HCLWR cores[12),13)].

Because the high conversion light water reactors have intermediate neutron spectra as compared with conventional LWRs and fast reactors, the contribution of reaction rate in the resonance energy region is of significance. So the resonance treatment is very important for HCLWRs studies. The present calculations employ the PEACO routine of the SRAC code to treat resonance absorption, which calculates effective cross sections by the collision probability method for the energy range from thermal cut-off energy to 130.0eV with 4600 groups for cross section representation and 460 groups for flux calculation.

The effective cross sections with 107-energy group structure were made for the fuel, cladding and moderator regions in the unit pin cell calculation. As for the B_4C absorber and its cladding, the effective cross sections were calculated from the supercell model where the B_4C rod was surrounded by the homogenized mixture of fuel rods and moderator. The above calculated effective cross sections of the fuel, cladding, H_2O, B_4C absorber and its cladding were used in the following assembly calculations. It should be noted that the effective cross sections for the fuel rod were made without consideration of the influence from the control rod insertion or withdrawal. The whole fuel assembly calculations were performed also based on the collision probability method with the macroscopic cross sections generated in the previous cell calculations. As for the assembly calculations, the white (isotropic) reflective boundary condition was assumed to save computational

times.

Table 3 shows the 107-energy group structure of the SRAC user's library. The assembly calculations with the SRAC code were performed not only with the finest 107-energy groups but also with condensed 69, 28 and 8 groups. Table 4 shows the condensation scheme of the group constants from the 107 groups.

3. Results and discussions

3.1 Macroscopic heterogeneity effects

We discuss here on the integrated parameters such as k_{eff}, conversion ratio, distributions of one-group condensed fluxes, cross sections and reaction rates etc. More detailed results will be presented in the next section considering the nuclide-wise and energy-wise contributions.

Figures 3-14 show the distributions of reaction rates, fluxes, one-group macroscopic cross sections, power form factors(power densities divided by averaged one) and conversion ratios in the fuel assemblies obtained from the VIM calculations. Table 5 shows the k_{eff} values and conversion ratios from the VIM and SRAC calculations. It is seen that the k_{eff} values agree within 0.5% between the results of the VIM and SRAC calculations, even of the SRAC calculation with 8-energy groups. However it is seen from Figs.9 and 10 that the good agreement of the SRAC calculation with 8-energy groups was caused by the accidental compensations of underestimation and overestimation of power distribution as compared with the VIM results. The SRAC calculation with 8-energy groups underestimate the power peaking by about 7% as compared with VIM result. To get power distribution with sufficient accuracy, it is necessary to use fine group constants with more than the 28-energy group structure.

It is seen from Fig.5 that the flux depression by the B_4C rod is very deep and reaches into long distance relative to the degrees of flux increase due to the water hole and gap water. On the contrary, the reaction rates and macroscopic cross sections by the water hole and gap water are changed more considerably than those by the B_4C rod as seen in Figs.1-7.

Table 6 shows the distributions of reaction rate ratios in the employed fuel assemblies and unit pin cell on per-atom basis. Tables 7 and 8 show the ratios of the disturbed/undisturbed reaction rates in the adjacent region to the central heterogeneity calculated by the VIM code and the SRAC code with the different numbers of energy groups.

The word "undisturbed" means that the neutron balance components are not

times.

Table 3 shows the 107-energy group structure of the SRAC user's library. The assembly calculations with the SRAC code were performed not only with the finest 107-energy groups but also with condensed 69, 28 and 8 groups. Table 4 shows the condensation scheme of the group constants from the 107 groups.

3. Results and discussions

3.1 Macroscopic heterogeneity effects

We discuss here on the integrated parameters such as k_{eff}, conversion ratio, distributions of one-group condensed fluxes, cross sections and reaction rates etc. More detailed results will be presented in the next section considering the nuclide-wise and energy-wise contributions.

Figures 3-14 show the distributions of reaction rates, fluxes, one-group macroscopic cross sections, power form factors(power densities divided by averaged one) and conversion ratios in the fuel assemblies obtained from the VIM calculations. Table 5 shows the k_{eff} values and conversion ratios from the VIM and SRAC calculations. It is seen that the k_{eff} values agree within 0.5% between the results of the VIM and SRAC calculations, even of the SRAC calculation with 8-energy groups. However it is seen from Figs.9 and 10 that the good agreement of the SRAC calculation with 8-energy groups was caused by the accidental compensations of underestimation and overestimation of power distribution as compared with the VIM results. The SRAC calculation with 8-energy groups underestimate the power peaking by about 7% as compared with VIM result. To get power distribution with sufficient accuracy, it is necessary to use fine group constants with more than the 28-energy group structure.

It is seen from Fig.5 that the flux depression by the B_4C rod is very deep and reaches into long distance relative to the degrees of flux increase due to the water hole and gap water. On the contrary, the reaction rates and macroscopic cross sections by the water hole and gap water are changed more considerably than those by the B_4C rod as seen in Figs.1-7.

Table 6 shows the distributions of reaction rate ratios in the employed fuel assemblies and unit pin cell on per-atom basis. Tables 7 and 8 show the ratios of the disturbed/undisturbed reaction rates in the adjacent region to the central heterogeneity calculated by the VIM code and the SRAC code with the different numbers of energy groups.

The word "undisturbed" means that the neutron balance components are not

purturbed by the central heterogeneity, that is to say, those in the fuel assembly with only MOX fuel rods. It is shown from the VIM results that the ratio of Pu-240 capture to Pu-239 fission (C_0/F_9) and (C_2/F_9) in the fuel rods adjacent to the B_4C rod is decreased by about 9% from the undisturbed while others are almost unchanged. The ratios (F_5/F_9), (F_1/F_9), and (C_2/F_9) in the fuel rods adjacent to the water hole are respectively reduced by about 10%, 7%, and 15%, as compared with the undisturbed. The results by VIM and SRAC for the reaction rate ratios are in a good agreement within the statistical errors of the VIM except for those near the gap water and the ratio C_2/F_9, of which the maximum deviations are 4.7%(0.7%)* and 9.4%(2.8%)*, respectively.

It is seen in Tables 7 and 8 that the VIM results on the fission rates of Pu-239, U-235, and Pu-241 in the fuel rods adjacent to the B_4C rod are decreased by about 16% from the undisturbed while those adjacent to the water hole are increased by about 32%, 18%, and 22%, respectively. The U-238 fission rates are not sensitive to such kind of heterogeneities. As compared with the undisturbed, the total capture rate in the fuel rods adjacent to the B_4C rod is decreased by about 16% while adjacent to the water hole is increased by about 20%.

The results of the VIM and SRAC calculation with 107-energy groups on the reaction rates in the fuel rods adjacent to the B_4C rod show a good agreement within the statistical errors of the VIM except for the capture rates of Pu-239 and Pu-242, where these discrepancies are 2.1%(1.2%)* and 15.4%(1.2%)*, respectively. For the total capture rate these nuclides do not seem to cause significant discrepancies between the VIM and SRAC results because of their small contributions. The total fission rate near the water hole by the SRAC with 107-energy groups is underestimated by 2.3%(1.1%)* from the VIM, which is attributed mainly to the underestimation of the Pu-239 fission rate of 2.8%(1.1%)*. The discrepancy in the total capture rate near the water hole between the VIM and SRAC with the 107-energy groups is 2.4%(1.2%)*, which seems to be caused by underestimations of the U-238 and Pu-239 capture rates of 3.1%(1.2%)* and 3.5%(1.2%)*, respectively.

Summarizing the above results, the reaction rate changes by the water hole and gap water are larger than by the B_4C rod, and the discrepancies between the results of VIM and SRAC also show the same trends. As for

*statistical error of the VIM calculation

the Pu-242 capture rate, the VIM and SRAC results do not show good agreement i.e. the maximum deviation of 15.4%(1.2%)* is seen in the SRAC results with 107-energy groups. Figures 12 and 13 show the comparisons of one-group macroscopic cross section distributions in the fuel assemblies from the VIM and SRAC calculations, where the results of VIM show severe space dependent fluctuations. However, as seen later in Fig.40, the multi-group Pu-242 capture cross section shows a good agreement between the VIM and SRAC results in the unit pin cell calculation.

3.2 Microscopic heterogeneity effects

Figures 14-18 show the energy group-wise reaction rates, neutron spectra, and macroscopic cross sections calculated with the VIM for the unit pin cell and the monitoring region-2 in the fuel assemblies. In these figures, the word "center" stands for the center of the employed fuel assembly.

To get more detailed information on the differences of reaction rates in the region-2 from those in the unit pin cell, the reaction rate differences obtained by VIM were decomposed into three contributors, i.e. the contributions of neutron spectrum shifts, cross section changes based on the 107-energy groups corresponding to the energy structure of SRAC, and their higher order components. The differences of reaction rates were calculated as following ;

Difference of reaction rates

$$= \sum_{g=1}^{107} \{\sigma_{A,g}\Phi_{A,g} - \sigma_{P,g}\Phi_{P,g}\}$$

$$= \sum_{g=1}^{107} \{(\Phi_{A,g}-\Phi_{P,g})\sigma_{P,g} + (\sigma_{A,g}-\sigma_{P,g})\Phi_{P,g} + (\Phi_{A,g}-\Phi_{P,g})(\sigma_{A,g}-\sigma_{P,g})\},$$

where the subscripts A and P mean the values obtained from the fuel assembly and pin cell calculations, respectively, and other notation is conventional.

The decomposed differences of reaction rates are shown in Figs.19-26. From these figures, it can be clearly shown that the most changes of the reaction rates by the insertion or withdrawal of the B_4C rod are caused by neutron spectrum shifts in the thermal and fast energy regions. The contributions of above three terms to reaction rate changes are large in turn of the first, second and third.

The Figures 27-30 show the contributions of individual isotopes to total reaction rate changes near the heterogeneities under consideration. It is seen that main contributions to the total fission and capture rate changes are made by Pu-239 fission rates and U-238 capture rates, respectively.

The second term of the difference of reaction rates are further more classified into individual isotopic contributions, which are shown in Figs.31-34. The second term and third term are not considered in the SRAC calculations because the group constants for the assembly calculations were made without consideration of heterogeneities in the fuel assembly. The second term in the fuel rods adjacent to the B_4C rod is less influential than that adjacent to the water hole. Near the B_4C rod, the second term in different energy regions is accidentally almost compensated itself while it affects the reaction rate changes near the water hole. The fission of Pu-239 and capture of U-238 are again main contributors for the second term. The effect of the third term on the reaction rate changes is very small.

The reaction rates, neutron spectra, and macroscopic cross sections obtained with VIM and SRAC in the unit pin cell calculations are compared in Figs.35-39 and those in the fuel assembly are shown in Figs.1-9 in the appendix. Figures 9-23 in the appendix show the comparisons of individual isotopic microscopic cross sections obtained by VIM in the unit pin cell and in the region-2 of the fuel assemblies. The neutron spectrum obtained by SRAC in the unit pin cell calculation is slightly hardened as compared with that by VIM. while it shows a good agreement in the assembly calculations. The 107-group macroscopic cross sections of the SRAC in the pin cell almost agree with those obtained by VIM.

From the microscopic analyses above mentioned, it is shown that most of the reaction rate changes due to the heterogeneity are caused by spectrum shifts, but the contribution of the cross sections changes based on 107-energy groups is not negligible, especially for the fission of Pu-239, and capture of U-238. The contribution of the cross section changes can not be found out from one-group analyses because of the accidental compensations in different energy regions. Such situation was observed in the fuel rods adjacent to the B_4C rod. In order to increase the accuracy for the assembly calculation with SRAC, it will be necessary to consider the heterogeneity effects in the generation of the fine group constants for the fuel near the control rod, or to increase the number of energy groups in the resonance region.

4. Conclusions

The reaction rates in the HCLWR fuel assembly are affected more remarkably by water hole or water gap than by B_4C rod. Most of the reaction changes due to the heterogeneities are explained as the results of neutron spectrum shifts on the basis of 107-energy groups corresponding to the energy structure of the SRAC code. The contribution of the changes of cross sections with 107-groups due to the heterogeneities to the reaction rate changes is not always negligibly small, because self compensations accidentally occurs in different energy regions. The contribution of change of cross sections is large especially for the heterogeneity caused by water hole or water gap and the main contributors of it are fission of Pu-239 and capture of U-238. Fission rate near the B_4C rod is reduced by about 13% while it is increased by about 26% near the water hole, as compared with the undisturbed, which is mainly caused by Pu-239 nuclide.

The SRAC calculation with 28-energy groups can predict the neutron balance components in the HCLWR fuel assembly with the heterogeneities within about 5% except for Pu-242 capture rate, as compared with the VIM results. The SRAC calculation with 8-energy groups underestimates power peaking by about 7%, which occurs in the fuel rods adjacent to the gap water surrounding the fuel assembly. To reduce the uncertainties of prediction of neutron balance components in the SRAC calculations for the HCLWR fuel assembly, it is necessary to generate fine group constants of the fuel near control rods with consideration of the heterogeneity or to increase the number of energy groups in the resonance energy region.

Acknowledgements

The authors would like to thank Mr. MORIMOTO Y. of Hitachi Ltd. and Mr. AKIE H. in JAERI for their useful comments in calculations with SRAC and drawing the figures.

4. Conclusions

The reaction rates in the HCLWR fuel assembly are affected more remarkably by water hole or water gap than by B_4C rod. Most of the reaction changes due to the heterogeneities are explained as the results of neutron spectrum shifts on the basis of 107-energy groups corresponding to the energy structure of the SRAC code. The contribution of the changes of cross sections with 107-groups due to the heterogeneities to the reaction rate changes is not always negligibly small, because self compensations accidentally occurs in different energy regions. The contribution of change of cross sections is large especially for the heterogeneity caused by water hole or water gap and the main contributors of it are fission of Pu-239 and capture of U-238. Fission rate near the B_4C rod is reduced by about 13% while it is increased by about 26% near the water hole, as compared with the undisturbed, which is mainly caused by Pu-239 nuclide.

The SRAC calculation with 28-energy groups can predict the neutron balance components in the HCLWR fuel assembly with the heterogeneities within about 5% except for Pu-242 capture rate, as compared with the VIM results. The SRAC calculation with 8-energy groups underestimates power peaking by about 7%, which occurs in the fuel rods adjacent to the gap water surrounding the fuel assembly. To reduce the uncertainties of prediction of neutron balance components in the SRAC calculations for the HCLWR fuel assembly, it is necessary to generate fine group constants of the fuel near control rods with consideration of the heterogeneity or to increase the number of energy groups in the resonance energy region.

Acknowledgements

The authors would like to thank Mr. MORIMOTO Y. of Hitachi Ltd. and Mr. AKIE H. in JAERI for their useful comments in calculations with SRAC and drawing the figures.

References

1. Edlund M.C. : "High Conversion Ratio Plutonium Recycle in Pressurized Water Reactors," Ann. Nucl. Energy, 2, 801 (1975).
2. Uotinen V.O. et al. : "Technical feasibility of a Pressurized Water Reactor Design with a Low-Water-Volume-Fraction Lattice," EPRI-NP-1833 (1981).
3. Penndorf K., Schult F. and Bunemann D. : "Some Neutron Physical Consequences of Maximizing the Conversion Ratio of Pressurized Water Reactors Operated in the Uranium-Plutonium Cycle," Nucl. Technol., 59, 256 (1982).
4. Hiroshi Akie, Yukio Ishiguro and Hideki Takano : "Summary Report on the International Benchmark Calculations for High Conversion Light Water Reactor Lattices," JAERI-M 88-200(NEACRP-L-309) (1988).
5. Hettergott E., Chawla R. and Gmur K. : "Analysis of Test Lattice Experiments in the Light Water High-Conversion Reactor PROTEUS," EPRI-NP-3190 (1983).
6. Chawla R. et al. : "Reactivity and Reaction Rate Ratio Changes with Moderator Voidage in a Light Water High Conversion Reactor Lattice," Nucl. Technol., 67, 360 (1984).
7. Berger H.-D., Bohme R., Chawla R., Gmur K. : "Investigation of Importance-weighted Infinite Multiplication Constants in Clean and Poisoned LWHCR Lattices," Proc. of the 1988 Inter. Reactor Physics Conference, Sept. 18-22, Jackson Hole, Wyoming, Vol. Ⅱ, Ⅱ-343-351, (1988).
8. Seiler R. Gmur K., Hager H. and Paratte J.M. "Experimental Studies of Macroscopic and Cell Heterogeneities in HCLWRs," Proc. of the 1988 Inter. Reactor Physics Conference, Sept. 18-22, Jackson Hole, Wyoming, Vol. Ⅱ, Ⅱ-353-360, (1988).
9. Levitt L. B. : "The Probability Table Method for Treating Unresolved Resonances in Monte Carlo Criticality Calculations," Trans. Am. Nucl. Soc., 14, 648 (1971).
10. Tsuchihashi K. el al. : "Revised SRAC Code System," JAERI-1302 (1986).
11. Mori T. et al. : "Development of Cross Section Library Preparation Code System for a Continuous Energy Monte Carlo Code," Private Communication, (1987) (in Japanese).

12. Takano H. et al. : "The Effects of Fission Products on Burnup Characteristics in High Conversion Light Water reactors," Nucl. Technol., 80, 250 (1988).
13. Ishiguro Y. and Kaneko K. : "Generalized Dancoff Factor in Complex Lattice Arrangement,"J. Nucl. Sci. Technol., 22 853 (1985).

Table 1 Compositions and atomic number densities ($\times 10^{24}/cm^3$)

Fuel (MOX)		Moderator	
U^{235}	4.0515×10^{-5}	H^{1}	6.65200×10^{-2}
U^{238}	1.9962×10^{-2}	O^{16}	3.33260×10^{-2}
Pu^{239}	1.4790×10^{-3}		
Pu^{240}	5.3114×10^{-4}		
Pu^{241}	1.8544×10^{-4}		
Pu^{242}	9.3866×10^{-5}		
O^{16}	4.3460×10^{-2}		
Cladding (sus-394)		Control Rod (B_4C)	
Cr(nat.)	8.5360×10^{-3}	B^{10}	7.53400×10^{-2}
Ni(nat.)	5.1180×10^{-3}	B^{11}	5.67520×10^{-3}
Fe(nat.)	3.1250×10^{-2}	C^{12}	2.02690×10^{-2}
Al^{27}	6.0800×10^{-3}		
Mo(nat.)	7.3540×10^{-4}		
Mn^{55}	1.0010×10^{-3}		
Si(nat.)	8.1240×10^{-4}		
N^{14}	1.3230×10^{-5}		

Table 2 List of VIM material library

Material	Temperature (k)	ID	File
Pu^{240}	300	10300	JENDL-2
Pu^{241}	300	20300	JENDL-2
U^{235}	300	30300	JENDL-2
U^{238}	300	40300	JENDL-2
Pu^{239}	300	50300	JENDL-2
Pu^{242}	300	110300	JENDL-2
Cr(nat.)	300	210300	JENDL-2
Ni(nat.)	300	220300	JENDL-2
Fe(nat.)	300	230300	JENDL-2
Al^{27}	300	240300	JENDL-2
O^{16}	300	260300	ENDF/B-IV
C^{12}	300	270300	JENDL-2
Mo(nat.)	300	280300	JENDL-2
Mn^{55}	300	290300	JENDL-2
B^{10}	300	310300	JENDL-2
B^{11}	300	320300	JENDL-2
H^{1}	300	350300	JENDL-2
Si(nat.)	300	380300	JENDL-2
N^{14}	300	420300	ENDF/B-IV
H¥H_2O[a]	300	900300	ENDF/B-IV[b]

[a] hydrogen of H_2O (chemical binding effect is considered in thermal scattering law)

[b] thermal data are based on ENDF/B-III.

Table 3 Energy group structure of SRAC user's library

number of fast group 61
number of thermal group 46

Group	Energy	ΔU	Group	Energy	ΔU	Group	Energy	ΔU
1	0.10000E+08	0.25	37	0.12341E+04	0.25	73	0.53158E+00	0.12
2	0.77880E+07	0.25	38	0.96112E+03	0.25	74	0.46912E+00	0.13
3	0.60653E+07	0.25	39	0.74852E+03	0.25	75	0.41399E+00	0.06
4	0.47237E+07	0.25	40	0.58295E+03	0.25	76	0.38926E+00	0.06
5	0.36788E+07	0.25	41	0.45400E+03	0.25	77	0.36528E+00	0.07
6	0.28651E+07	0.25	42	0.35357E+03	0.25	78	0.34206E+00	0.07
7	0.22313E+07	0.25	43	0.27536E+03	0.25	79	0.31961E+00	0.07
8	0.17377E+07	0.25	44	0.21445E+03	0.25	80	0.29792E+00	0.07
9	0.13534E+07	0.25	45	0.16702E+03	0.25	81	0.27699E+00	0.08
10	0.10540E+07	0.25	46	0.13007E+03	0.25	82	0.25683E+00	0.08
11	0.82085E+06	0.25	47	0.10130E+03	0.25	83	0.23742E+00	0.08
12	0.63928E+06	0.25	48	0.78893E+02	0.25	84	0.21878E+00	0.09
13	0.49787E+06	0.25	49	0.61442E+02	0.25	85	0.20090E+00	0.09
14	0.38774E+06	0.25	50	0.47851E+02	0.25	86	0.18378E+00	0.09
15	0.30197E+06	0.25	51	0.37266E+02	0.25	87	0.16743E+00	0.10
16	0.23518E+06	0.25	52	0.29023E+02	0.25	88	0.15183E+00	0.10
17	0.18316E+06	0.25	53	0.22603E+02	0.25	89	0.13700E+00	0.11
18	0.14264E+06	0.25	54	0.17604E+02	0.25	90	0.12293E+00	0.11
19	0.11109E+06	0.25	55	0.13710E+02	0.25	91	0.10963E+00	0.12
20	0.86517E+05	0.25	56	0.10677E+02	0.25	92	0.97080E-01	0.13
21	0.67380E+05	0.25	57	0.83153E+01	0.25	93	0.85397E-01	0.14
22	0.52475E+05	0.25	58	0.64760E+01	0.25	94	0.74276E-01	0.15
23	0.40868E+05	0.25	59	0.50435E+01	0.25	95	0.64017E-01	0.16
24	0.31828E+05	0.25	60	0.39279E+01	0.25	96	0.54520E-01	0.17
25	0.24788E+05	0.25	61	0.30590E+01	0.25	97	0.45785E-01	0.19
26	0.19305E+05	0.25	62	0.23824E+01	0.25	98	0.37813E-01	0.21
27	0.15034E+05	0.25	63	0.18554E+01	0.12	99	0.30602E-01	0.24
28	0.11709E+05	0.25	64	0.16374E+01	0.12	100	0.24154E-01	0.27
29	0.91188E+04	0.25	65	0.14450E+01	0.13	101	0.18467E-01	0.31
30	0.71017E+04	0.25	66	0.12752E+01	0.13	102	0.13543E-01	0.37
31	0.55308E+04	0.25	67	0.11253E+01	0.12	103	0.93805E-02	0.45
32	0.43074E+04	0.25	68	0.99312E+00	0.12	104	0.59804E-02	0.58
33	0.33546E+04	0.25	69	0.87643E+00	0.13	105	0.33423E-02	0.82
34	0.26126E+04	0.25	70	0.77344E+00	0.12	106	0.14663E-02	1.43
35	0.20347E+04	0.25	71	0.68256E+00	0.12	107	0.35238E-03	3.56
36	0.15846E+04	0.25	72	0.60236E+00	0.13	108	0.10000E-04	

Table 4 Energy group condensation schemes for fuel assembly calculation with the SRAC code

107-group cut(→ 69 group → 28 group → 8 group)								
group no.	69	28	8	group no.	69	28	group no.	69
1	2*	6	10	24	51	92	47	81
2	4	10	28	25	53	94	48	82
3	6	18	61	26	55	97	49	83
4	8	28	67	27	61	100	50	84
5	10	45	74	28	62	107	51	85
6	12	53	79	29	63		52	86
7	14	55	89	30	64		53	87
8	16	61	107	31	65		54	88
9	18	62		32	66		55	89
10	20	63		33	67		56	90
11	22	64		34	68		57	91
12	24	66		35	69		58	92
13	26	67		36	70		59	93
14	28	69		37	71		60	94
15	30	72		38	72		61	95
16	32	74		39	73		62	96
17	34	75		40	74		63	97
18	35	77		41	75		64	98
19	37	79		42	76		65	99
20	41	81		43	77		66	100
21	45	83		44	78		67	101
22	47	86		45	79		68	103
23	49	89		46	80		69	107

* Lower boundary numbers in the 107-groups.

Table 5 Effective multiplication factors and conversion ratios calculated by the VIM and SRAC codes

Case name	k_{eff}					conversion ratio	
	VIM	SRAC				VIM	SRAC
		107g*	69g	28g	8g		
Pin cell	1.1332 ±0.0013+	1.1359 (1.0024)++				0.78268 (0.6%)	0.78615 (0.9956)
MOX only	1.1435 ±0.0009	1.1451 (1.0014)	1.1459 (1.0021)	1.1442 (1.0006)	1.1394 (0.9964)		
B_4C rod	1.1251 ±0.0010	1.1284 (1.0029)	1.1293 (1.0037)	1.1274 (1.0020)	1.1222 (0.9974)		
Water hole	1.1412 ±0.0010	1.1461 (1.0043)	1.1470 (1.0051)	1.1452 (1.0035)	1.1401 (0.9990)		

* the number of energy groups

\+ standard deviation

++ SRAC/VIM

Table 6 Comparison of reaction rate ratio distributions in the fuel assembly between VIM and SRAC

U -235 FISSION / PU-239 FISSION (F5/F9)

DISTANCE (CM)	MOX FUEL ONLY	WITH A B4C ROD	WITH A WATER HOLE
0.0	0.908 (1.008) *		
	(1.8%) +		
1.07	0.912 (1.000)	0.911 (1.010)	0.819 (1.015)
	(0.9%)	(1.1%)	(1.0%)
2.14	0.903 (1.008)	0.914 (1.001)	0.888 (1.011)
	(0.7%)	(0.8%)	(0.8%)
3.21	0.910 (0.997)	0.919 (0.989)	0.902 (1.001)
	(0.8%)	(0.7%)	(0.8%)
4.28	0.901 (1.010)	0.907 (1.004)	0.895 (1.016)
	(0.9%)	(0.8%)	(0.8%)
5.35	0.908 (0.998)	0.906 (1.001)	0.910 (0.996)
	(0.8%)	(0.7%)	(0.8%)
6.42	0.906 (0.998)	0.903 (1.002)	0.901 (1.003)
	(0.8%)	(0.9%)	(0.7%)
7.49	0.906 (0.998)	0.905 (0.999)	0.904 (1.000)
	(0.8%)	(0.9%)	(0.8%)
8.56	0.898 (1.000)	0.898 (1.002)	0.903 (0.995)
	(0.8%)	(0.7%)	(0.9%)
9.63	0.894 (0.999)	0.895 (0.998)	0.895 (0.997)
	(0.8%)	(0.8%)	(0.8%)
10.70	0.857 (1.015)	0.862 (1.010)	0.860 (1.012)
	(0.9%)	(0.9%)	(0.7%)
11.77	0.779 (1.026)	0.785 (1.019)	0.784 (1.020)
	(0.8%)	(0.8%)	(0.8%)
PIN CELL	0.909 (1.005)		
	(0.3%)		

PU-241 FISSION / PU-239 FISSION (F1/F9)

DISTANCE (CM)	MOX FUEL ONLY	WITH A B4C ROD	WITH A WATER HOLE
0.0	1.684 (1.009)		
	(1.9%)		
1.07	1.698 (0.998)	1.674 (1.005)	1.581 (1.015)
	(0.9%)	(1.1%)	(0.9%)
2.14	1.686 (1.004)	1.684 (1.003)	1.677 (1.005)
	(0.8%)	(0.9%)	(0.9%)
3.21	1.690 (1.001)	1.693 (0.997)	1.686 (1.002)
	(0.9%)	(0.8%)	(0.9%)
4.28	1.679 (1.010)	1.684 (1.006)	1.675 (1.012)
	(0.9%)	(0.9%)	(0.8%)
5.35	1.695 (0.998)	1.697 (0.996)	1.686 (1.004)
	(0.7%)	(0.8%)	(0.8%)
6.42	1.696 (0.997)	1.691 (0.999)	1.677 (1.008)
	(0.8%)	(0.9%)	(0.7%)
7.49	1.696 (0.998)	1.693 (0.998)	1.691 (1.000)
	(0.8%)	(0.9%)	(0.9%)
8.56	1.698 (0.994)	1.676 (1.007)	1.684 (1.002)
	(0.9%)	(0.6%)	(0.9%)
9.63	1.686 (1.000)	1.685 (1.000)	1.697 (0.993)
	(0.8%)	(0.9%)	(0.8%)
10.70	1.649 (1.008)	1.660 (1.001)	1.648 (1.009)
	(0.9%)	(0.9%)	(0.7%)
11.77	1.553 (1.013)	1.562 (1.007)	1.558 (1.009)
	(0.8%)	(0.8%)	(0.9%)
PIN CELL	1.693 (0.997)		
	(0.3%)		

* VIM (SRAC/VIM)

\+ statistical error of VIM

Table 6 (Continued)

U -238 FISSION / PU-239 FISSION (F8/F9)

DISTANCE (CM)	MOX FUEL ONLY	WITH A B4C ROD	WITH A WATER HOLE
0.0	0.013 (1.008) (1.6%)		
1.07	0.013 (1.013) (0.8%)	0.015 (1.013) (0.9%)	0.010 (1.029) (0.8%)
2.14	0.013 (1.006) (0.7%)	0.014 (1.001) (0.7%)	0.013 (1.018) (0.8%)
3.21	0.013 (1.005) (0.7%)	0.014 (0.985) (0.6%)	0.013 (1.015) (0.8%)
4.28	0.013 (1.025) (0.8%)	0.013 (1.010) (0.8%)	0.013 (1.028) (0.7%)
5.35	0.013 (1.005) (0.6%)	0.013 (1.002) (0.7%)	0.013 (1.001) (0.7%)
6.42	0.013 (1.006) (0.7%)	0.013 (1.008) (0.8%)	0.013 (1.003) (0.6%)
7.49	0.013 (1.005) (0.7%)	0.013 (1.007) (0.8%)	0.013 (1.005) (0.8%)
8.56	0.013 (1.009) (0.8%)	0.013 (1.019) (0.5%)	0.013 (1.001) (0.8%)
9.63	0.013 (1.014) (0.7%)	0.013 (1.008) (0.7%)	0.013 (0.993) (0.7%)
10.70	0.012 (1.017) (0.8%)	0.012 (1.018) (0.8%)	0.012 (1.005) (0.6%)
11.77	0.009 (1.047) (0.7%)	0.009 (1.040) (0.7%)	0.009 (1.045) (0.8%)
PIN CELL	0.013 (1.073) (0.3%)		

U -238 CAPTURE / PU-239 FISSION (C8/F9)

DISTANCE (CM)	MOX FUEL ONLY	WITH A B4C ROD	WITH A WATER HOLE
0.0	0.074 (1.004) (2.2%)		
1.07	0.074 (0.998) (1.0%)	0.075 (1.009) (1.2%)	0.062 (0.995) (1.2%)
2.14	0.073 (1.008) (0.9%)	0.076 (0.989) (1.1%)	0.071 (1.004) (1.1%)
3.21	0.073 (1.007) (1.0%)	0.075 (0.986) (0.9%)	0.073 (1.000) (0.9%)
4.28	0.071 (1.033) (1.1%)	0.073 (1.006) (1.2%)	0.071 (1.025) (0.9%)
5.35	0.074 (0.987) (1.0%)	0.073 (1.002) (1.0%)	0.072 (1.010) (1.0%)
6.42	0.072 (1.006) (0.9%)	0.072 (1.005) (1.1%)	0.072 (1.001) (1.1%)
7.49	0.073 (0.990) (1.0%)	0.072 (1.009) (1.0%)	0.074 (0.984) (1.0%)
8.56	0.071 (1.015) (0.9%)	0.070 (1.018) (1.0%)	0.072 (0.999) (1.1%)
9.63	0.070 (1.013) (0.9%)	0.070 (1.005) (1.1%)	0.072 (0.986) (1.1%)
10.70	0.065 (1.031) (1.1%)	0.066 (1.022) (1.1%)	0.066 (1.015) (1.0%)
11.77	0.058 (0.978) (1.0%)	0.058 (0.983) (1.0%)	0.058 (0.978) (1.1%)
PIN CELL	0.074 (1.011) (0.3%)		

Table 6 (Continued)

PU-240 CAPTURE / PU-239 FISSION (C0/F9)

DISTANCE (CM)	MOX FUEL ONLY	WITH A B4C ROD	WITH A WATER HOLE
0.0	1.309 (0.996) (4.0%)		
1.07	1.338 (0.980) (1.4%)	1.234 (1.022) (2.1%)	1.301 (0.996) (1.5%)
2.14	1.282 (1.023) (1.5%)	1.291 (0.998) (1.8%)	1.306 (1.008) (1.4%)
3.21	1.328 (0.988) (1.6%)	1.318 (0.987) (1.6%)	1.331 (0.991) (1.5%)
4.28	1.337 (0.977) (1.3%)	1.310 (0.992) (1.7%)	1.291 (1.015) (1.6%)
5.35	1.311 (1.004) (1.7%)	1.315 (0.996) (1.5%)	1.345 (0.979) (1.5%)
6.42	1.363 (0.965) (2.0%)	1.285 (1.021) (1.5%)	1.309 (1.006) (1.4%)
7.49	1.306 (1.008) (1.6%)	1.316 (0.998) (1.4%)	1.347 (0.979) (1.4%)
8.56	1.325 (1.001) (1.8%)	1.301 (1.017) (1.6%)	1.351 (0.982) (1.5%)
9.63	1.346 (0.988) (1.2%)	1.338 (0.992) (1.7%)	1.328 (1.002) (1.6%)
10.70	1.332 (1.003) (1.6%)	1.300 (1.026) (1.6%)	1.330 (1.004) (1.6%)
11.77	1.334 (0.996) (1.5%)	1.284 (1.034) (1.6%)	1.345 (0.988) (1.6%)
PIN CELL	1.310 (0.985) (0.5%)		

PU-242 CAPTURE / PU-239 FISSION (C2/F9)

DISTANCE (CM)	MOX FUEL ONLY	WITH A B4C ROD	WITH A WATER HOLE
0.0	1.018 (1.006) (7.8%)		
1.07	1.086 (0.938) (3.0%)	0.975 (1.009) (4.7%)	0.919 (0.963) (3.6%)
2.14	0.954 (1.068) (3.5%)	1.038 (0.965) (3.4%)	0.957 (1.057) (3.4%)
3.21	1.099 (0.924) (3.9%)	1.092 (0.920) (3.9%)	1.011 (1.008) (3.7%)
4.28	0.986 (1.038) (2.9%)	1.022 (0.995) (3.8%)	1.072 (0.957) (3.2%)
5.35	1.031 (0.991) (3.6%)	1.000 (1.017) (3.4%)	0.991 (1.033) (3.6%)
6.42	1.058 (0.965) (3.4%)	1.095 (0.929) (3.1%)	1.004 (1.018) (3.2%)
7.49	1.002 (1.023) (3.3%)	1.015 (1.007) (3.2%)	1.015 (1.010) (3.5%)
8.56	1.050 (0.976) (3.8%)	0.968 (1.055) (2.9%)	1.017 (1.008) (3.0%)
9.63	0.993 (1.031) (3.4%)	1.000 (1.022) (3.2%)	1.106 (0.926) (3.6%)
10.70	1.004 (0.987) (3.3%)	1.001 (0.988) (3.4%)	1.018 (0.973) (3.4%)
11.77	0.866 (0.987) (3.6%)	0.943 (0.906) (2.8%)	0.872 (0.980) (3.2%)
PIN CELL	1.017 (0.979) (1.1%)		

Table 7 Comparison of reaction rate ratios (disturbed/undisturbed) near a B_4C rod between VIM and SRAC. The ratios are normalized to 1.0 for fission rates at the distance of 11.77 cm from the central fuel rod

TOTAL FISSION

DISTANCE	VIM	SRAC			
(CM)		107	69	28	8
1.07	0.866 (1.1%)+	0.856(0.988)*	0.855(0.988)	0.861(0.994)	0.872(1.007)
2.14	0.936 (1.0%)	0.933(0.996)	0.933(0.996)	0.936(0.999)	0.940(1.004)
3.21	0.962 (1.0%)	0.965(1.003)	0.965(1.003)	0.967(1.005)	0.968(1.007)
4.28	0.982 (1.1%)	0.982(1.000)	0.982(1.000)	0.982(1.001)	0.983(1.002)
5.35	0.997 (1.0%)	0.990(0.993)	0.990(0.993)	0.990(0.993)	0.990(0.993)
11.77	1.000	1.000	1.000	1.000	1.000

PU-239 FISSION

DISTANCE	VIM	SRAC			
(CM)		107	69	28	8
1.07	0.852 (1.1%)	0.839(0.985)	0.839(0.985)	0.845(0.992)	0.857(1,006)
2.14	0.930 (1.0%)	0.926(0.996)	0.926(0.996)	0.929(0.999)	0.934(1.005)
3.21	0.957 (1.0%)	0.962(1.005)	0.962(1.005)	0.964(1.007)	0.966(1.009)
4.28	0.979 (1.1%)	0.980(1.001)	0.980(1.001)	0.981(1.002)	0.982(1.002)
5.35	0.997 (1.0%)	0.989(0.992)	0.989(0.992)	0.989(0.992)	0.989(0.992)
11.77	1.000	1.000	1.000	1.000	1.000

U -235 FISSION

DISTANCE	VIM	SRAC			
(CM)		107	69	28	8
1.07	0.844 (1.1%)	0.846(1.002)	0.846(1.002)	0.853(1.010)	0.861(1.020)
2.14	0.934 (1.0%)	0.930(0.996)	0.930(0.995)	0.933(0.999)	0.935(1.002)
3.21	0.960 (1.0%)	0.964(1.004)	0.964(1.004)	0.965(1.006)	0.966(1.006)
4.28	0.978 (1.1%)	0.981(1.003)	0.981(1.003)	0.982(1.004)	0.981(1.004)
5.35	0.987 (1.0%)	0.989(1.002)	0.989(1.002)	0.989(1.002)	0.989(1.002)
11.77	1.000	1.000	1.000	1.000	1.000

* SRAC (SRAC/VIM)

\+ statistical error of VIM

Table 7 (Continued)

U -238 FISSION

DISTANCE	VIM	SRAC			
(CM)		107	69	28	8
1.07	0.966 (1.1%)	0.958(0.992)	0.958(0.992)	0.959(0.993)	0.961(0.995)
2.14	0.976 (1.0%)	0.974(0.998)	0.974(0.998)	0.975(0.999)	0.976(1.000)
3.21	0.991 (1.0%)	0.984(0.993)	0.984(0.993)	0.984(0.993)	0.985(0.994)
4.28	0.996 (1.1%)	0.990(0.994)	0.990(0.994)	0.990(0.994)	0.990(0.994)
5.35	0.997 (1.0%)	0.993(0.997)	0.993(0.997)	0.993(0.997)	0.994(0.997)
11.77	1.000	1.000	1.000	1.000	1.000

PU-241 FISSION

DISTANCE	VIM	SRAC			
(CM)		107	69	28	8
1.07	0.835 (1.1%)	0.833(0.998)	0.832(0.997)	0.839(1.005)	0.856(1.026)
2.14	0.922 (1.0%)	0.923(1.001)	0.923(1.000)	0.926(1.004)	0.933(1.012)
3.21	0.953 (1.0%)	0.960(1.007)	0.960(1.007)	0.962(1.009)	0.965(1.012)
4.28	0.976 (1.1%)	0.979(1.004)	0.979(1.004)	0.980(1.004)	0.981(1.006)
5.35	0.992 (1.0%)	0.988(0.996)	0.988(0.996)	0.989(0.997)	0.989(0.997)
11.77	1.000	1.000	1.000	1.000	1.000

Table 7 (Continued)

TOTAL CAPTURE

DISTANCE	VIM	SRAC			
(CM)		107	69	28	8
1.07	0.845 (1.2%)	0.839(0.992)	0.839(0.992)	0.845(0.999)	0.854(1.010)
2.14	0.957 (1.1%)	0.927(0.968)	0.926(0.968)	0.929(0.970)	0.933(0.974)
3.21	0.977 (1.2%)	0.962(0.985)	0.962(0.985)	0.963(0.986)	0.964(0.987)
4.28	0.996 (1.1%)	0.980(0.984)	0.980(0.984)	0.981(0.985)	0.981(0.985)
5.35	1.000 (1.1%)	0.989(0.989)	0.989(0.989)	0.989(0.989)	0.989(0.989)
11.77	1.000	1.000	1.000	1.000	1.000

U -238 CAPTURE

DISTANCE	VIM	SRAC			
(CM)		107	69	28	8
1.07	0.870 (1.2%)	0.863(0.992)	0.863(0.991)	0.866(0.996)	0.871(1.001)
2.14	0.965 (1.1%)	0.938(0.973)	0.938(0.972)	0.939(0.973)	0.939(0.974)
3.21	0.988 (1.2%)	0.968(0.980)	0.967(0.979)	0.968(0.979)	0.967(0.979)
4.28	1.012 (1.1%)	0.983(0.971)	0.983(0.971)	0.983(0.971)	0.982(0.970)
5.35	0.987 (1.1%)	0.990(1.003)	0.990(1.003)	0.990(1.003)	0.989(1.002)
11.77	1.000	1.000	1.000	1.000	1.000

PU-240 CAPTURE

DISTANCE	VIM	SRAC			
(CM)		107	69	28	8
1.07	0.816 (1.2%)	0.807(0.989)	0.807(0.990)	0.814(0.998)	0.828(1.015)
2.14	0.973 (1.1%)	0.911(0.936)	0.911(0.936)	0.915(0.940)	0.922(0.947)
3.21	0.987 (1.2%)	0.954(0.967)	0.955(0.967)	0.957(0.969)	0.960(0.972)
4.28	0.997 (1.1%)	0.976(0.979)	0.976(0.980)	0.977(0.980)	0.979(0.982)
5.35	1.040 (1.1%)	0.986(0.948)	0.986(0.948)	0.987(0.949)	0.988(0.950)
11.77	1.000	1.000	1.000	1.000	1.000

Table 7 (Continued)

PU-239 CAPTURE

DISTANCE	VIM	SRAC			
(CM)		107	69	28	8
1.07	0.843 (1.2%)	0.825(0.979)	0.825(0.979)	0.833(0.989)	0.844(1.002)
2.14	0.936 (1.1%)	0.920(0.983)	0.920(0.983)	0.924(0.988)	0.928(0.992)
3.21	0.961 (1.2%)	0.960(0.999)	0.960(0.999)	0.961(1.000)	0.963(1.002)
4.28	0.976 (1.1%)	0.979(1.004)	0.979(1.004)	0.980(1.004)	0.980(1.004)
5.35	1.001 (1.1%)	0.988(0.988)	0.988(0.988)	0.989(0.988)	0.988(0.988)
11.77	1.000	1.000	1.000	1.000	1.000

PU-242 CAPTURE

DISTANCE	VIM	SRAC			
(CM)		107	69	28	8
1.07	0.702 (1.2%)	0.810(1.154)	0.813(1.158)	0.820(1.168)	0.851(1.212)
2.14	0.929 (1.1%)	0.911(0.980)	0.913(0.983)	0.917(0.987)	0.931(1.002)
3.21	0.874 (1.2%)	0.953(1.090)	0.955(1.092)	0.957(1.094)	0.963(1.101)
4.28	0.932 (1.1%)	0.975(1.046)	0.976(1.047)	0.977(1.048)	0.980(1.051)
5.35	0.889 (1.1%)	0.986(1.109)	0.986(1.110)	0.987(1.110)	0.988(1.112)
11.77	1.000	1.000	1.000	1.000	1.000

Table 8 Comparison of reaction rate ratios (disturbed/undisturbed) near a water hole between VIM and SRAC. The ratios are normalized to 1.0 for fission rates at the distance of 11.77 cm from the central fuel rod

TOTAL FISSION

DISTANCE	VIM	SRAC			
(CM)		107	69	28	8
1.07	1.259 (1.1%)+	1.229(0.977)*	1.228(0.976)	1.222(0.971)	1.183(0.940)
2.14	1.055 (1.1%)	1.040(0.986)	1.041(0.986)	1.039(0.984)	1.030(0.976)
3.21	1.027 (1.1%)	1.013(0.986)	1.013(0.986)	1.012(0.986)	1.010(0.983)
4.28	1.013 (1.1%)	1.005(0.992)	1.005(0.992)	1.005(0.992)	1.004(0.991)
5.35	1.007 (1.0%)	1.002(0.995)	1.002(0.995)	1.002(0.995)	1.002(0.995)
11.77	1.000	1.000	1.000	1.000	1.000

PU-239 FISSION

DISTANCE	VIM	SRAC			
(CM)		107	69	28	8
1.07	1.318 (1.1%)	1.280(0.972)	1.279(0.971)	1.272(0.966)	1.228(0.932)
2.14	1.065 (1.1%)	1.047(0.983)	1.047(0.983)	1.045(0.982)	1.036(0.973)
3.21	1.031 (1.1%)	1.014(0.984)	1.015(0.984)	1.014(0.983)	1.011(0.980)
4.28	1.015 (1.1%)	1.005(0.990)	1.006(0.990)	1.005(0.990)	1.004(0.989)
5.35	1.009 (1.0%)	1.002(0.994)	1.002(0.994)	1.002(0.994)	1.002(0.994)
11.77	1.000	1.000	1.000	1.000	1.000

U -235 FISSION

DISTANCE	VIM	SRAC			
(CM)		107	69	28	8
1.07	1.176 (1.1%)	1.167(0.992)	1.169(0.994)	1.162(0.988)	1.131(0.962)
2.14	1.041 (1.1%)	1.033(0.992)	1.034(0.993)	1.032(0.991)	1.026(0.986)
3.21	1.017 (1.1%)	1.011(0.994)	1.011(0.994)	1.010(0.994)	1.009(0.993)
4.28	1.002 (1.1%)	1.004(1.002)	1.004(1.003)	1.004(1.002)	1.004(1.002)
5.35	1.004 (1.0%)	1.002(0.997)	1.002(0.997)	1.002(0.997)	1.002(0.998)
11.77	1.000	1.000	1.000	1.000	1.000

* SRAC (SRAC/VIM)

\+ statistical error of VIM

Table 8 (Continued)

U -238 FISSION

DISTANCE	VIM	SRAC			
(CM)		107	69	28	8
1.07	1.023 (1.1%)	1.012(0.989)	1.012(0.989)	1.009(0.986)	1.002(0.979)
2.14	1.011 (1.1%)	1.009(0.998)	1.009(0.998)	1.008(0.996)	1.004(0.993)
3.21	1.010 (1.1%)	1.005(0.996)	1.005(0.996)	1.004(0.995)	1.002(0.993)
4.28	1.007 (1.1%)	1.003(0.996)	1.003(0.996)	1.003(0.996)	1.001(0.994)
5.35	1.010 (1.0%)	1.002(0.992)	1.002(0.992)	1.002(0.992)	1.001(0.991)
11.77	1.000	1.000	1.000	1.000	1.000

PU-241 FISSION

DISTANCE	VIM	SRAC			
(CM)		107	69	28	8
1.07	1.223 (1.1%)	1.212(0.991)	1.212(0.991)	1.204(0.985)	1.158(0.947)
2.14	1.055 (1.1%)	1.042(0.987)	1.042(0.988)	1.040(0.986)	1.029(0.975)
3.21	1.026 (1.1%)	1.014(0.988)	1.014(0.989)	1.013(0.988)	1.010(0.984)
4.28	1.009 (1.1%)	1.005(0.996)	1.006(0.996)	1.005(0.996)	1.004(0.995)
5.35	0.999 (1.0%)	1.002(1.003)	1.003(1.003)	1.002(1.003)	1.002(1.003)
11.77	1.000	1.000	1.000	1.000	1.000

Table 8 (Continued)

TOTAL CAPTURE

DISTANCE	VIM	SRAC			
(CM)		107	69	28	8
1.07	1.194 (1.2%)	1.165(0.976)	1.161(0.973)	1.153(0.966)	1.115(0.934)
2.14	1.055 (1.2%)	1.033(0.979)	1.033(0.979)	1.031(0.978)	1.026(0.972)
3.21	1.028 (1.2%)	1.011(0.984)	1.012(0.984)	1.011(0.984)	1.010(0.983)
4.28	1.009 (1.2%)	1.004(0.995)	1.005(0.996)	1.004(0.995)	1.004(0.995)
5.35	1.001 (1.2%)	1.002(1.001)	1.002(1.001)	1.002(1.001)	1.002(1.001)
11.77	1.000	1.000	1.000	1.000	1.000

U -238 CAPTURE

DISTANCE	VIM	SRAC			
(CM)		107	69	28	8
1.07	1.095 (1.2%)	1.061(0.969)	1.053(0.961)	1.049(0.958)	1.039(0.949)
2.14	1.037 (1.2%)	1.016(0.980)	1.016(0.979)	1.015(0.979)	1.014(0.978)
3.21	1.030 (1.2%)	1.006(0.976)	1.006(0.977)	1.006(0.977)	1.006(0.977)
4.28	1.019 (1.2%)	1.002(0.983)	1.002(0.984)	1.002(0.984)	1.003(0.984)
5.35	0.984 (1.2%)	1.001(1.017)	1.001(1.017)	1.001(1.017)	1.002(1.018)
11.77	1.000	1.000	1.000	1.000	1.000

PU-240 CAPTURE

DISTANCE	VIM	SRAC			
(CM)		107	69	28	8
1.07	1.271 (1.2%)	1.265(0.996)	1.266(0.996)	1.248(0.982)	1.157(0.911)
2.14	1.076 (1.2%)	1.051(0.977)	1.052(0.977)	1.050(0.976)	1.039(0.966)
3.21	1.025 (1.2%)	1.019(0.994)	1.019(0.994)	1.018(0.993)	1.015(0.990)
4.28	0.972 (1.2%)	1.008(1.037)	1.008(1.037)	1.007(1.037)	1.006(1.035)
5.35	1.027 (1.2%)	1.004(0.978)	1.004(0.978)	1.004(0.978)	1.003(0.977)
11.77	1.000	1.000	1.000	1.000	1.000

Table 8 (Continued)

PU-239 CAPTURE

DISTANCE	VIM	SRAC			
(CM)		107	69	28	8
1.07	1.315 (1.2%)	1.269(0.965)	1.268(0.964)	1.260(0.958)	1.221(0.928)
2.14	1.068 (1.2%)	1.045(0.979)	1.045(0.979)	1.043(0.977)	1.036(0.970)
3.21	1.037 (1.2%)	1.014(0.977)	1.014(0.978)	1.014(0.977)	1.012(0.975)
4.28	1.015 (1.2%)	1.005(0.990)	1.005(0.990)	1.005(0.990)	1.005(0.990)
5.35	1.012 (1.2%)	1.002(0.991)	1.002(0.991)	1.002(0.991)	1.002(0.991)
11.77	1.000	1.000	1.000	1.000	1.000

PU-242 CAPTURE

DISTANCE	VIM	SRAC			
(CM)		107	69	28	8
1.07	1.107 (1.2%)	1.112(1.004)	1.109(1.002)	1.103(0.996)	1.049(0.947)
2.14	1.061 (1.2%)	1.040(0.980)	1.038(0.978)	1.036(0.976)	1.018(0.959)
3.21	0.943 (1.2%)	1.018(1.080)	1.017(1.078)	1.015(1.077)	1.008(1.070)
4.28	1.095 (1.2%)	1.008(0.920)	1.007(0.920)	1.007(0.919)	1.004(0.917)
5.35	0.963 (1.2%)	1.004(1.043)	1.004(1.043)	1.003(1.042)	1.002(1.041)
11.77	1.000	1.000	1.000	1.000	1.000

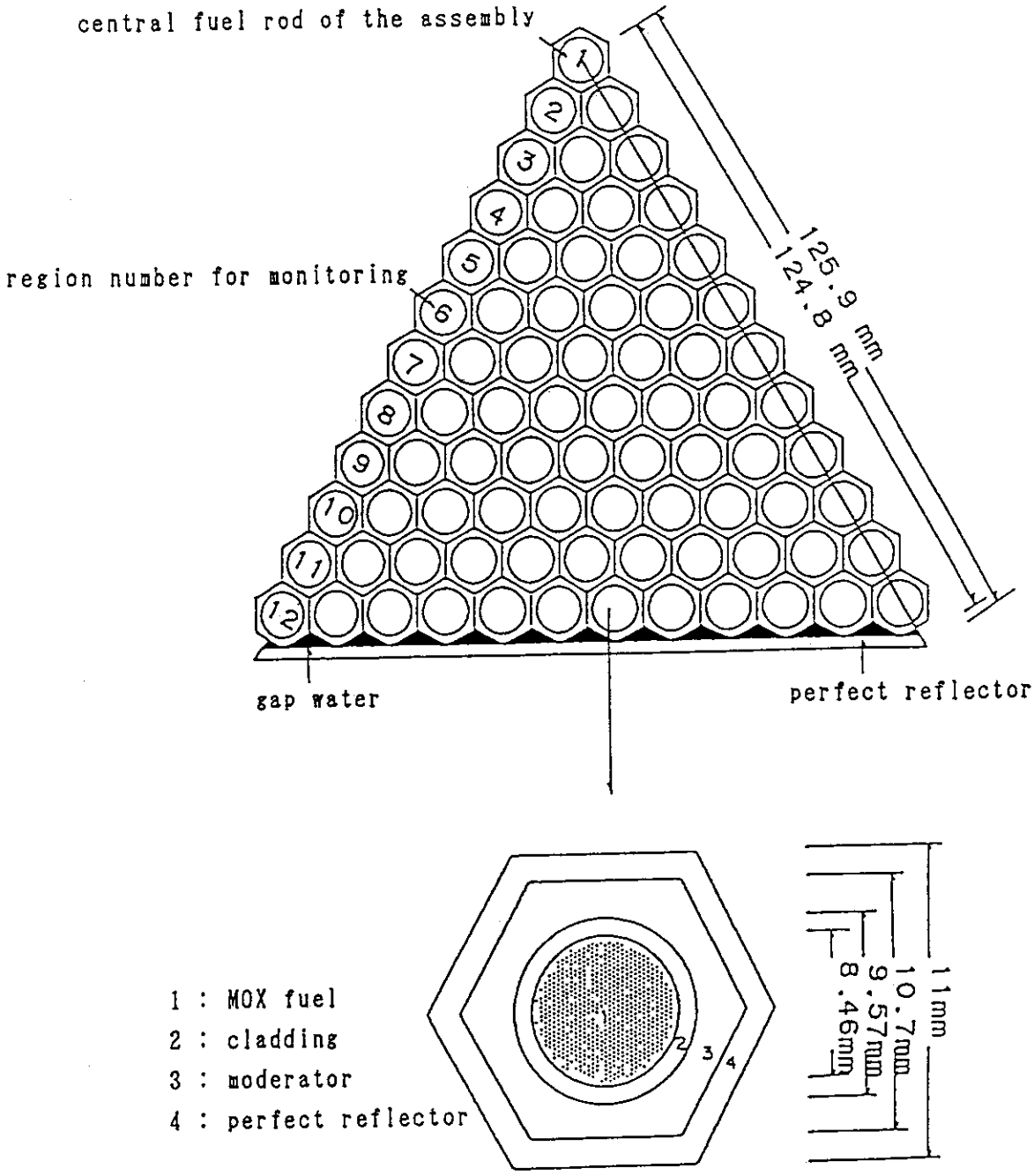

Figure 1 Geometrical model of one-sixth hexagonal fuel assembly and unit pin cell for the VIM and SRAC calculation

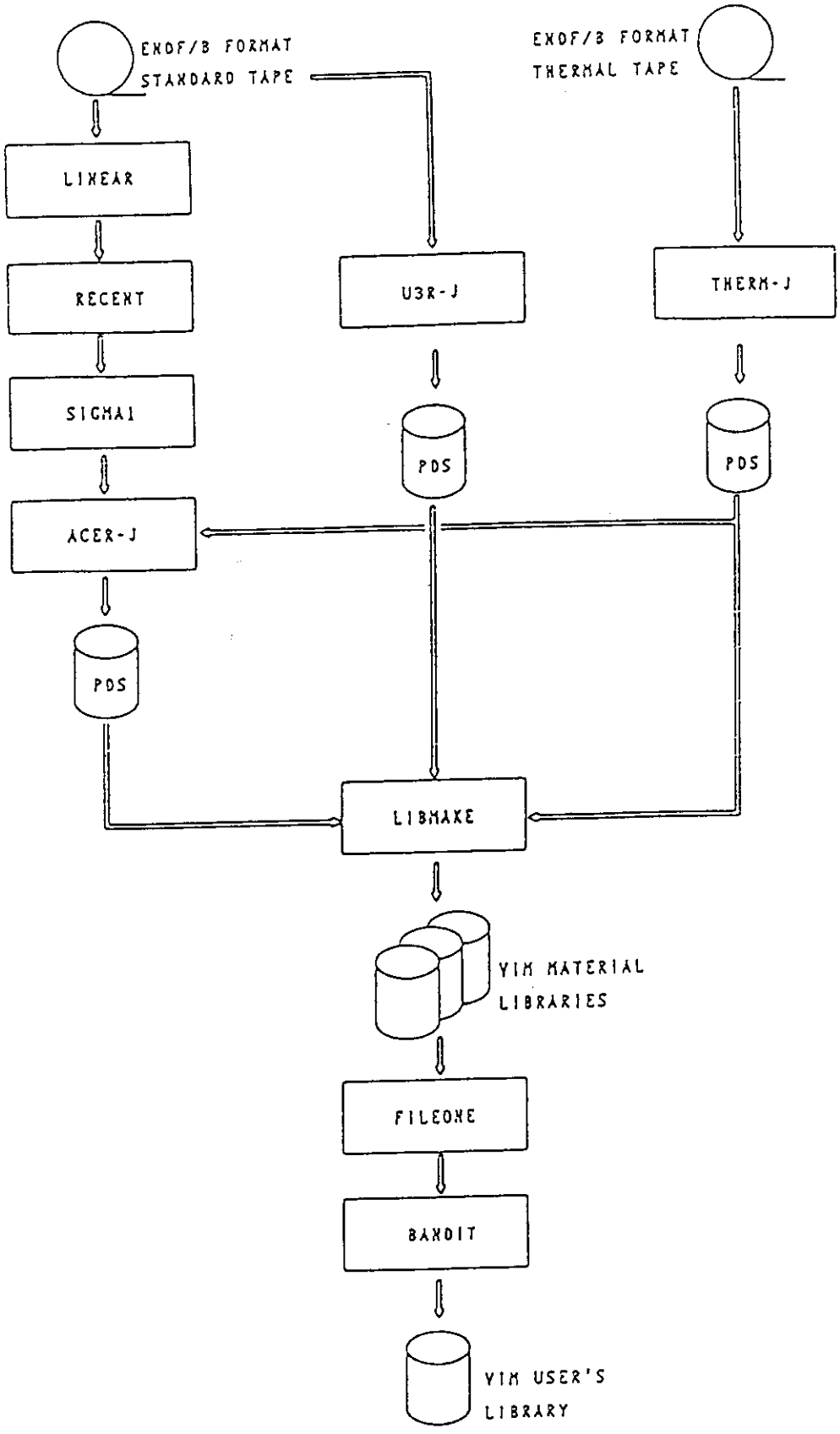

Figure 2 Flow diagram to generate the VIM user's library

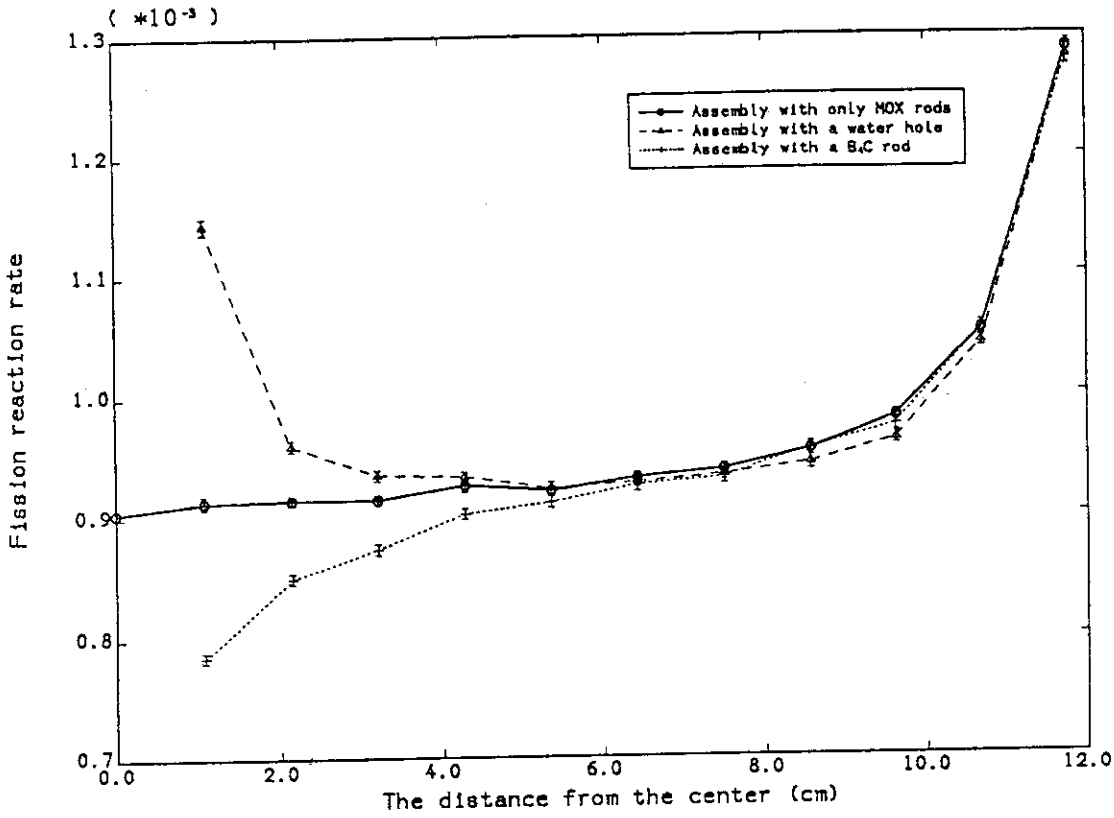

Figure 3 Distributions of fission reaction rate in the fuel assemblies

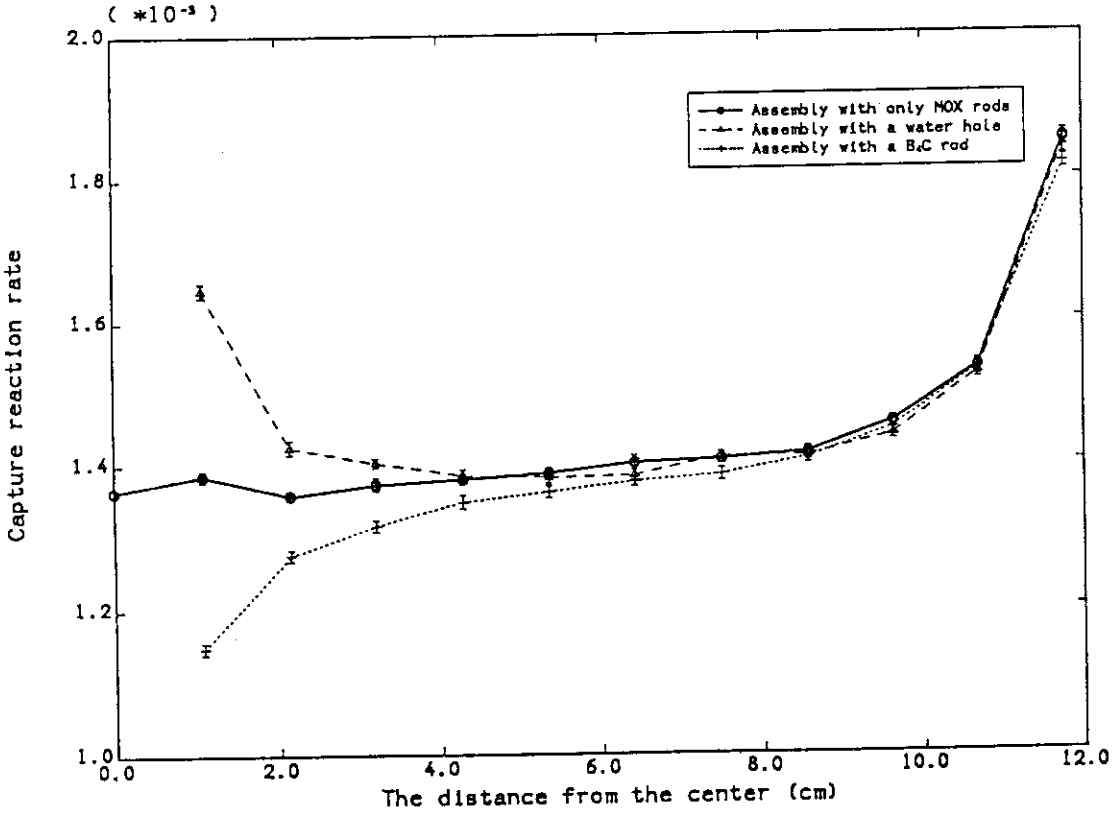

Figure 4 Distributions of capture reaction rate in the fuel assemblies

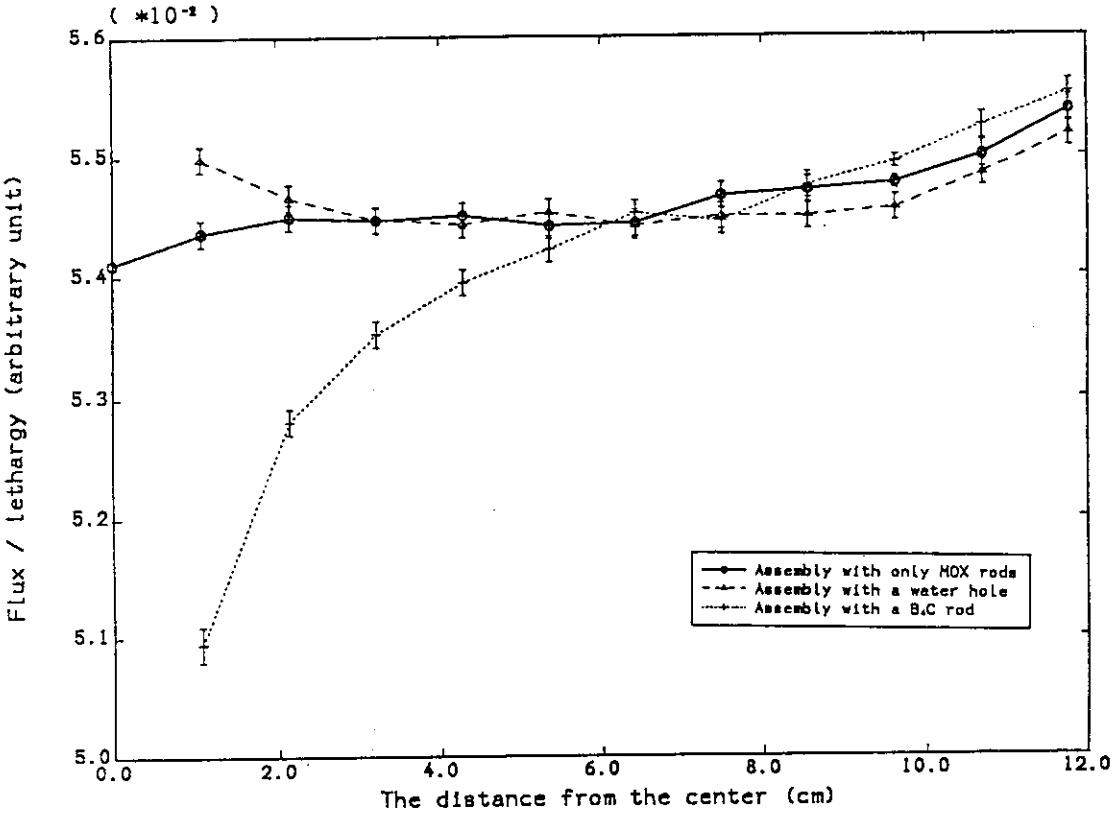

Figure 5 Distributions of 1-group flux in the fuel assemblies

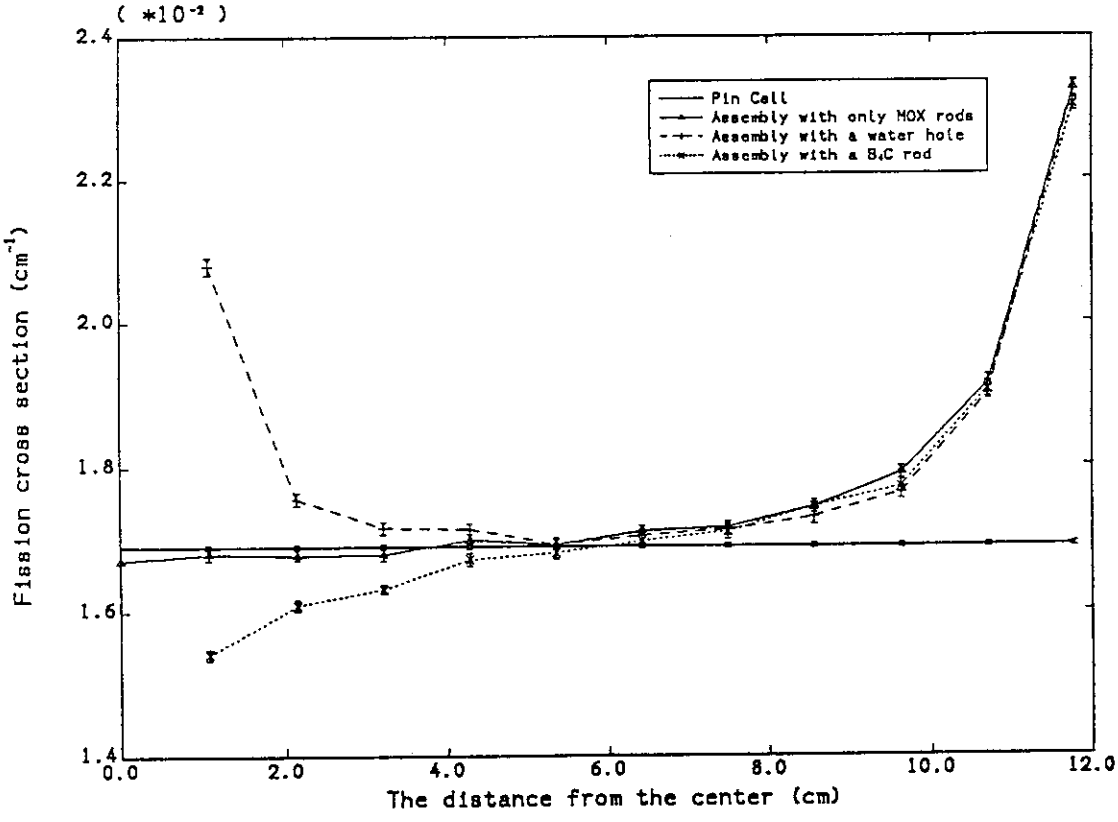

Figure 6 Distributions of 1-group macroscopic fission cross section in the fuel assemblies

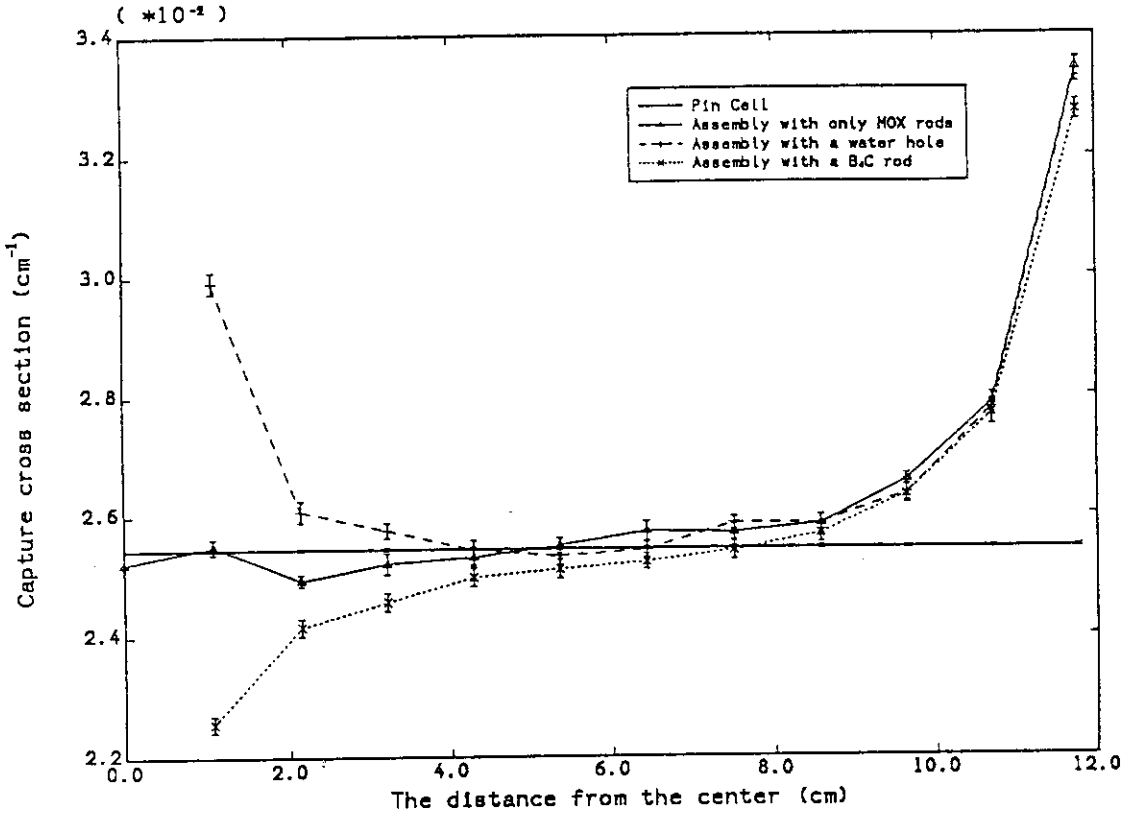

Figure 7 Distributions of 1-group macroscopic capture cross section in the fuel assemblies

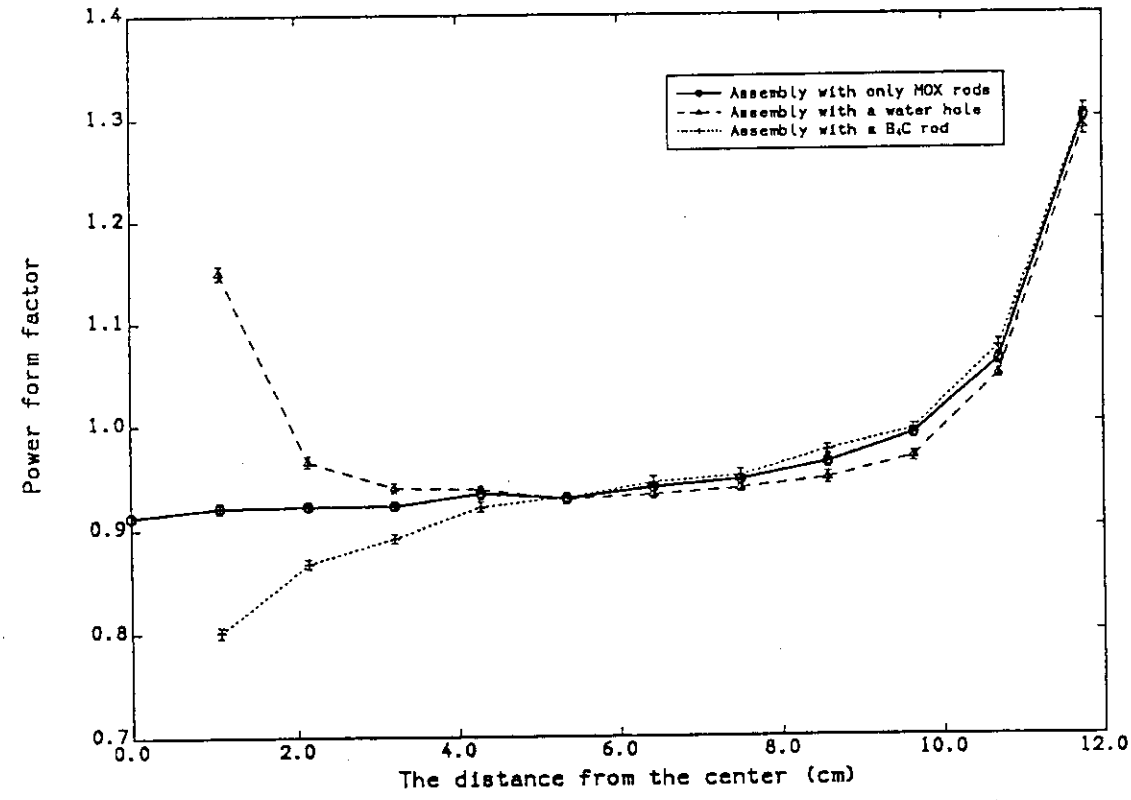

Figure 8 Distributions of power form factor in the fuel assemblies

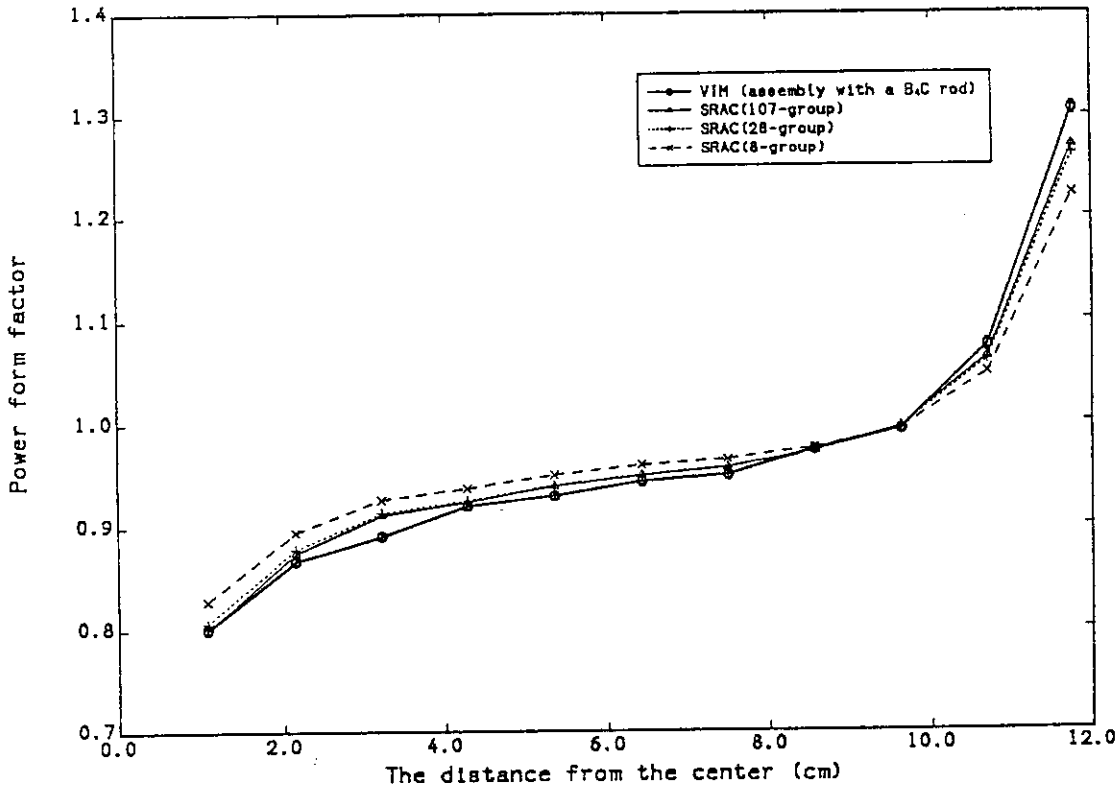

Figure 9 Comparison of power form factor distribition in the fuel assembly with a B_4C rod between VIM and SRAC

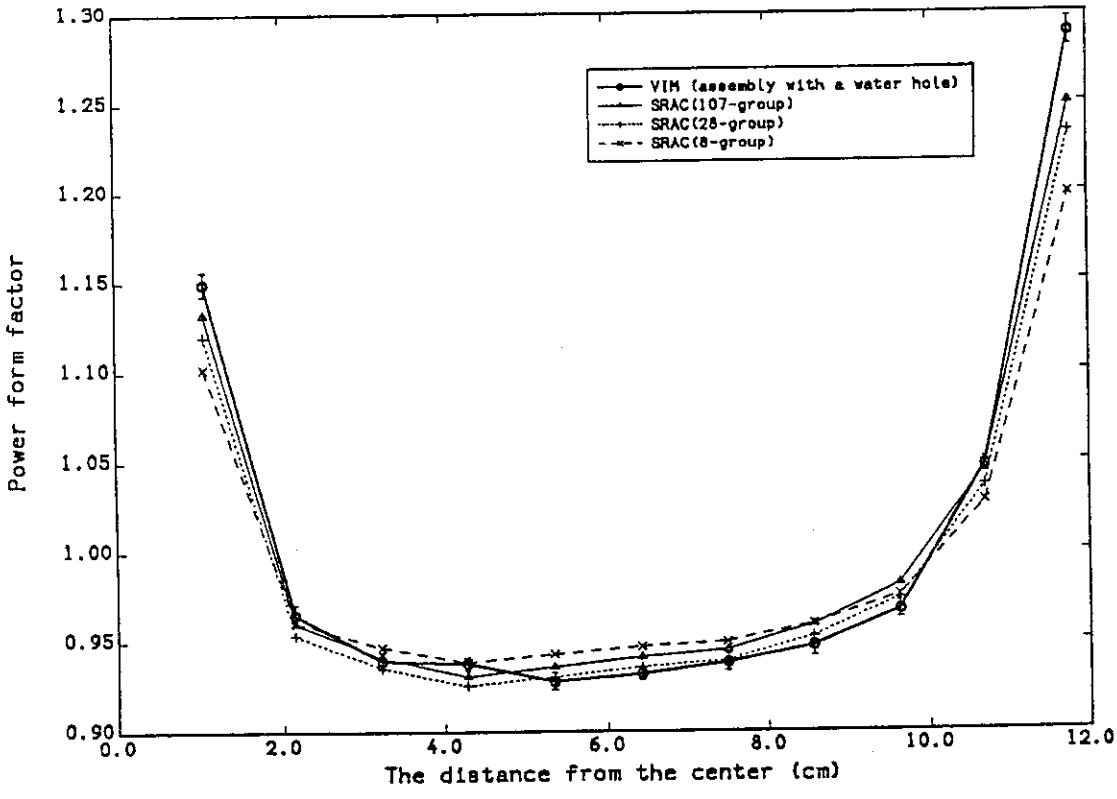

Figure 10 Comparison of power form factor distribution in the fuel assembly with a water hole between VIM and SRAC

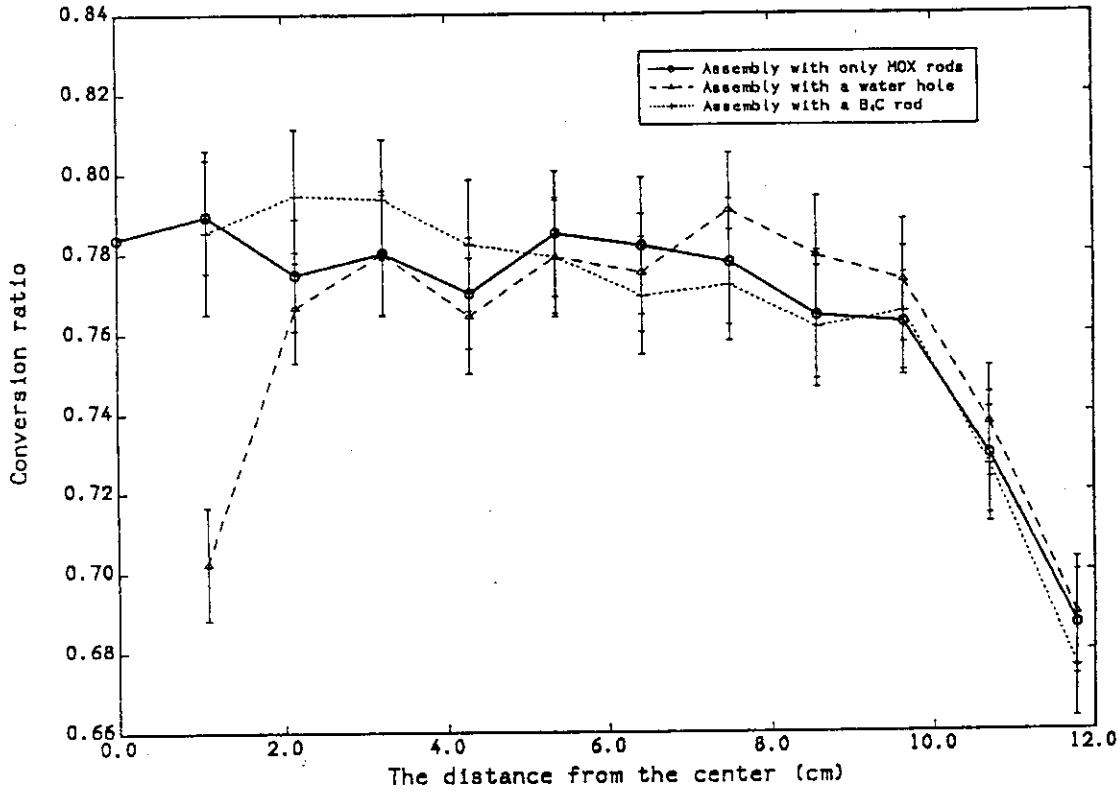

Figure 11 Space dependent conversion ratios in the fuel assemblies

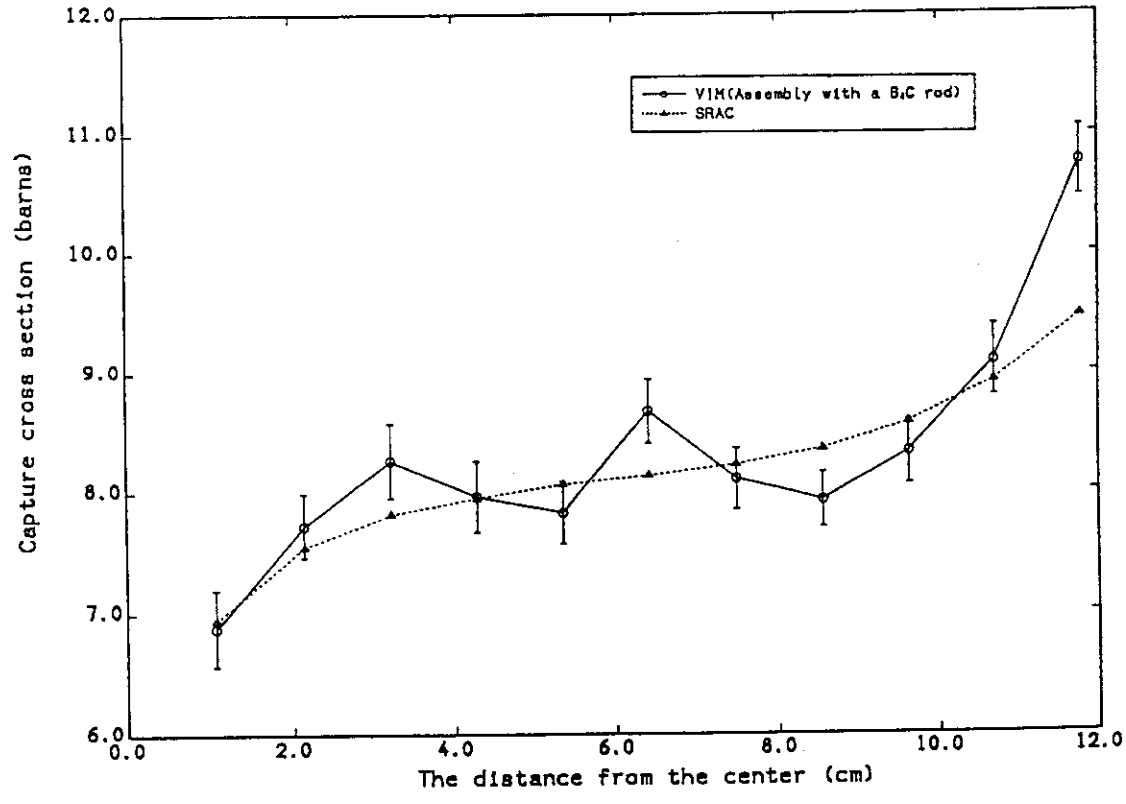

Figure 12 Comparison of ^{242}Pu 1-group macroscopic capture cross section in the assembly with a B_4C rod between VIM and SRAC

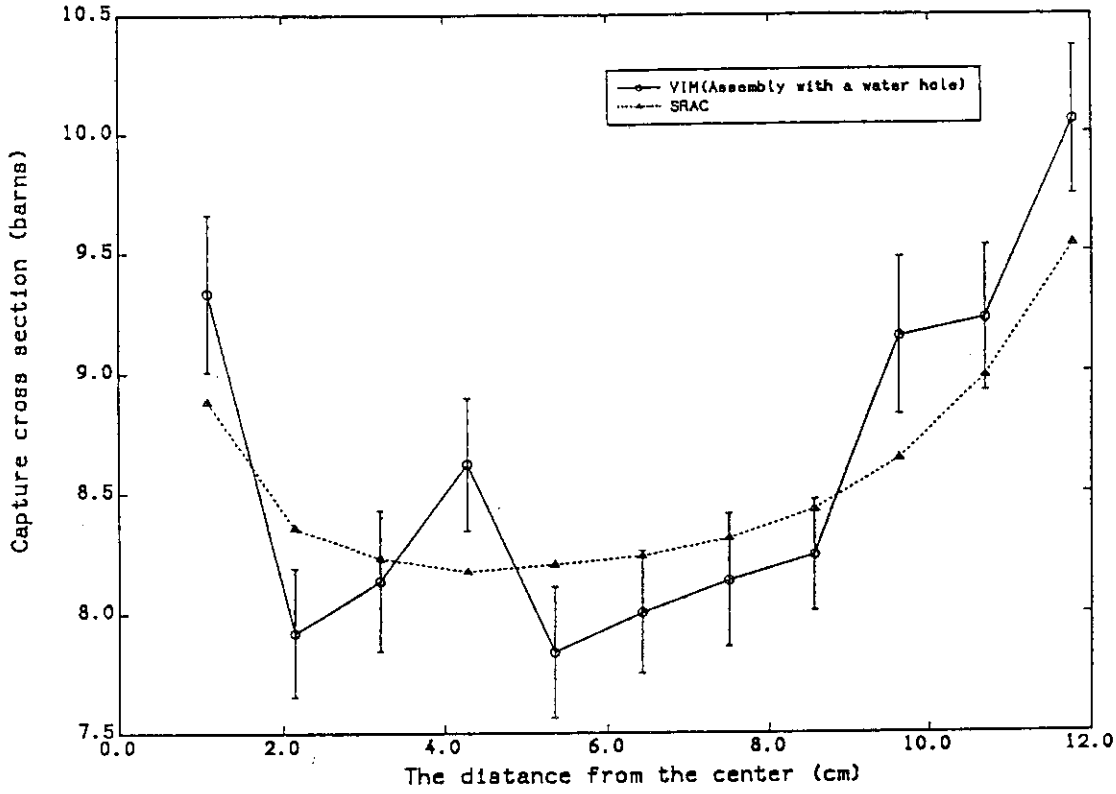

Figure 13 Comparison of ^{242}Pu 1-group macroscopic capture cross section in the assembly with a water hole between VIM and SRAC

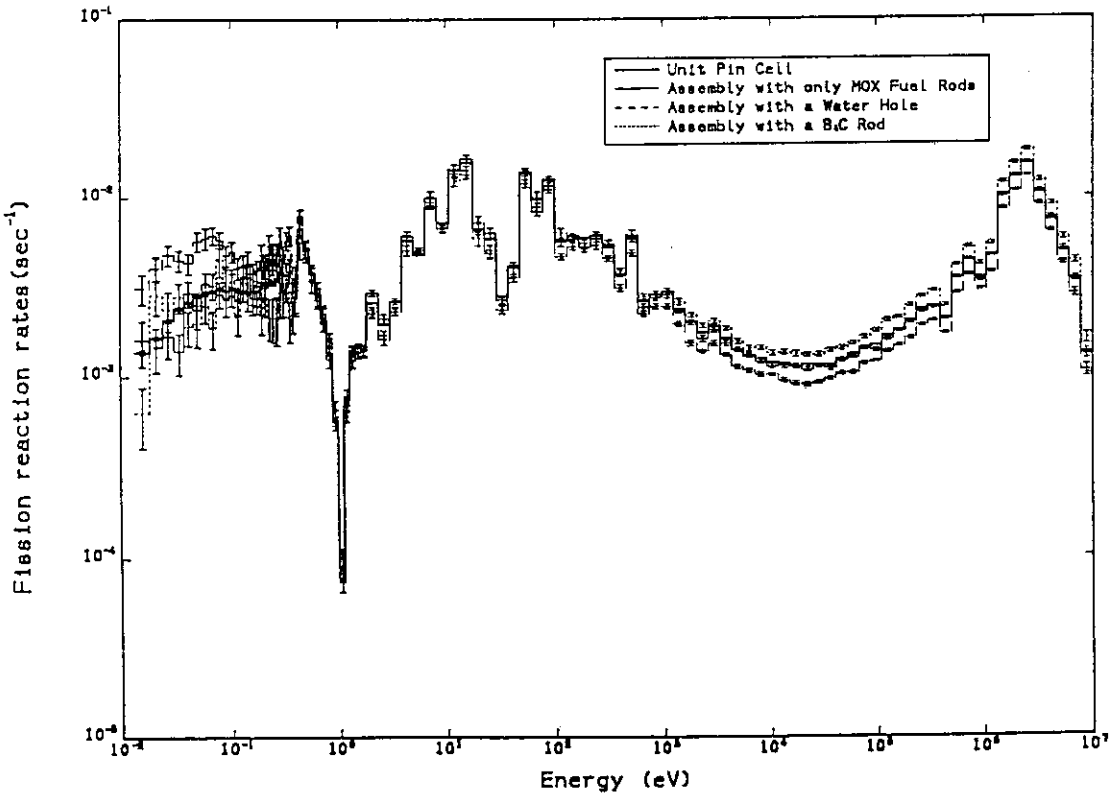

Figure 14 Comparison of multi-group fission reaction rate between the unit pin cell and the region 2 in the fuel assemblies

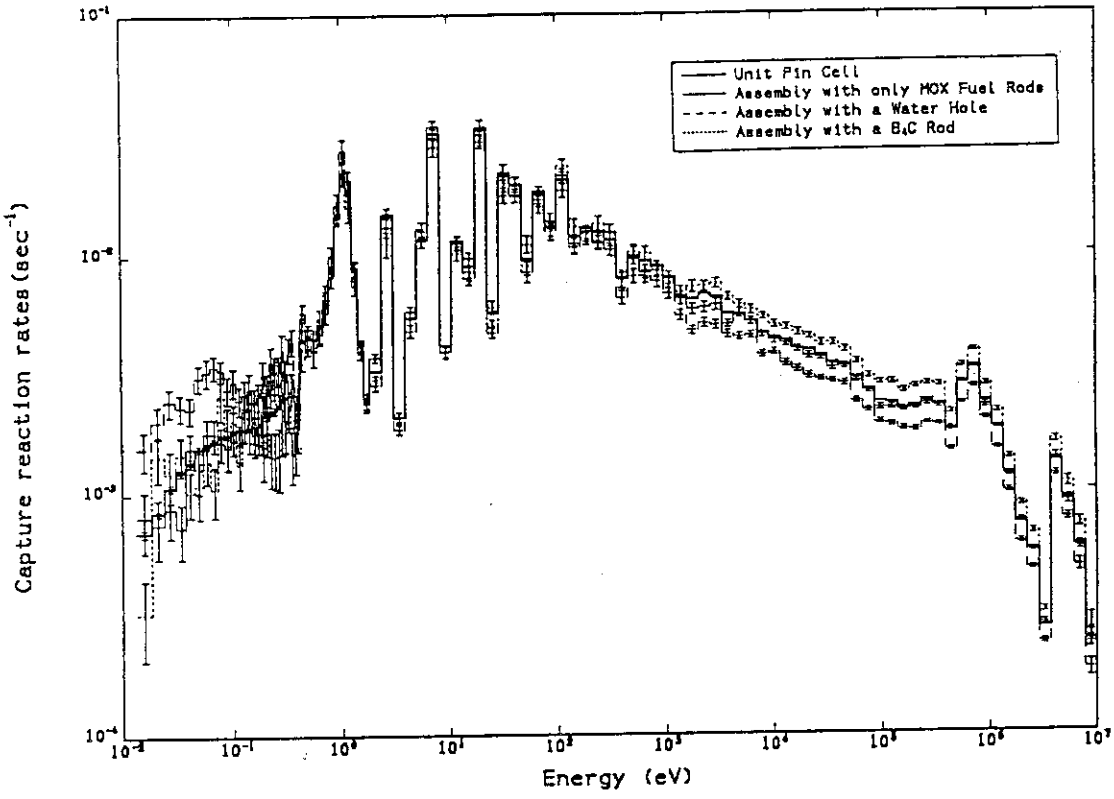

Figure 15 Comparison of multi-group capture reaction rate between the unit pin cell and the region 2 in the fuel assemblies

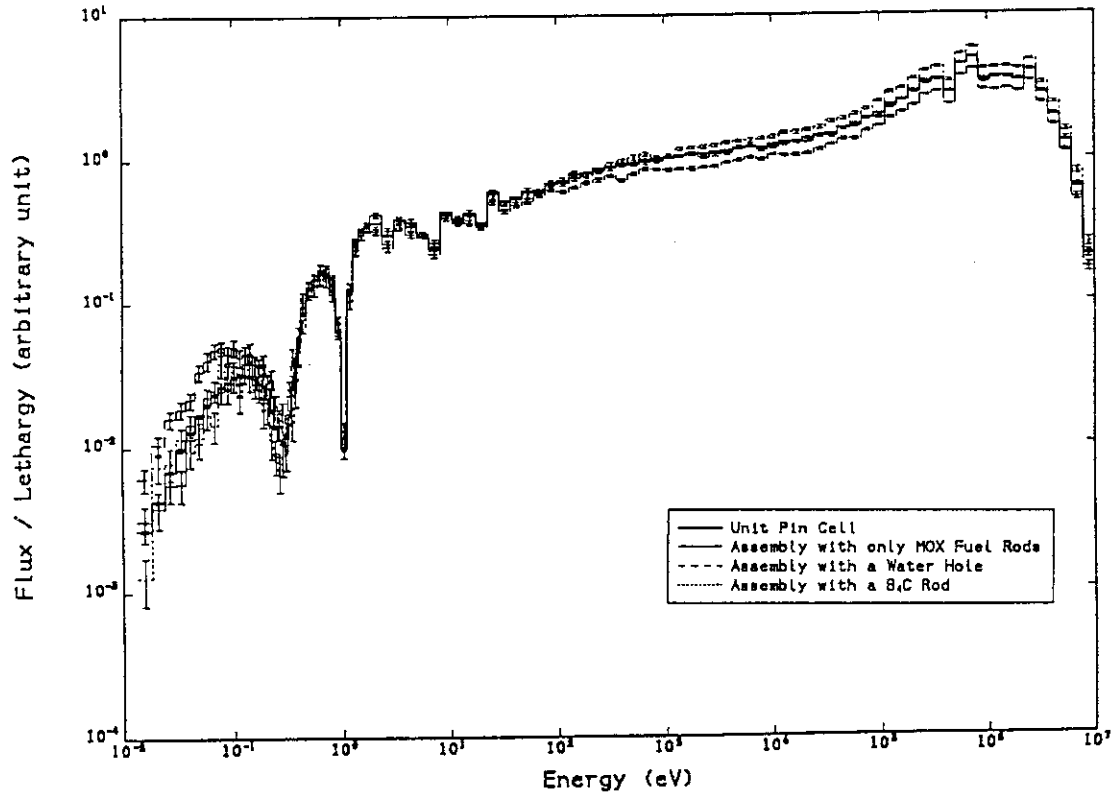

Figure 16 Comparison of multi-group neutron spectrum between the unit pin cell and the region 2 in the fuel assemblies

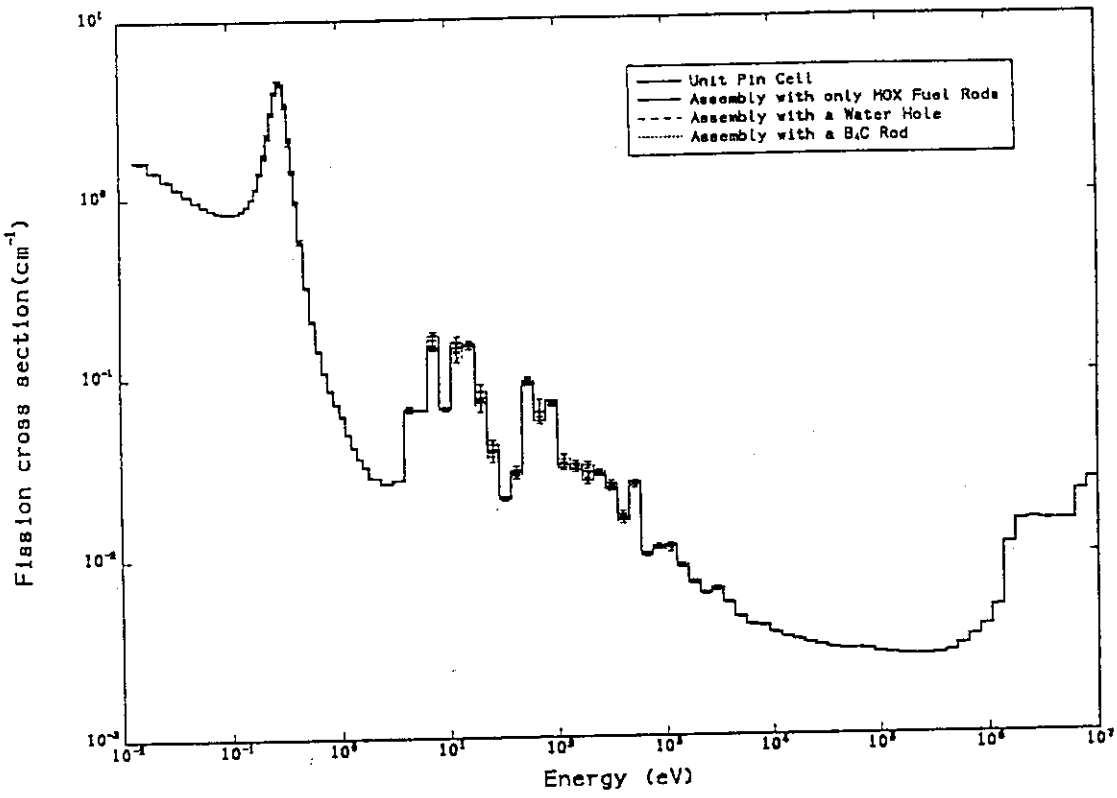

Figure 17 Comparison of multi-group macroscopic fission cross section the unit pin cell and the region 2 in the fuel assemblies

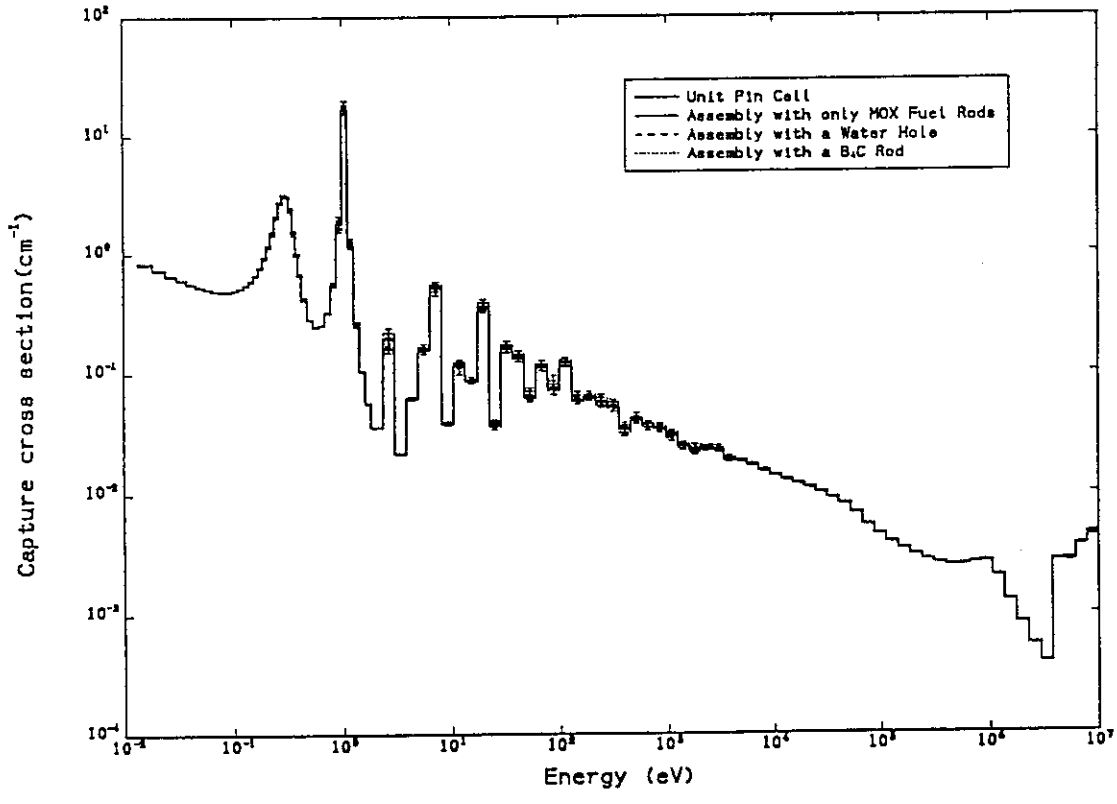

Figure 18 Comparison of multi-group macroscopic capture cross section the unit pin cell and the region 2 in the fuel assemblies

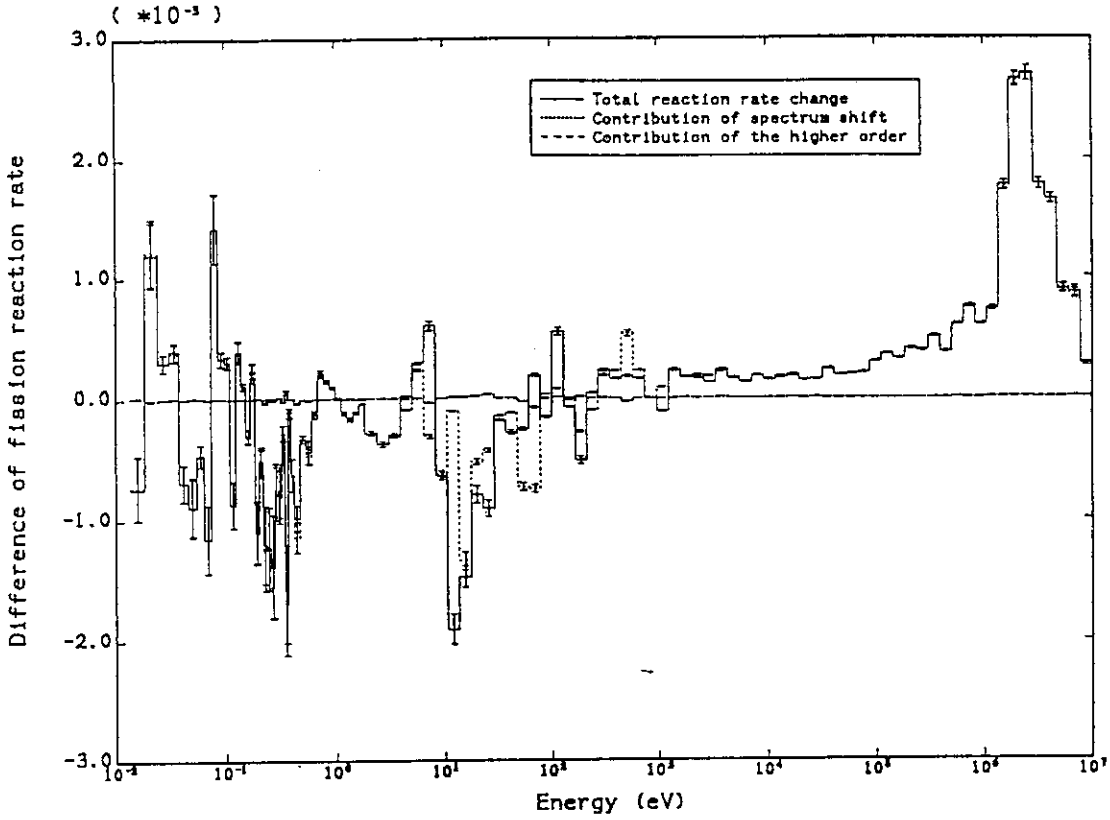

Figure 19 Contribution of spectrum shift and the higer order to the fission rate change in the fuel rods adjacent to the B_4C rod

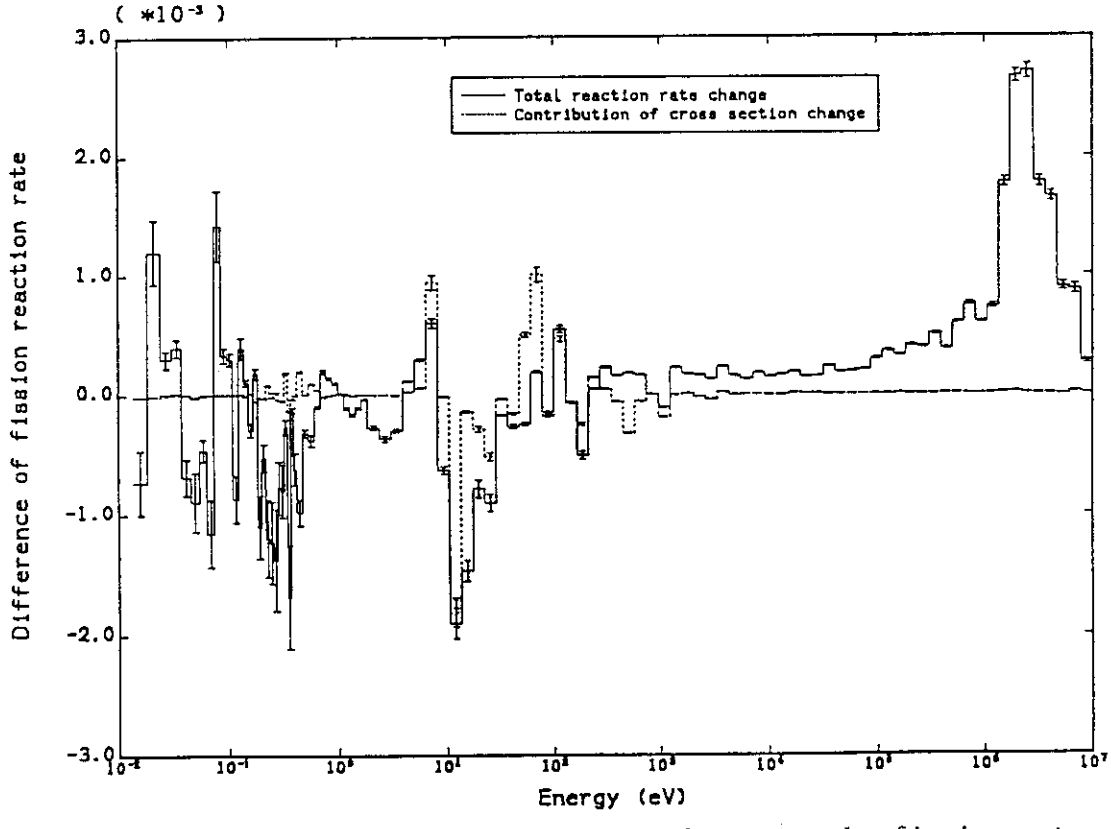

Figure 20 Contribution of cross section change to the fission rate change in the fuel rods adjacent to the B_4C rod

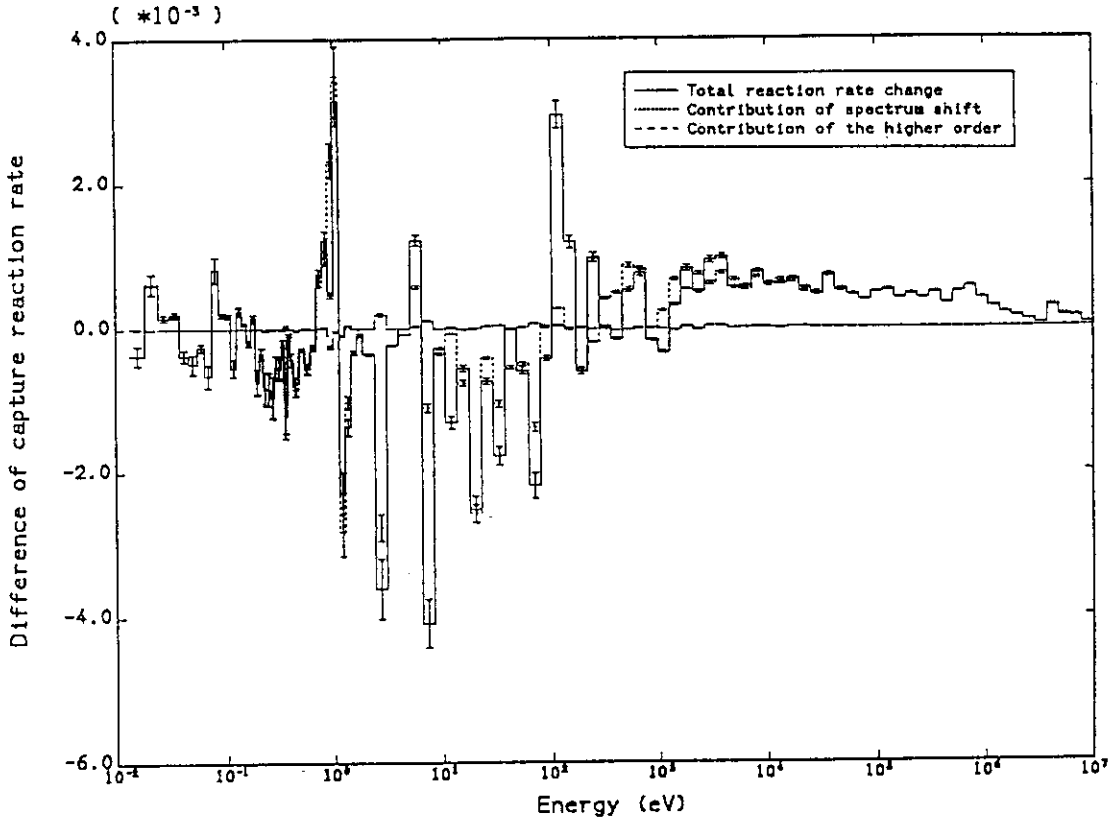

Figure 21 Contribution of spectrum shift and the higer order to the capture rate change in the fuel rods adjacent to the B_4C rod

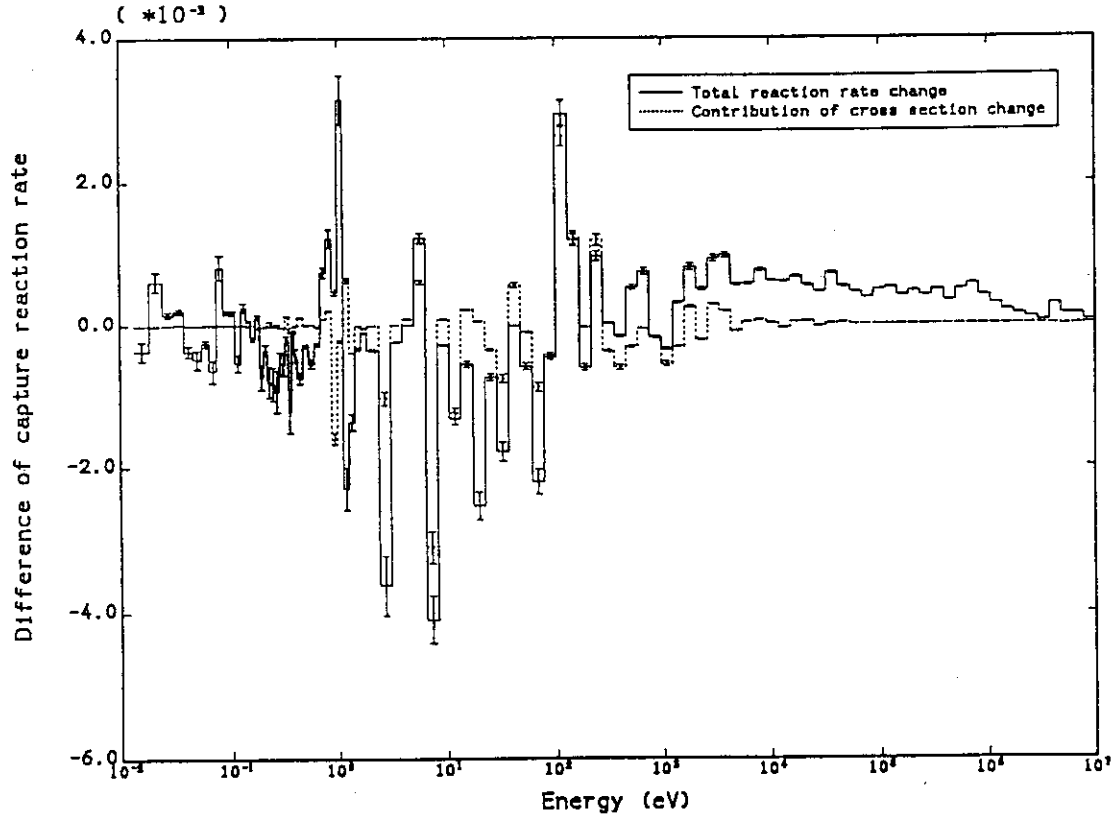

Figure 22 Contribution of cross section change to the cpature rate change in the fuel rods adjacent to the B_4C rod

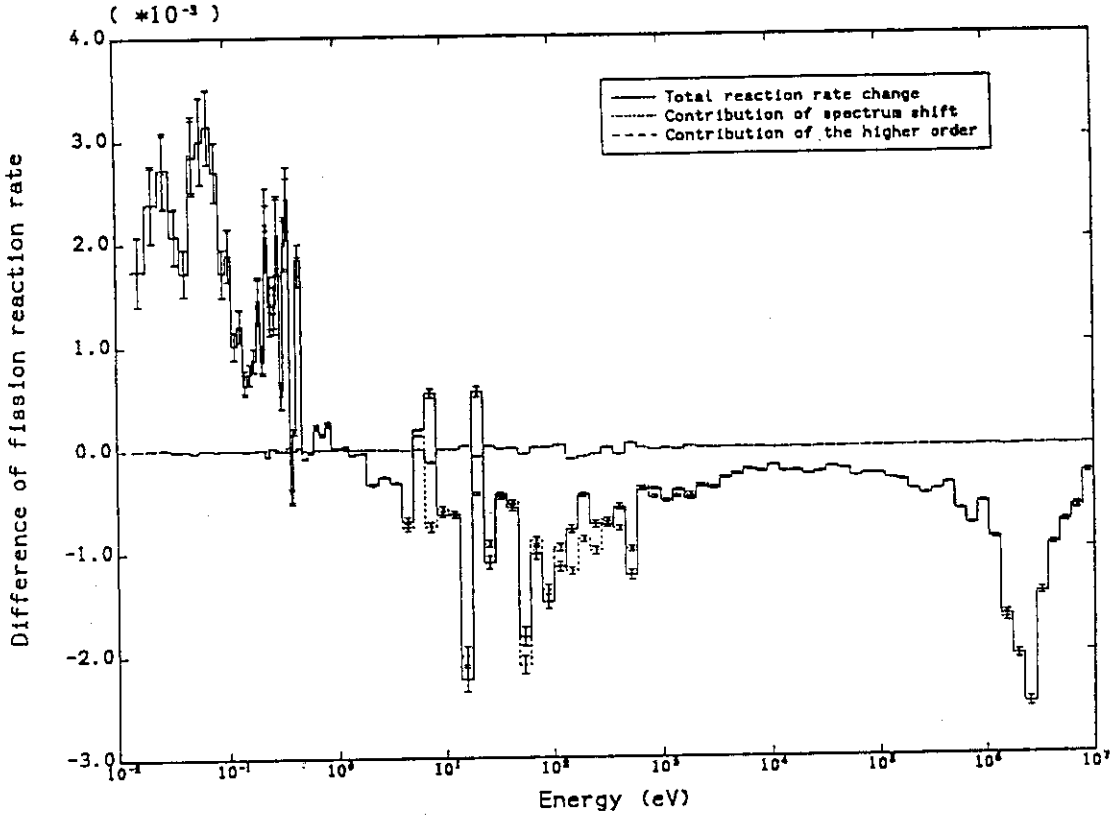

Figure 23 Contribution of flux shift and the higher order to the fission rate change in the fuel rods adjacent to the water hole

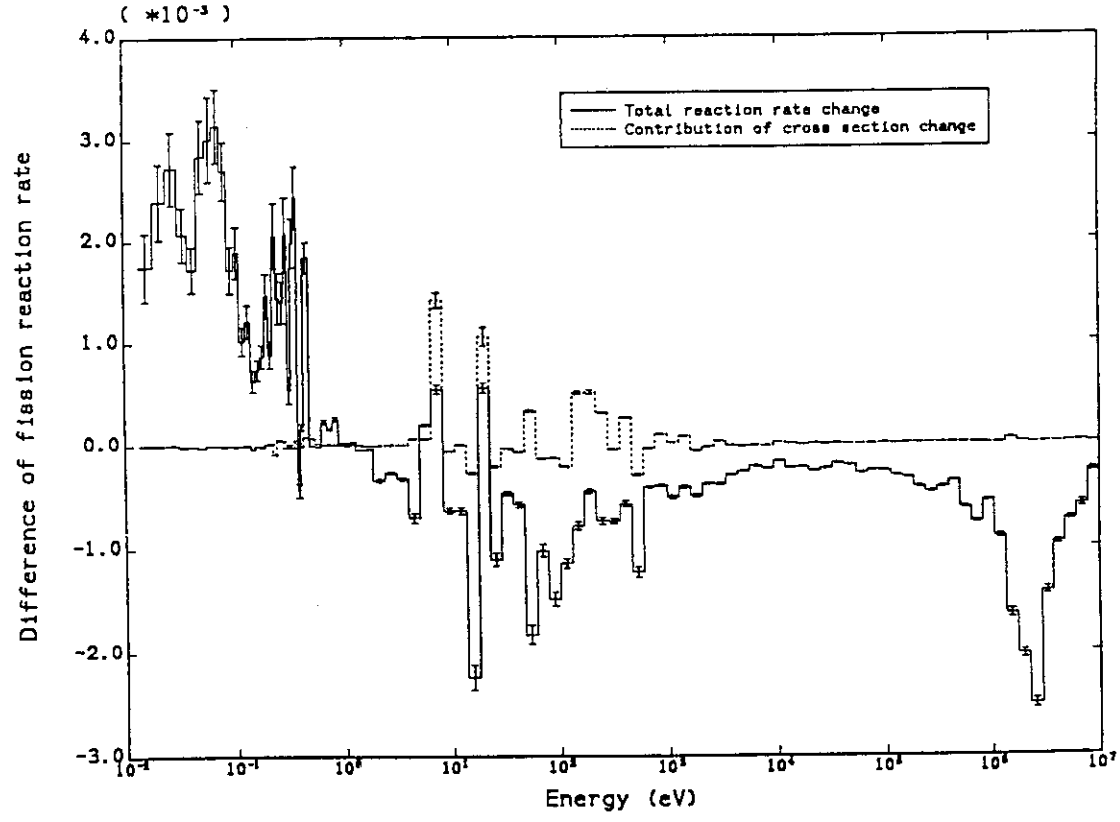

Figure 24 Contribution of cross section change to the fission rate change in the fuel rods adjacent to the water hole

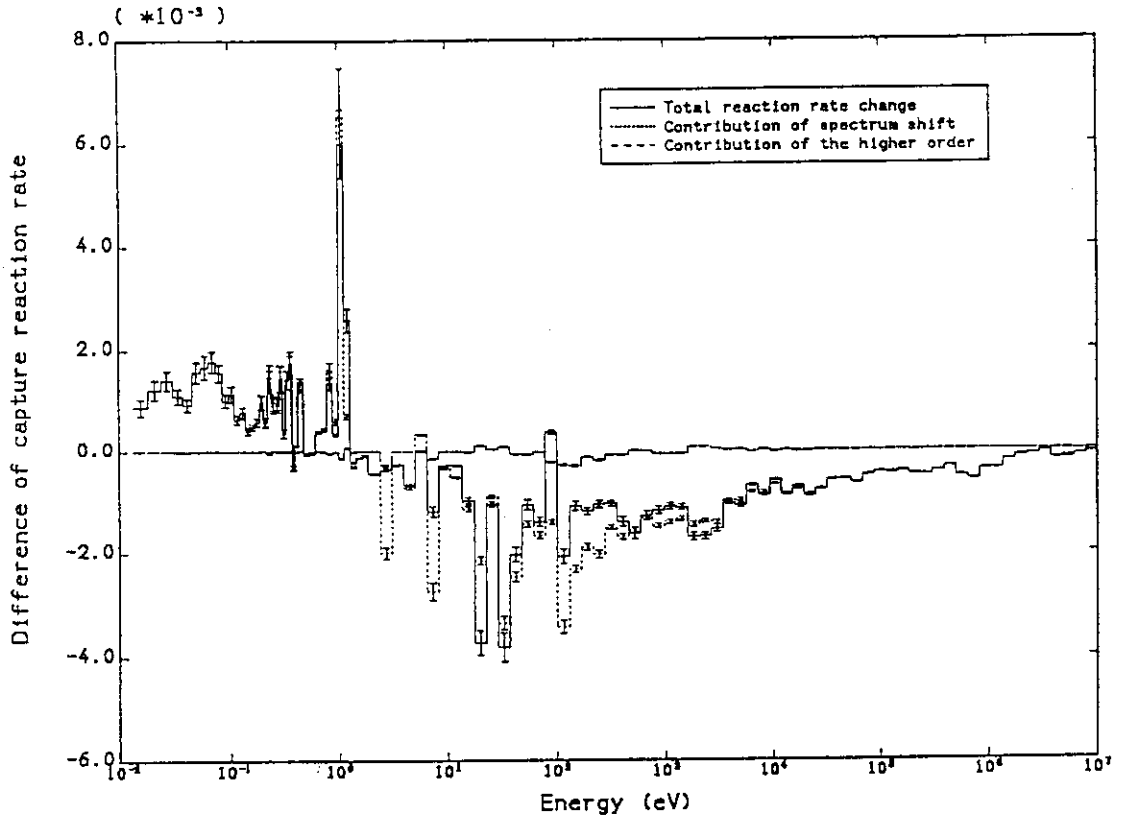

Figure 25 Contribution of flux shift and the higher order to the capture rate change in the fuel rods adjacent to the water hole

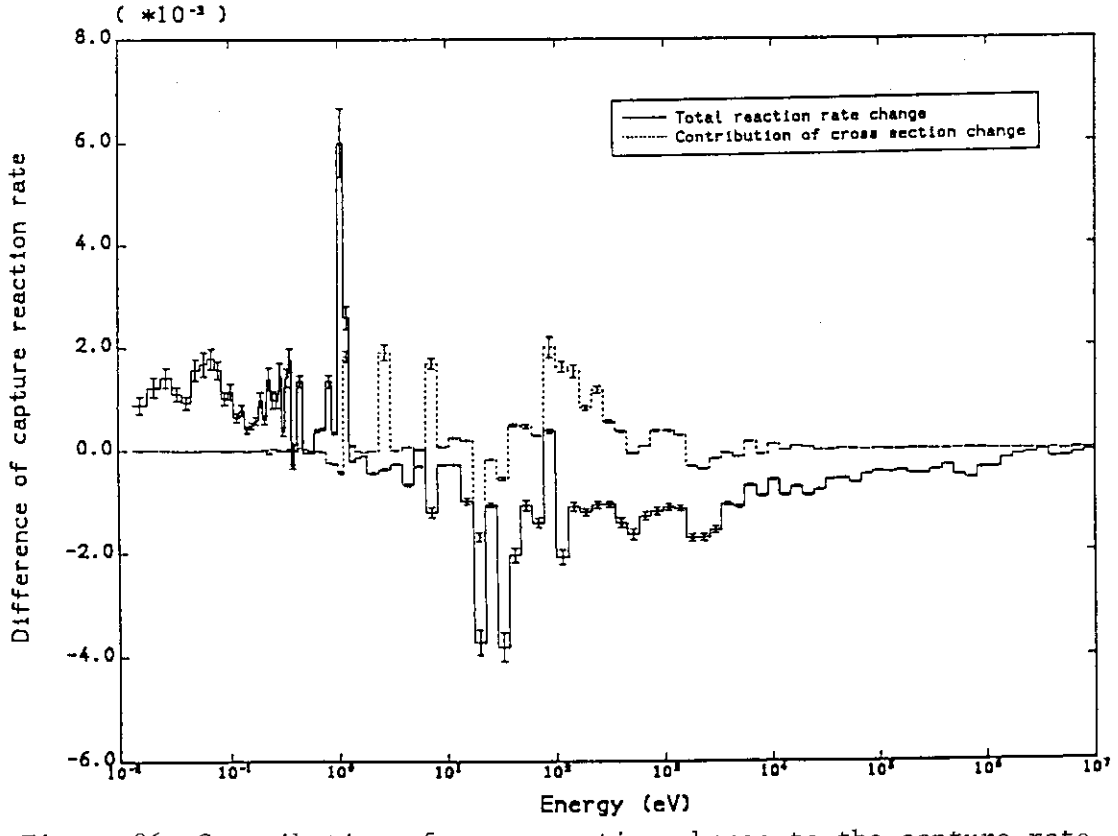

Figure 26 Contribution of cross section change to the capture rate change in the fuel rods adjacent to the water hole

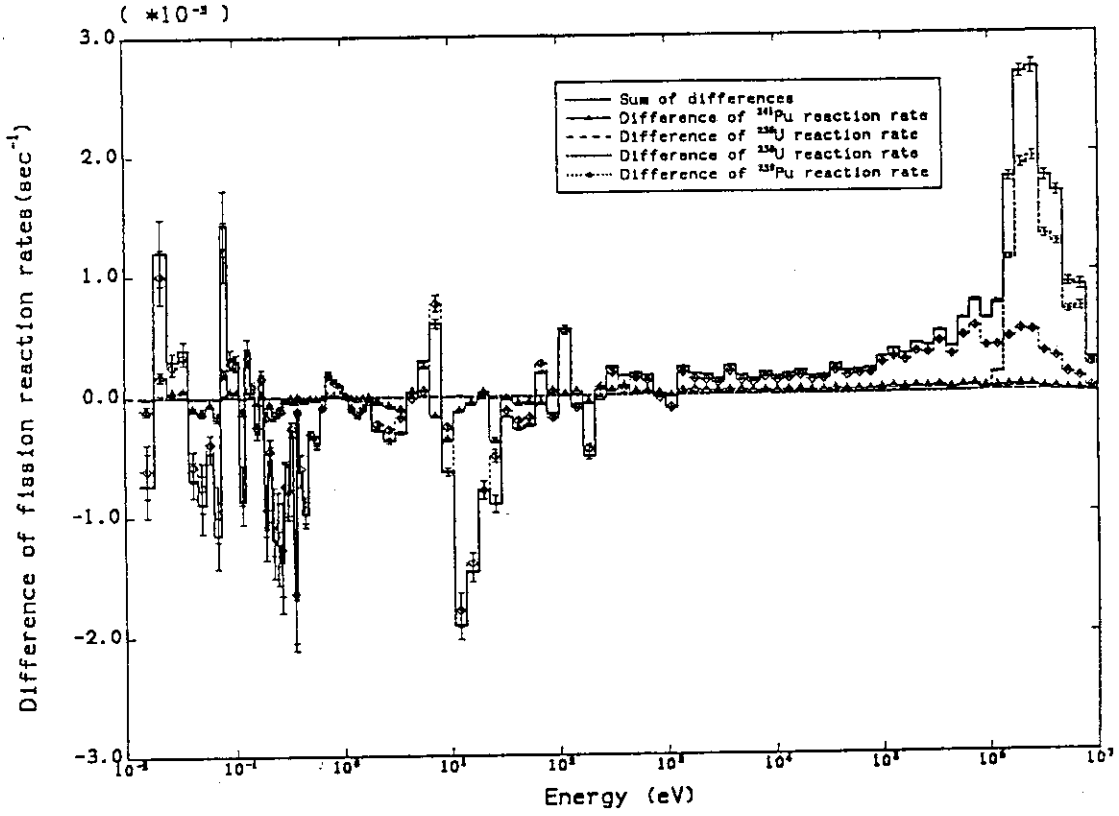

Figure 27 Contributions of individual isotopes to the fission rate change in the fuel rods adjacent to the B_4C rod

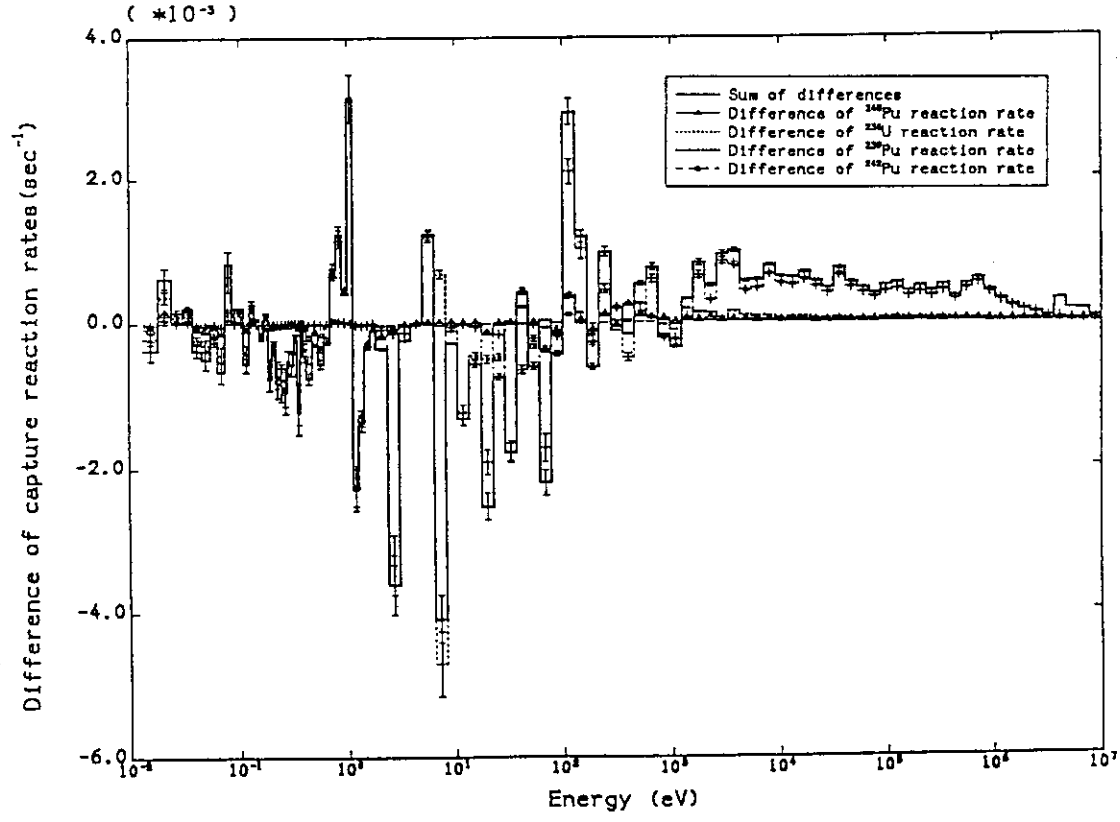

Figure 28 Contributions of individual isotopes to the capture rate change in the fuel rods adjacent to the B_4C rod

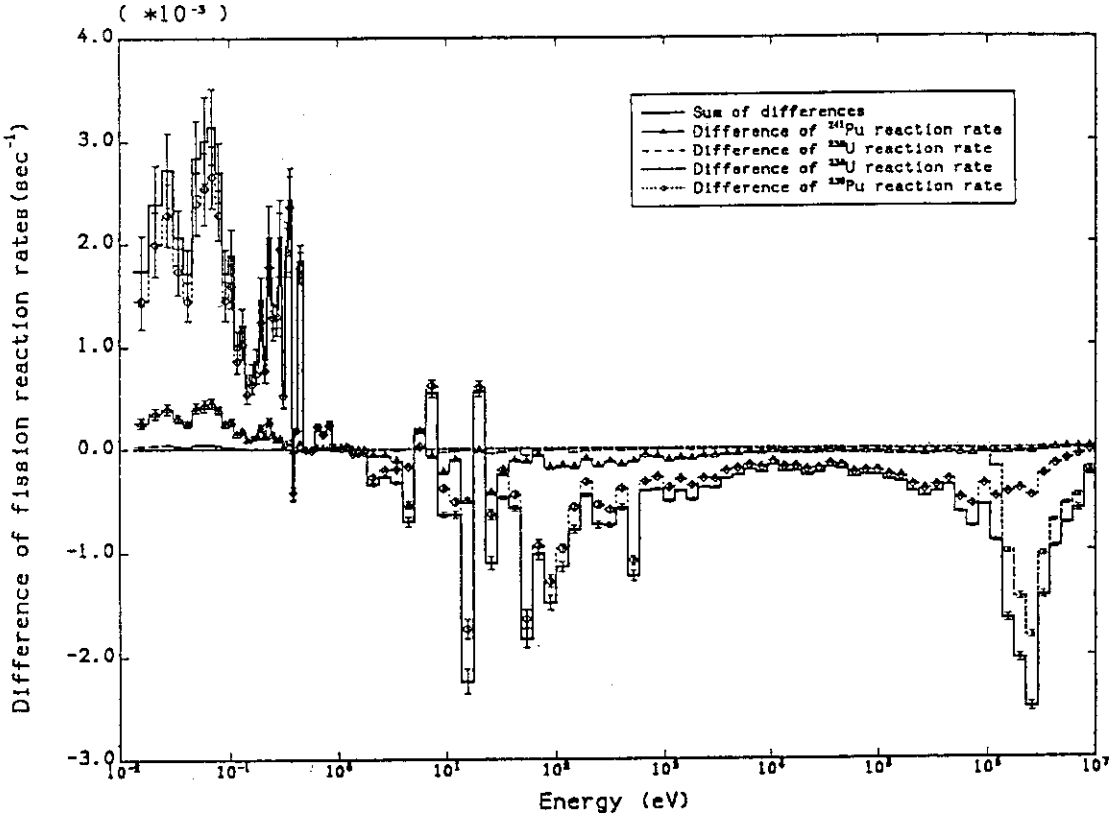

Figure 29 Contributions of individual isotopes to the fission rate change in the fuel rods adjacent to the water hole

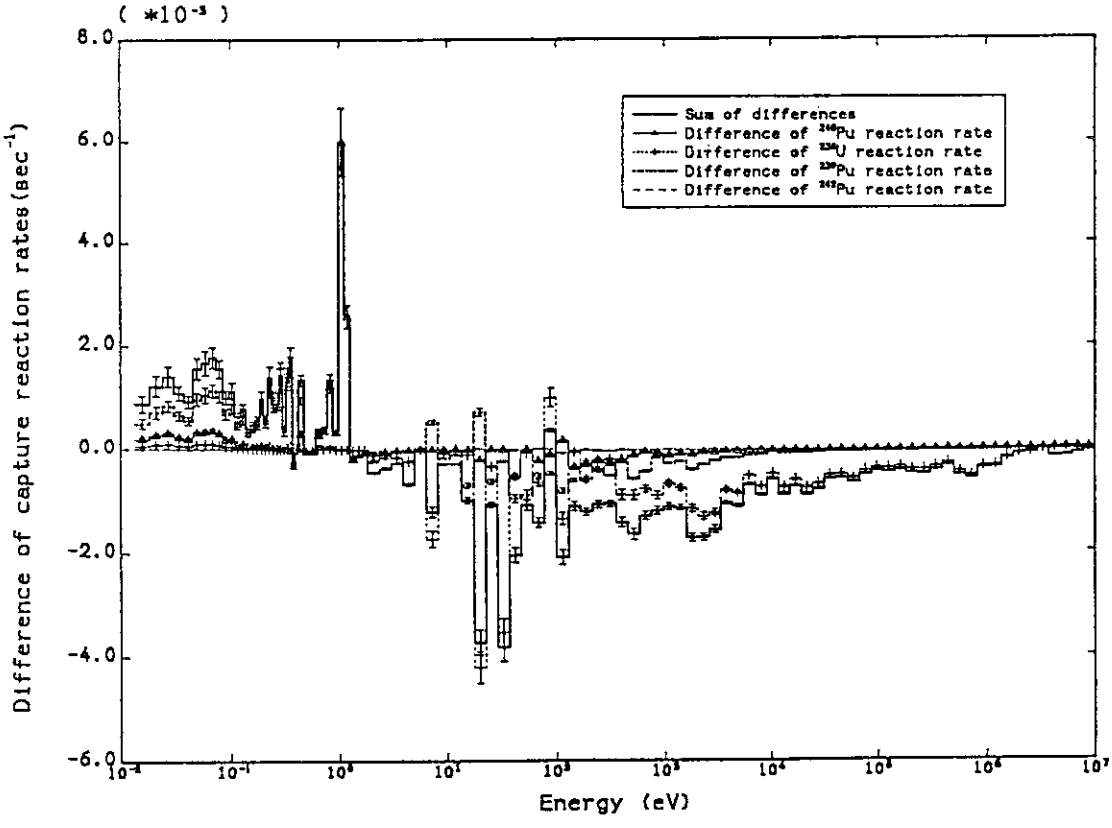

Figure 30 Contributions of individual isotopes to the capture rate change in the fuel rods adjacent to the water hole

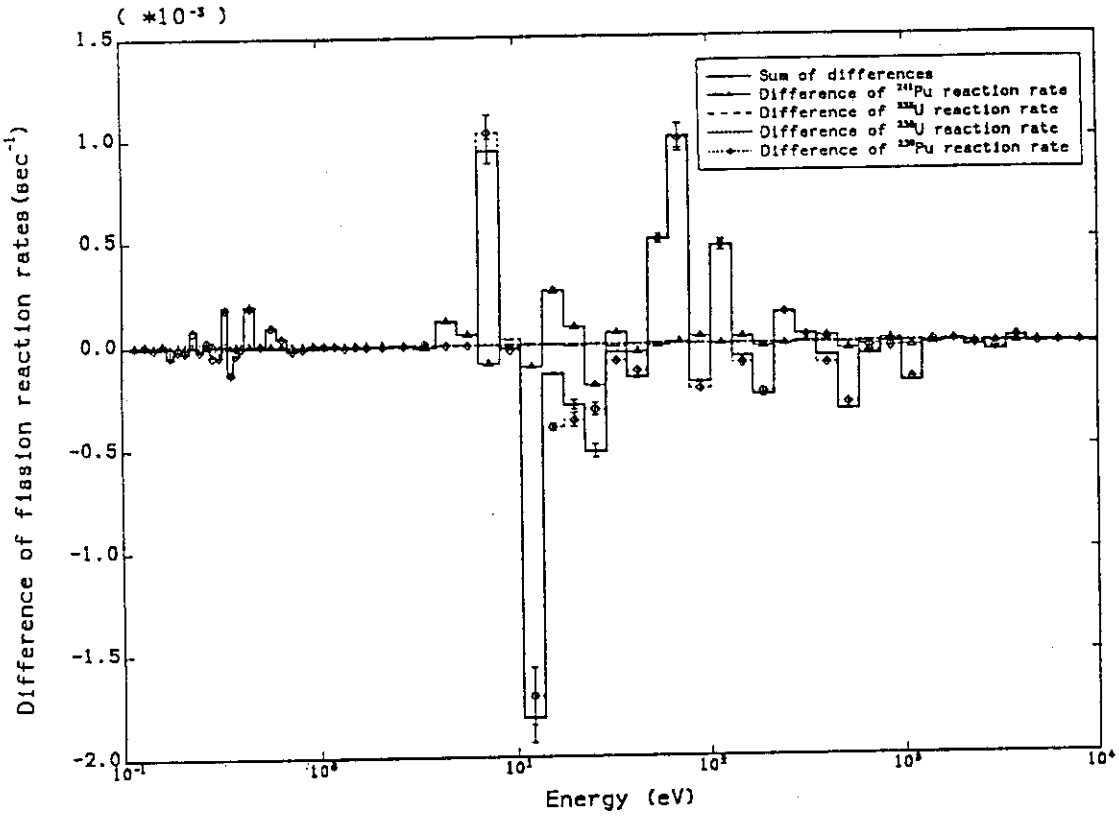

Figure 31 Contributions of individual isotopic cross section change to the fission rate change in the fuel rods adjacent to the B_4C rod

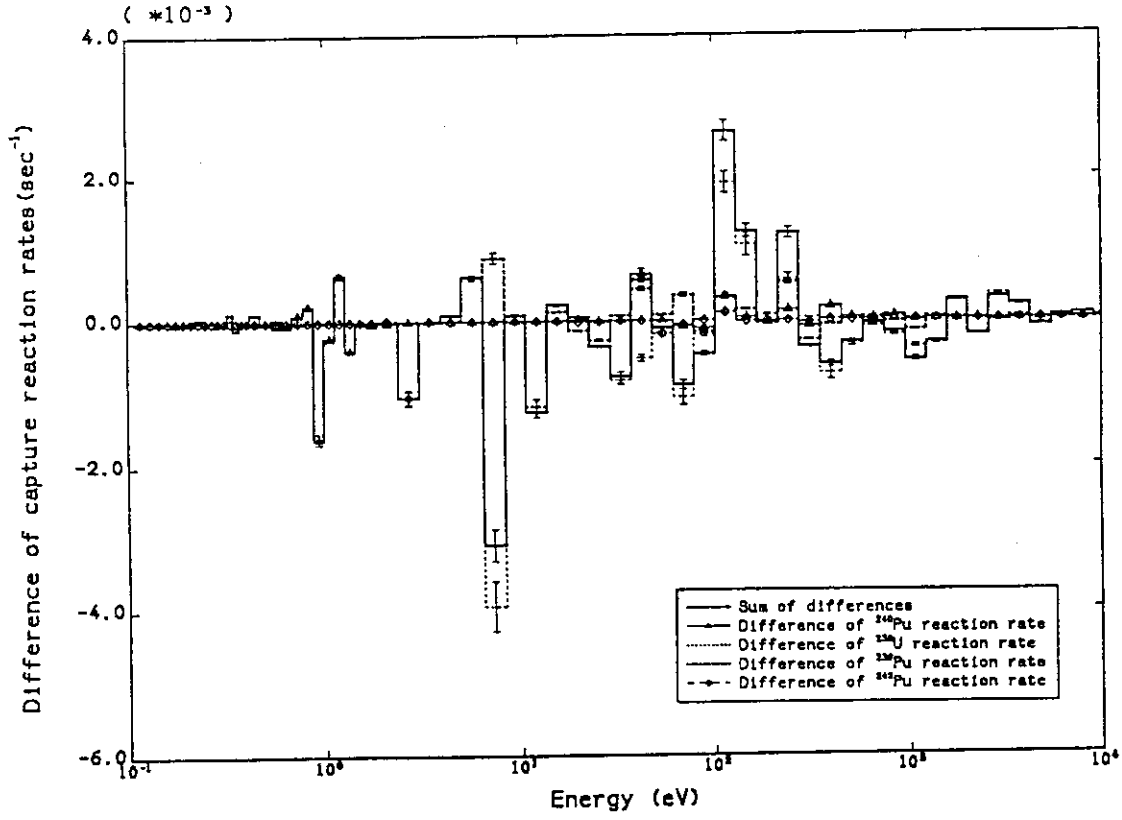

Figure 32 Contributions of individual isotopic cross section change to the capture rate change in the fuel rods adjacent to the B_4C rod

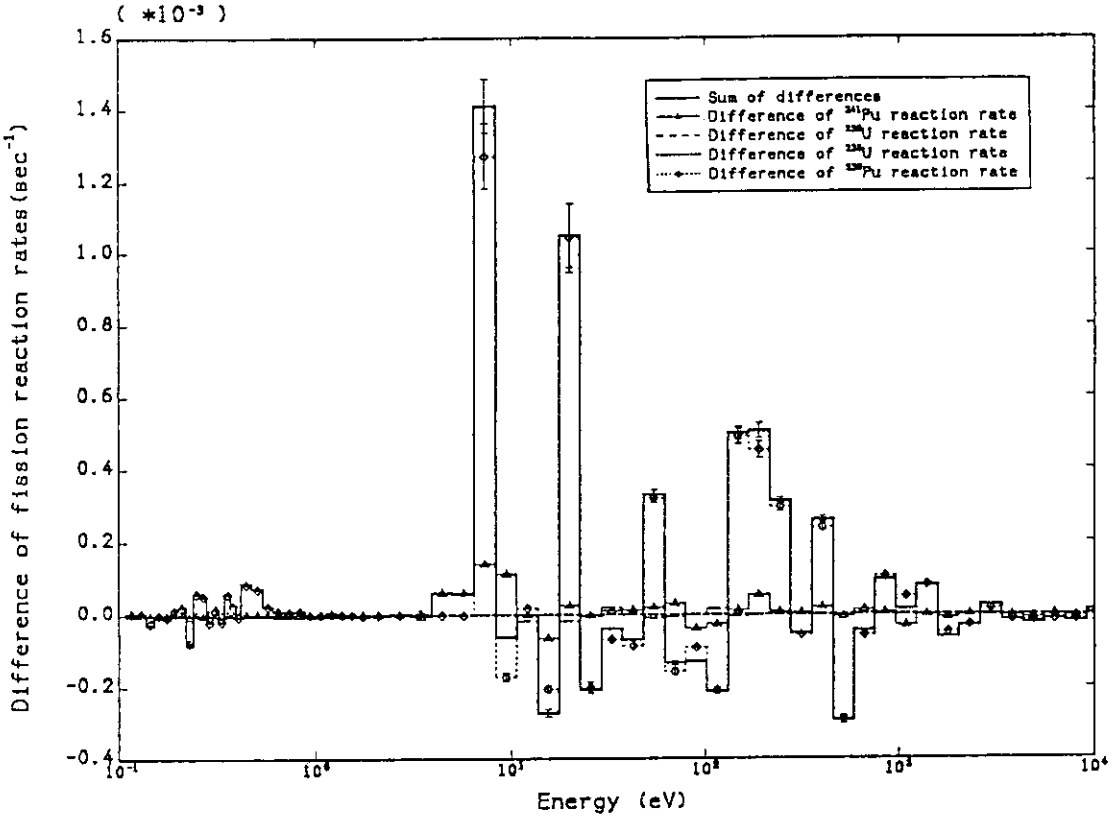

Figure 33 Contributions of individual isotopic cross section change to the fission rate change in the fuel rods adjacent to the water hole

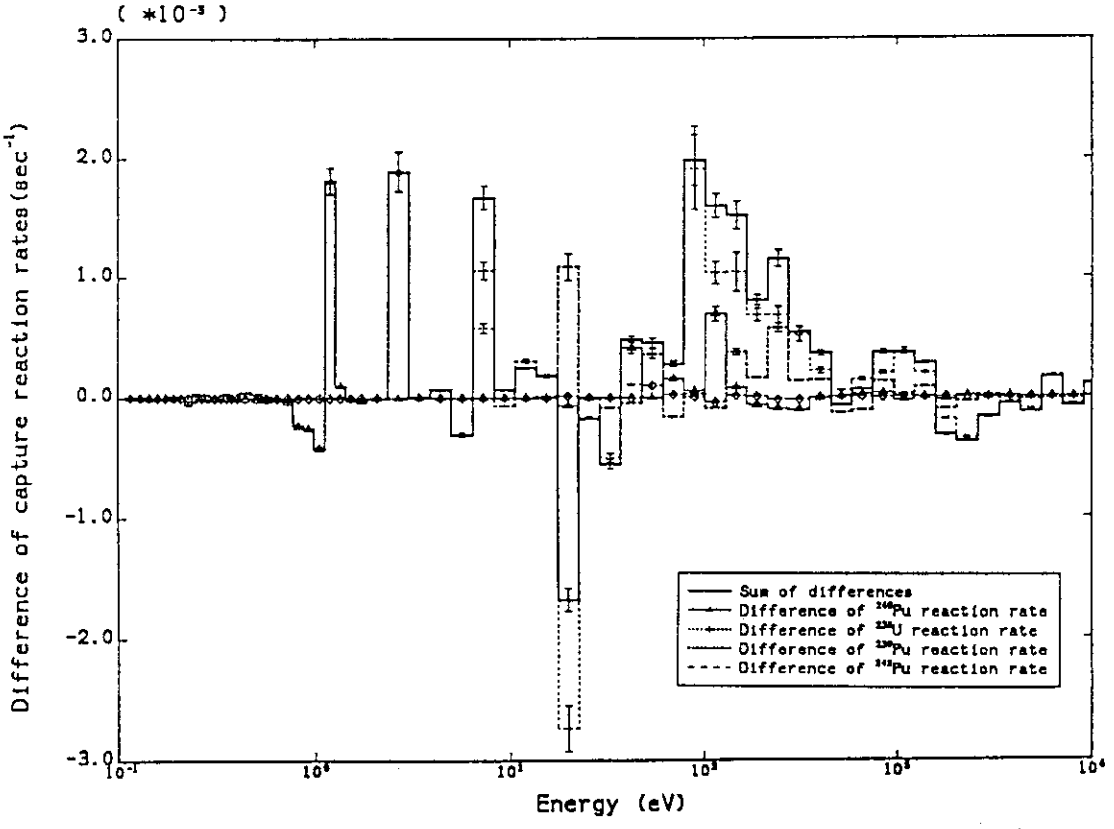

Figure 34 Contributions of individual isotopic cross section change to the capture rate change in the fuel rods adjacent to the water hole

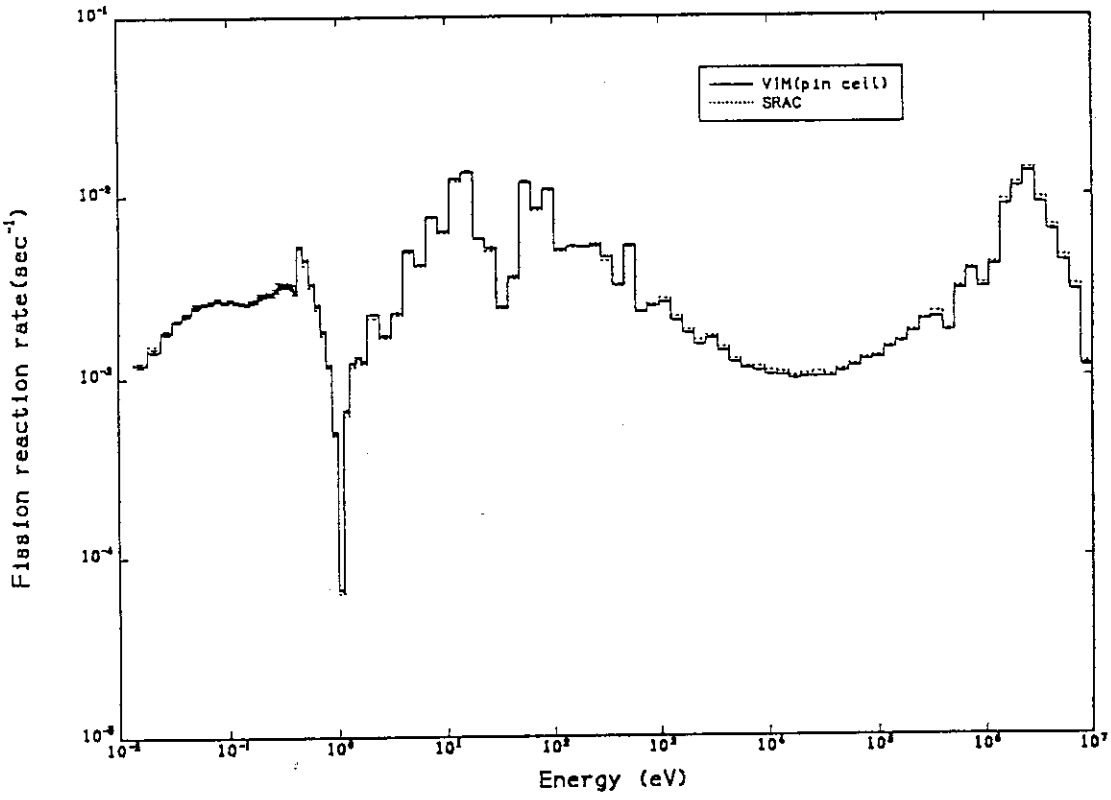

Figure 35 Comparison of multi-group fission rate in the unit pin cell between VIM and SRAC

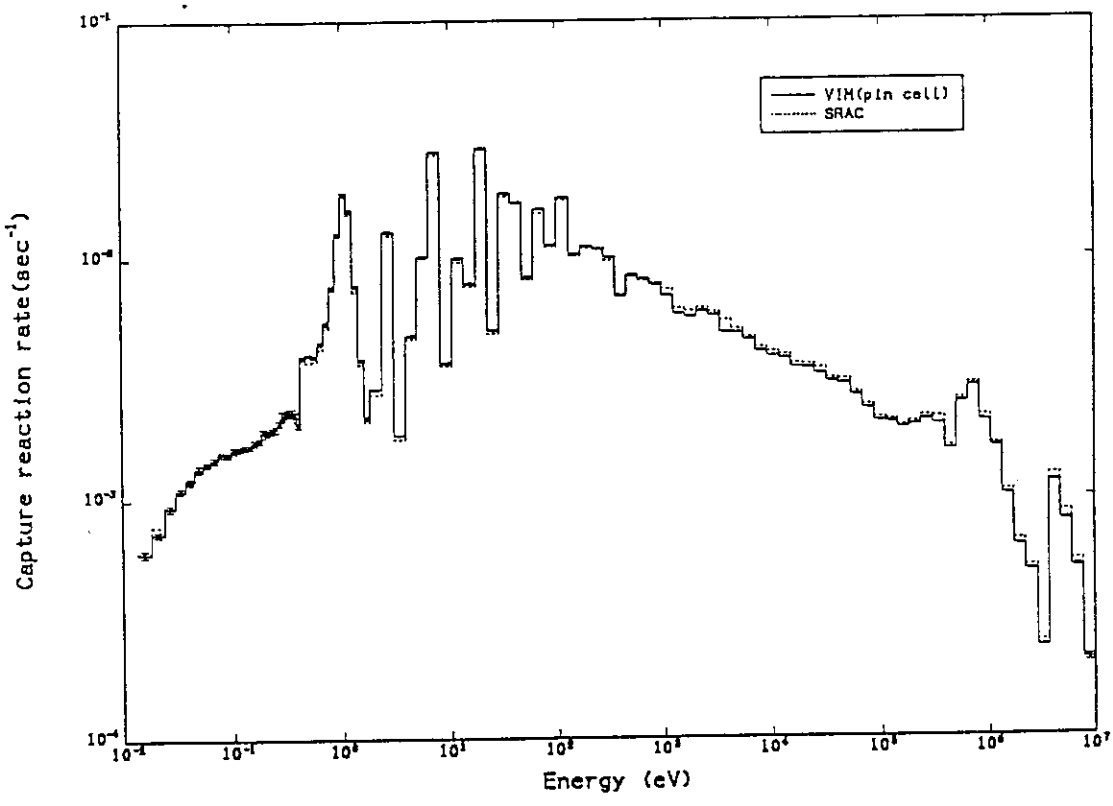

Figure 36 Comparison of multi-group capture rate in the unit pin cell between VIM and SRAC

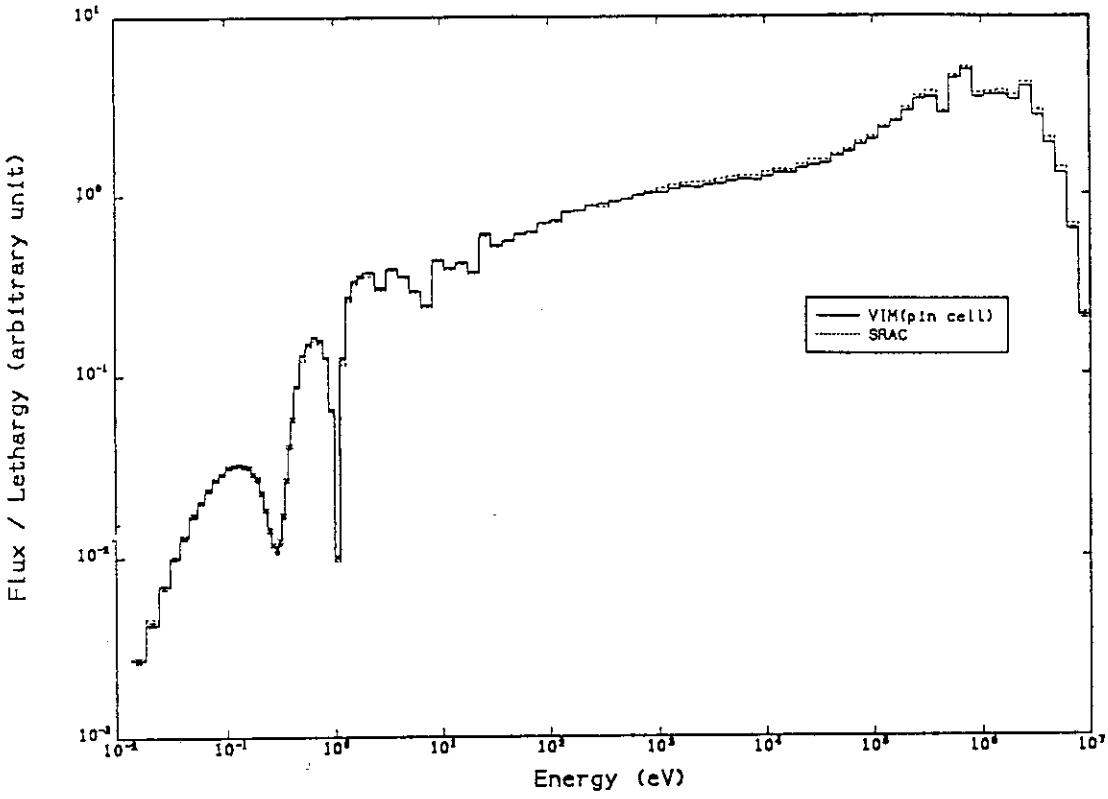

Figure 37 Comparison of neutron spectrum in the unit pin cell between VIM and SRAC

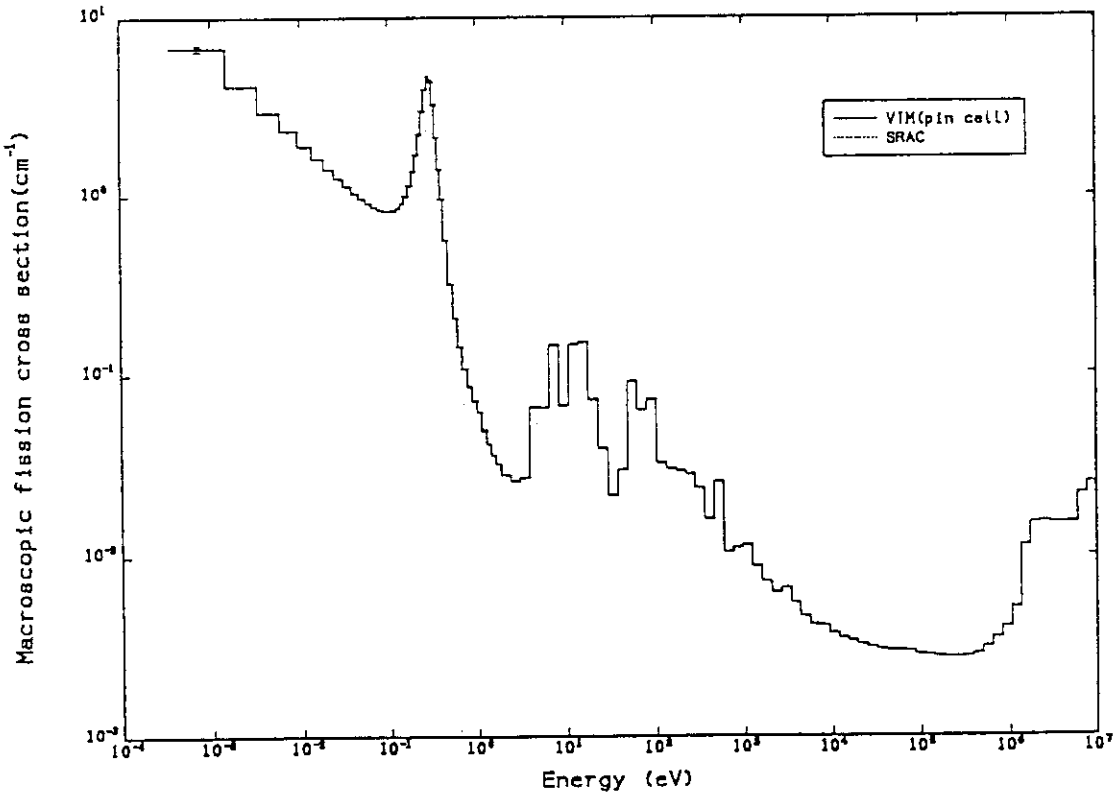

Figure 38 Comparison of multi-group macroscopic fission cross section in the unit pin cell between VIM and SRAC

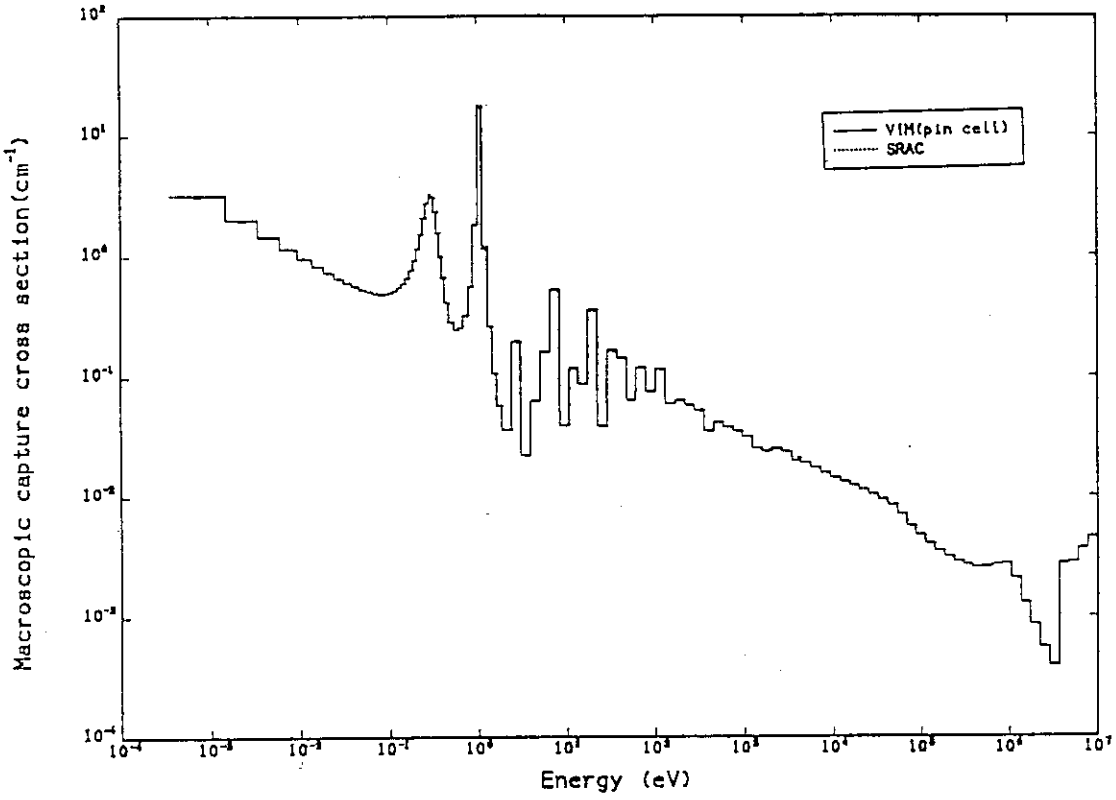

Figure 39 Comparison of multi-group macroscopic caputure cross section in the unit pin cell between VIM and SRAC

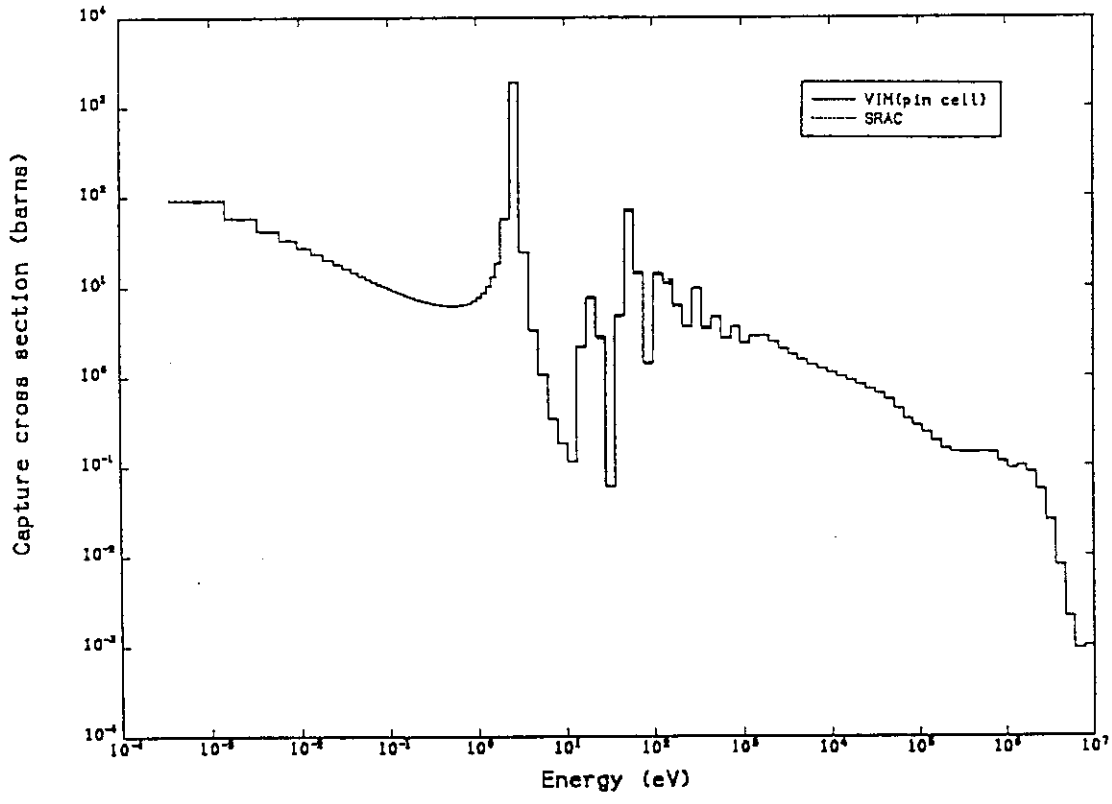

Figure 40 Comparison of multi-group ^{242}Pu capture cross section in the unit pin cell between VIM and SRAC

Appendix (Supplementary figures)

Here, the reaction rates, neutron spectra, and macroscopic cross sections obtained with VIM and SRAC in the fuel assembly calculations are shown in Figs. A.1-A.9. Figures A.9-A.23 show the comparisons of individual isotopic microscopic cross sections obtained by VIM in the unit pin cell and in the fuel rods adjacent to the B_4C rod or water hole.

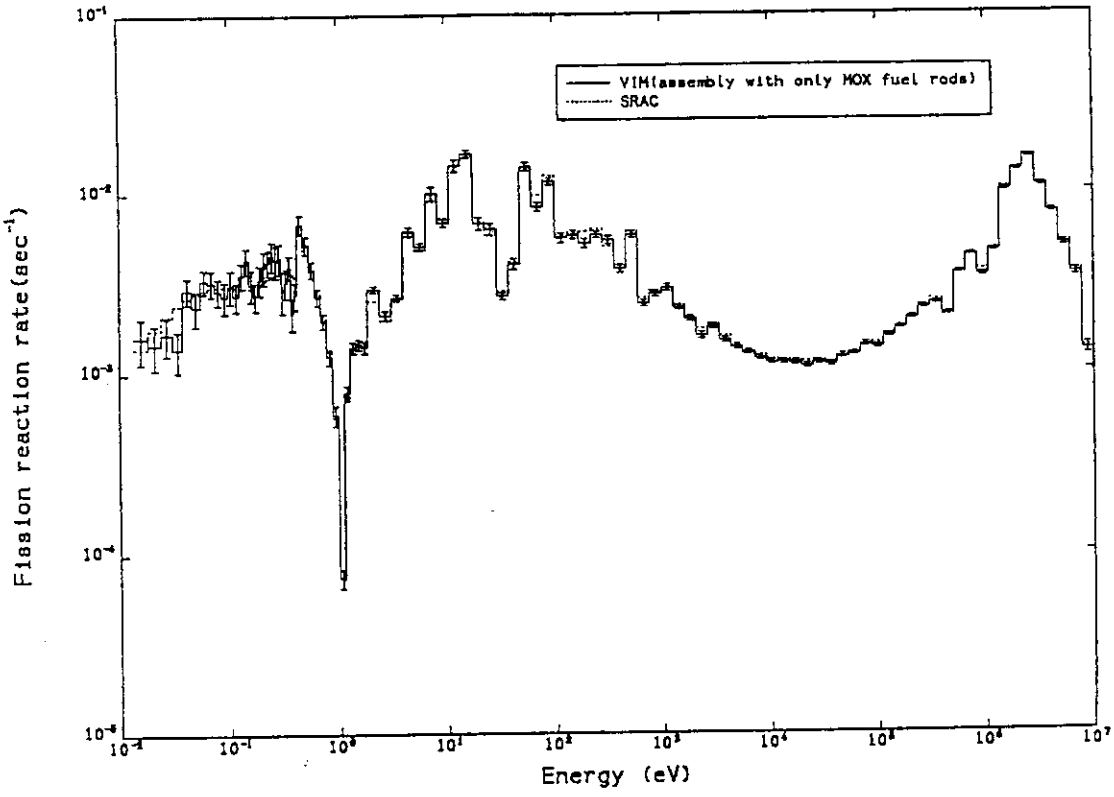

Figure A.1 Comparison of multi-group fission rate in the region 2 of the assembly with only MOX fuel rods between VIM and SRAC

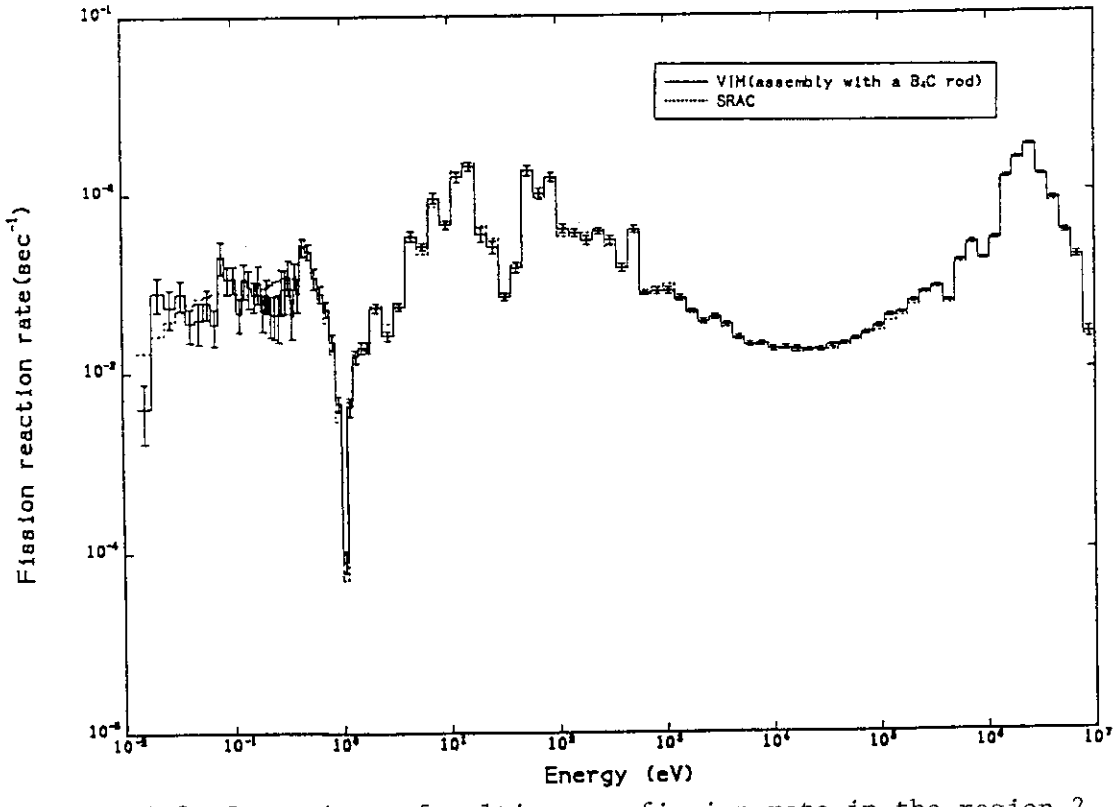

Figure A.2 Comparison of multi-group fission rate in the region 2 of the assembly with a B_4C rod between VIM and SRAC

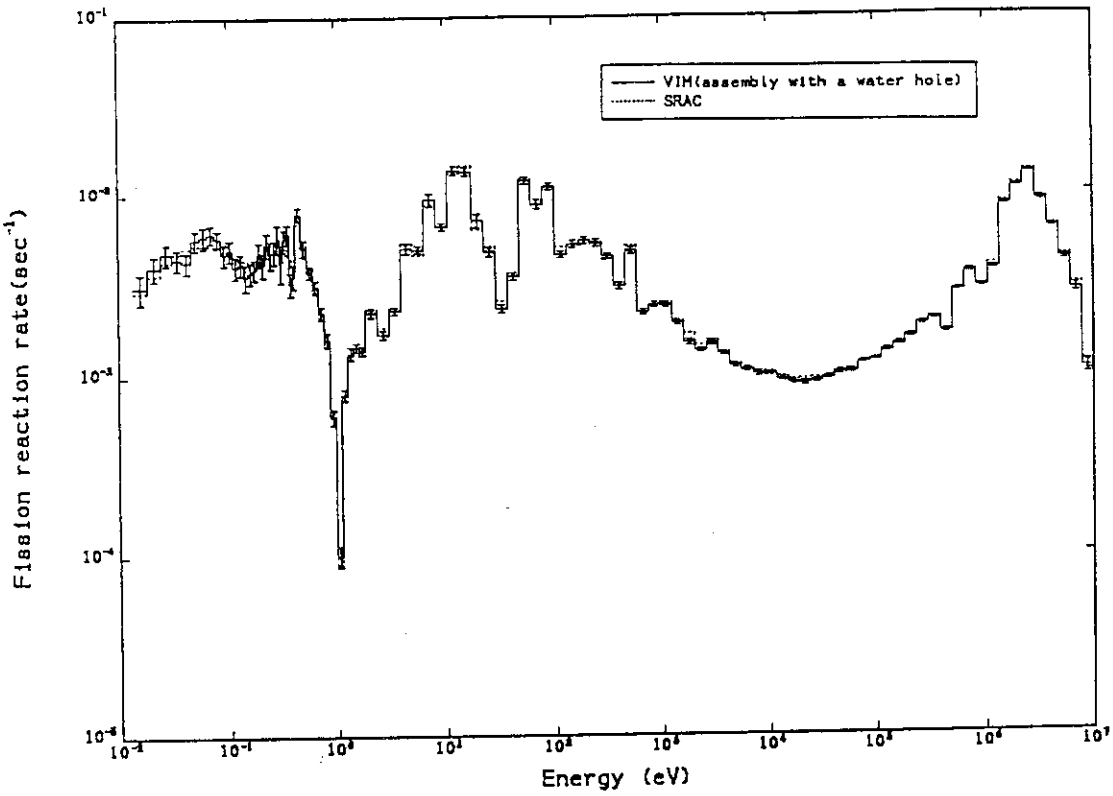

Figure A.3 Comparison of multi-group fission rate in the region 2 of the assembly with a water hole between VIM and SRAC

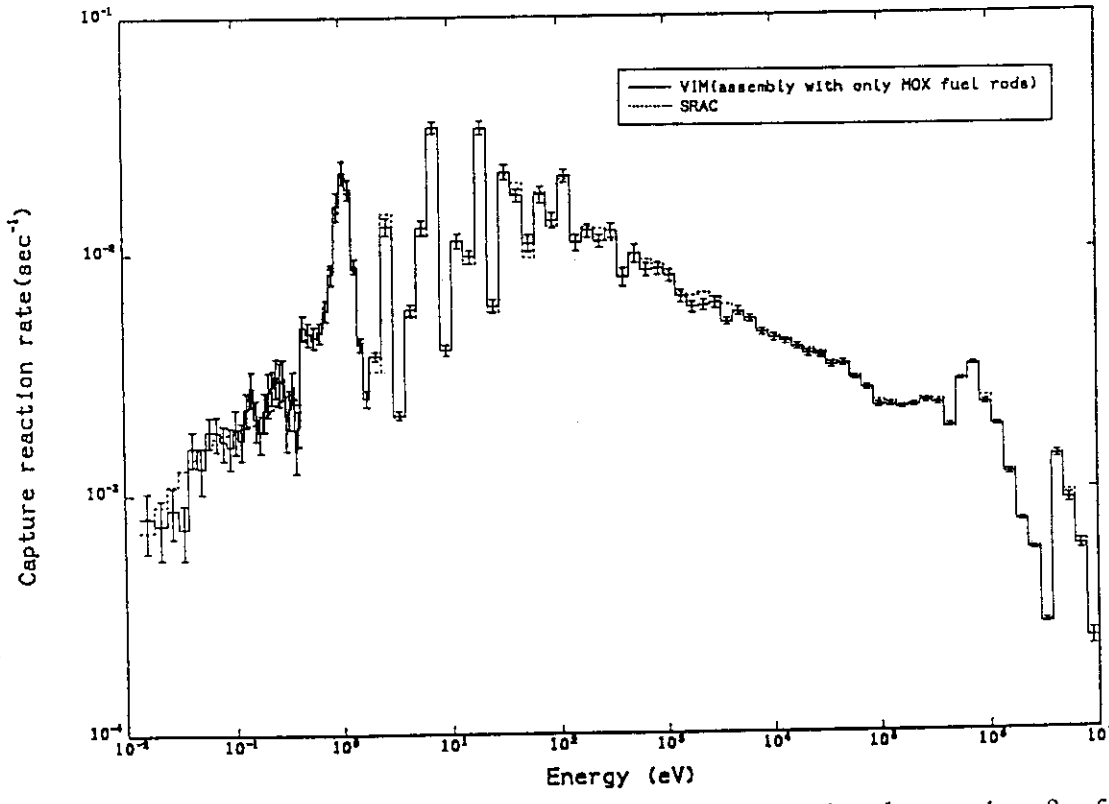

Figure A.4 Comparison of multi-group capture rate in the region 2 of the assembly with only MOX fuel rods between VIM and SRAC

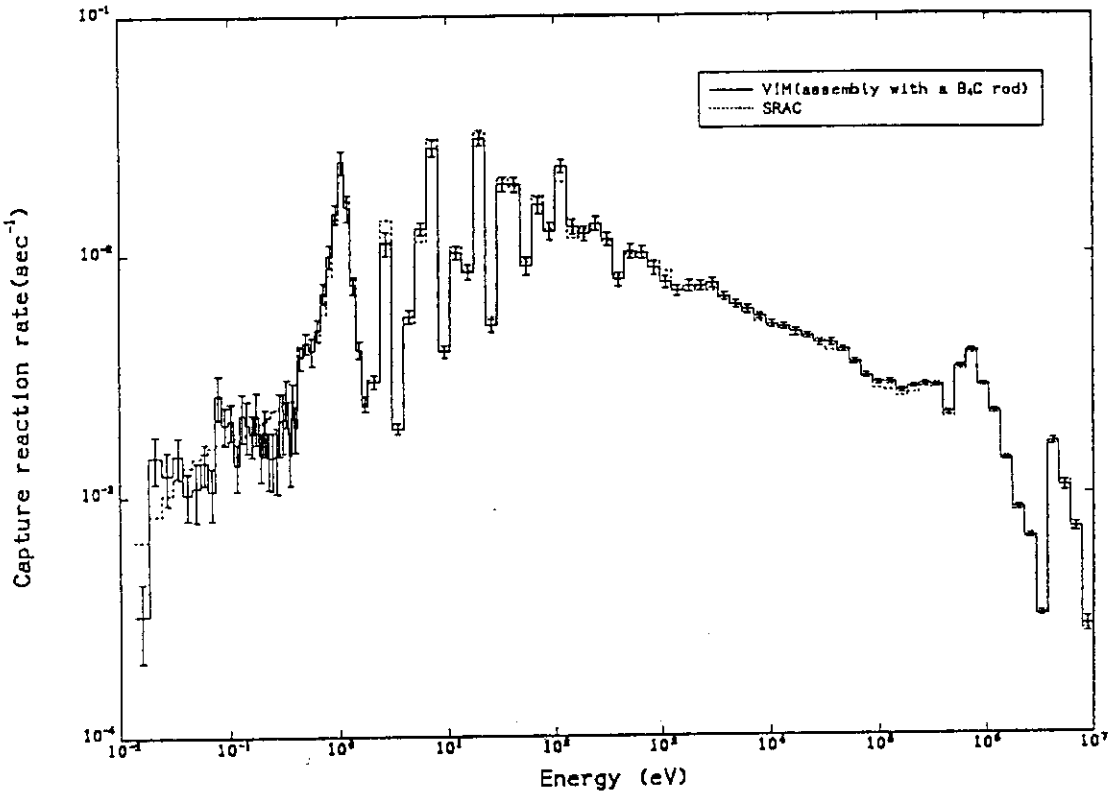

Figure A.5 Comparison of multi-group capture rate in the region 2 of the assembly with a B_4C rod between VIM and SRAC

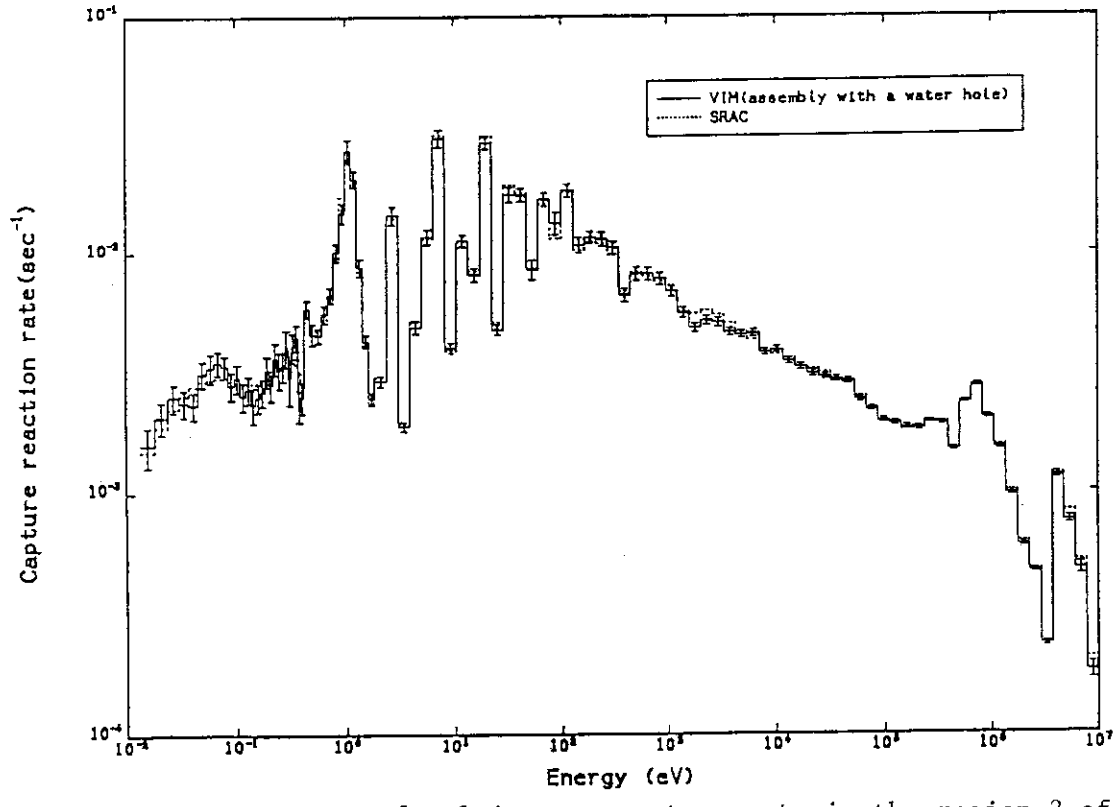

Figure A.6 Comparison of multi-group capture rate in the region 2 of the assembly with a water hole between VIM and SRAC

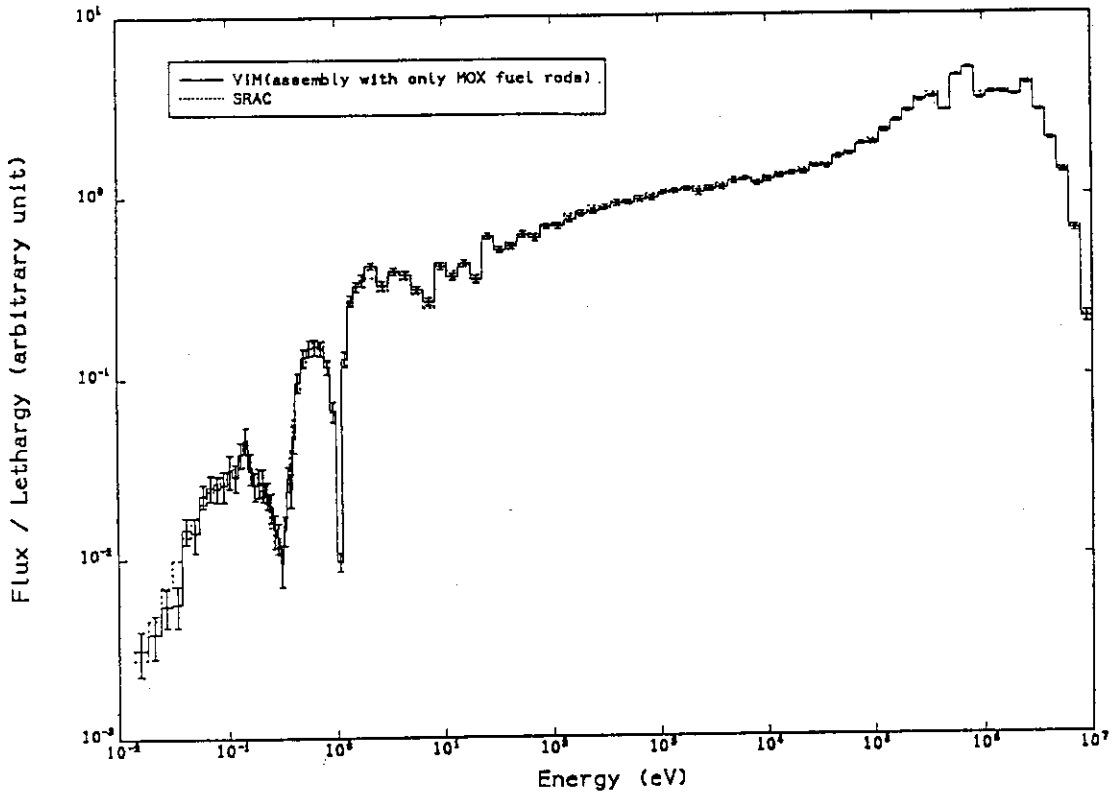

Figure A.7 Comparison of neutron spectrum in the region 2 of the assembly with only MOX fuel rods between VIM and SRAC

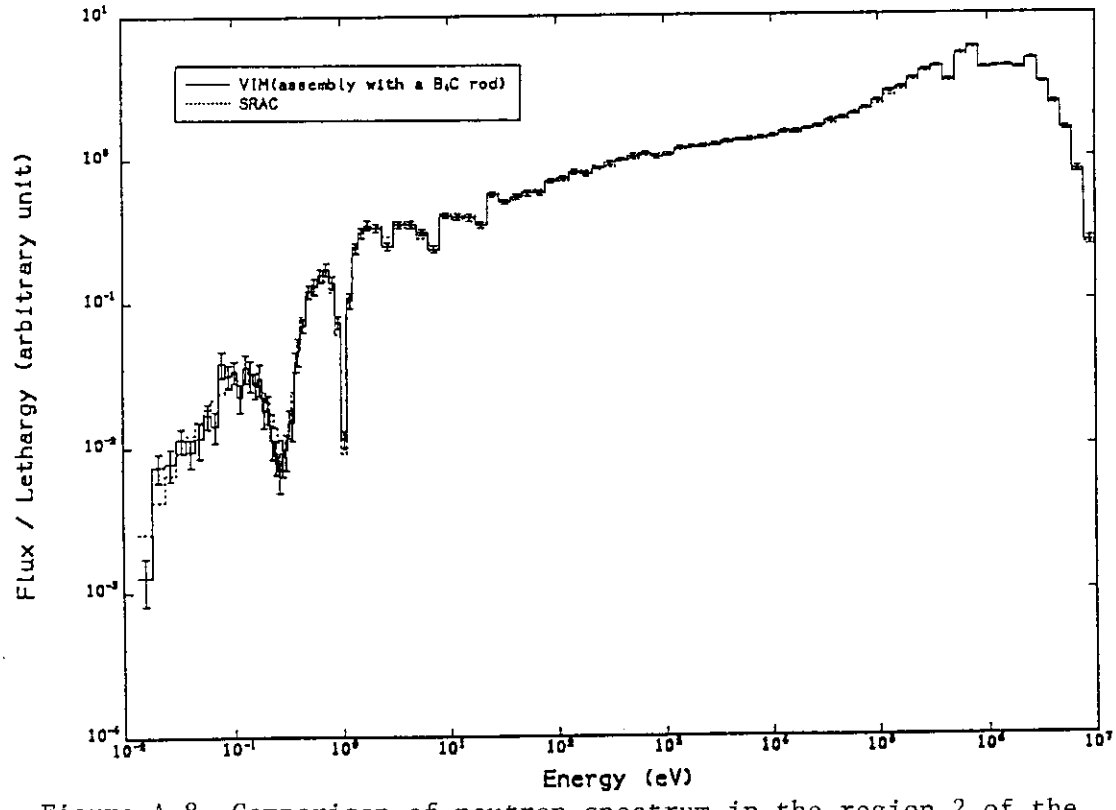

Figure A.8 Comparison of neutron spectrum in the region 2 of the assembly with a B_4C rod between VIM and SRAC

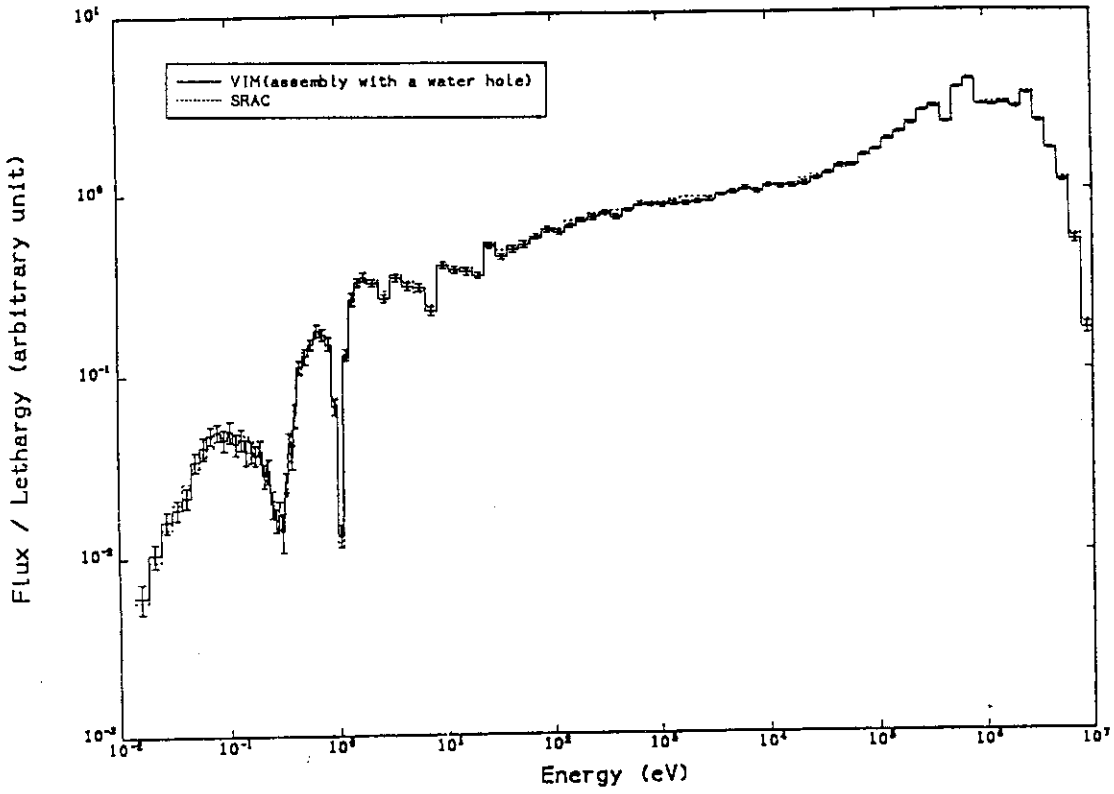

Figure A.9 Comparison of neutron spectrum in the region 2 of the assembly with a water hole between VIM and SRAC

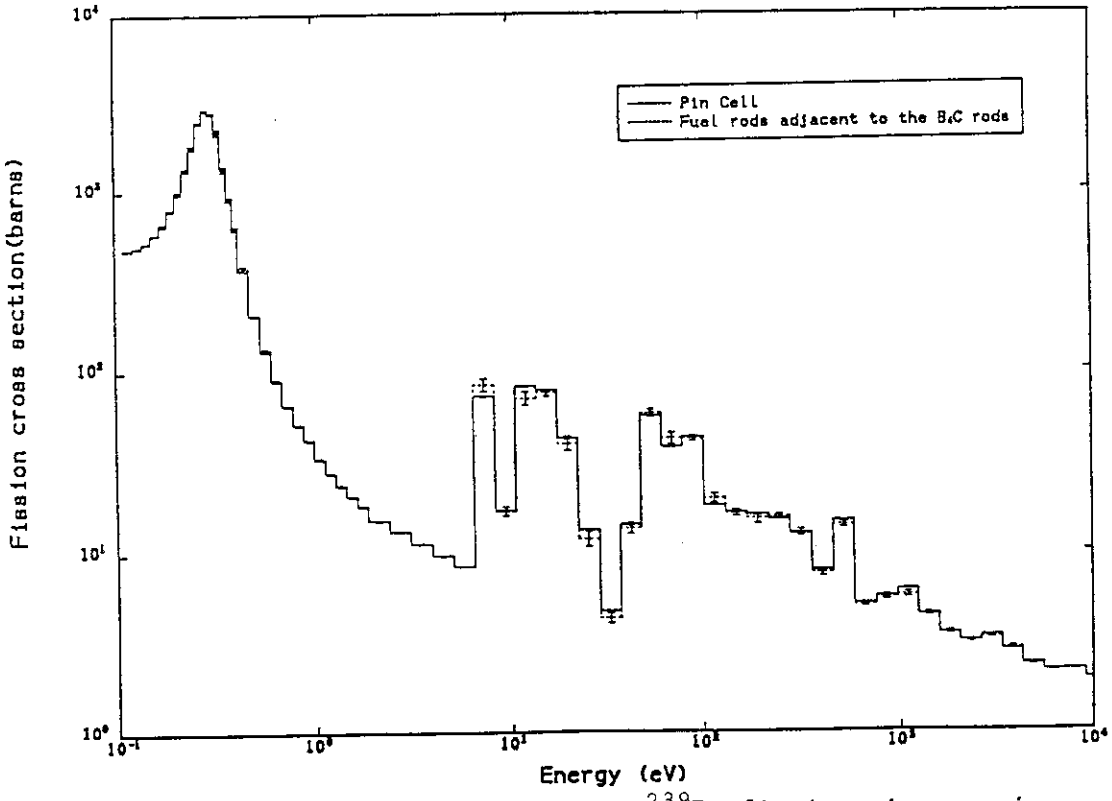

Figure A.10 Comparison of multi-group ^{239}Pu fission microscopic cross section between the unit pin cell and the fuel rods adjacent to the B_4C rod from the VIM calculation

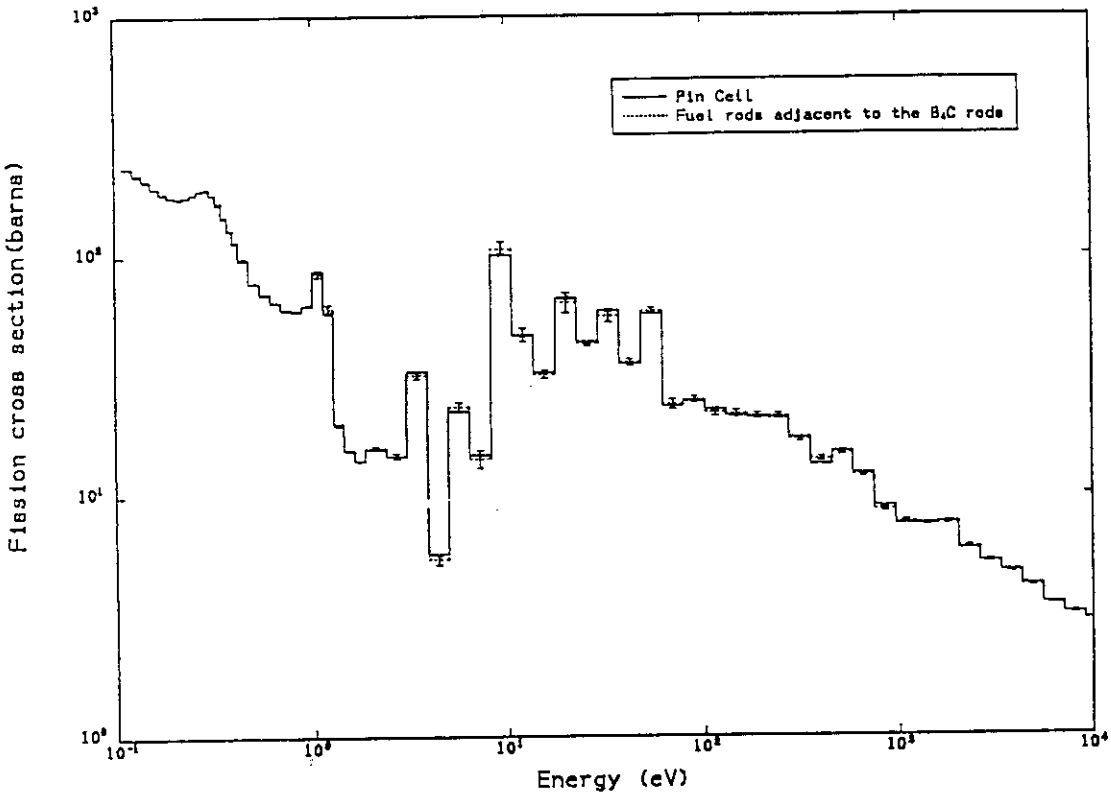

Figure A.11 Comparison of multi-group ^{235}U fission microscopic cross section between the unit pin cell and the fuel rods adjacent to the B_4C rod from the VIM calculation

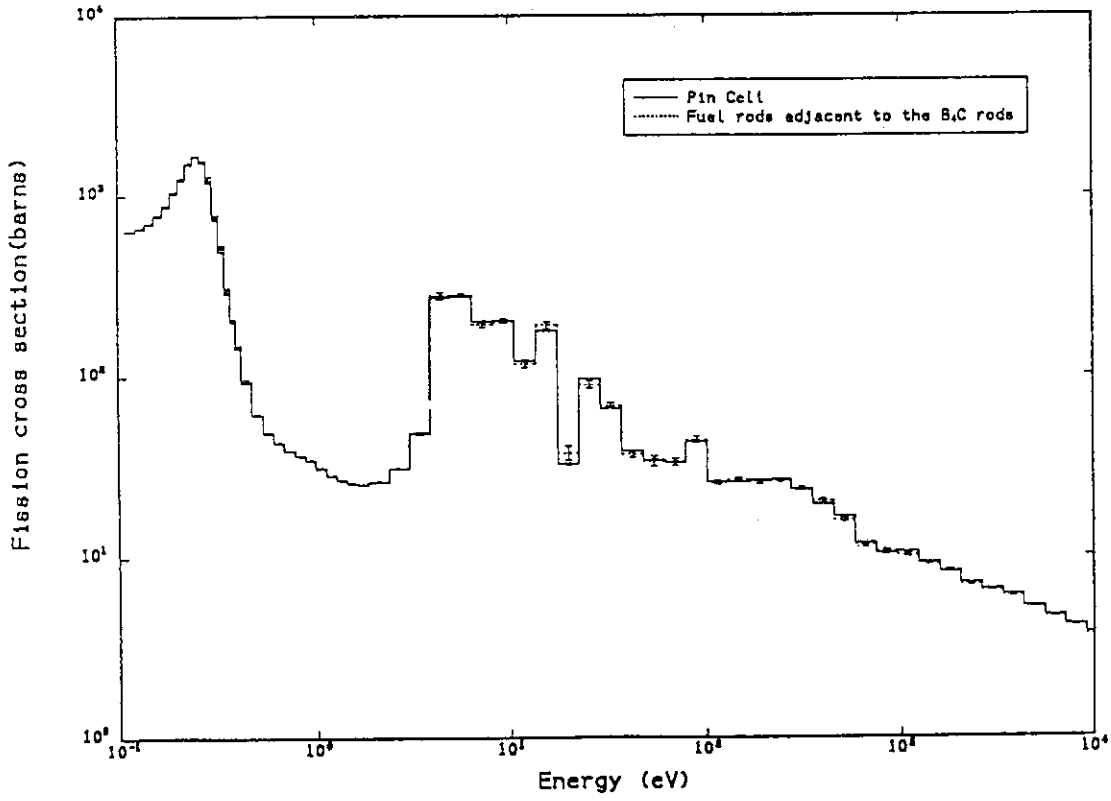

Figure A.12 Comparison of multi-group ^{241}Pu fission microscopic cross section between the unit pin cell and the fuel rods adjacent to the B_4C rod from the VIM calculation

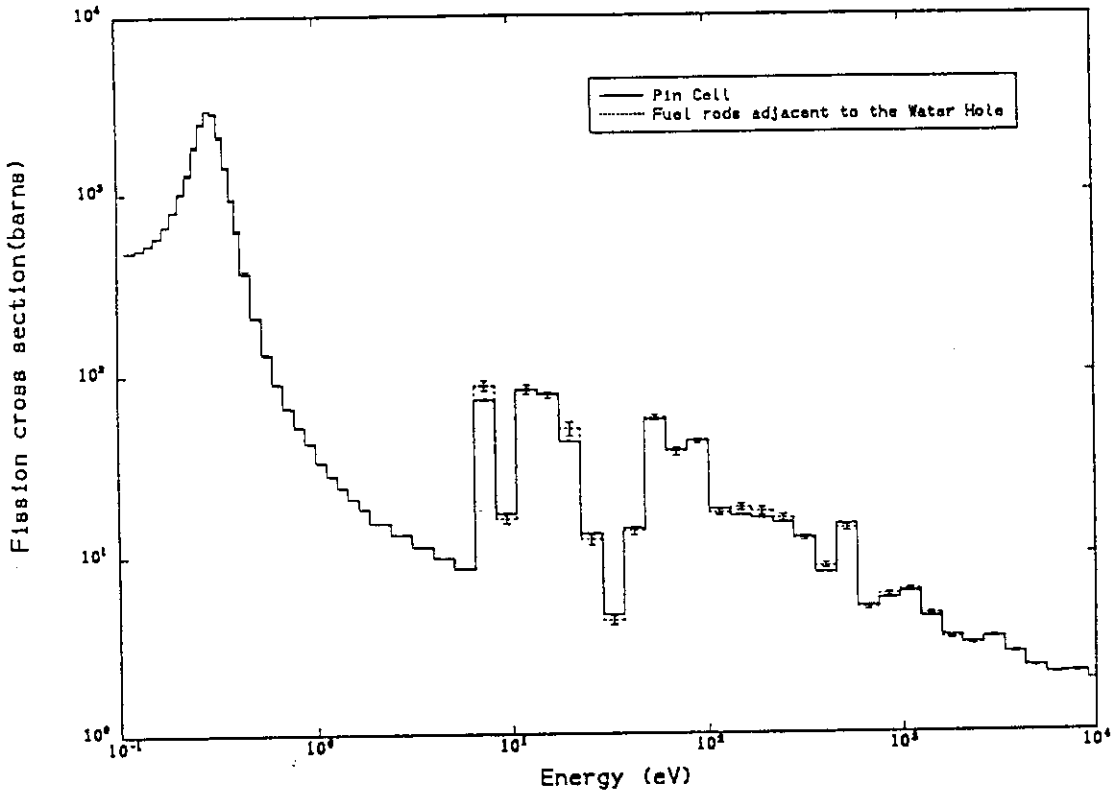

Figure A.13 Comparison of multi-group ^{239}Pu fission microscopic cross section between the unit pin cell and the fuel rods adjacent to the water hole from the VIM calculation

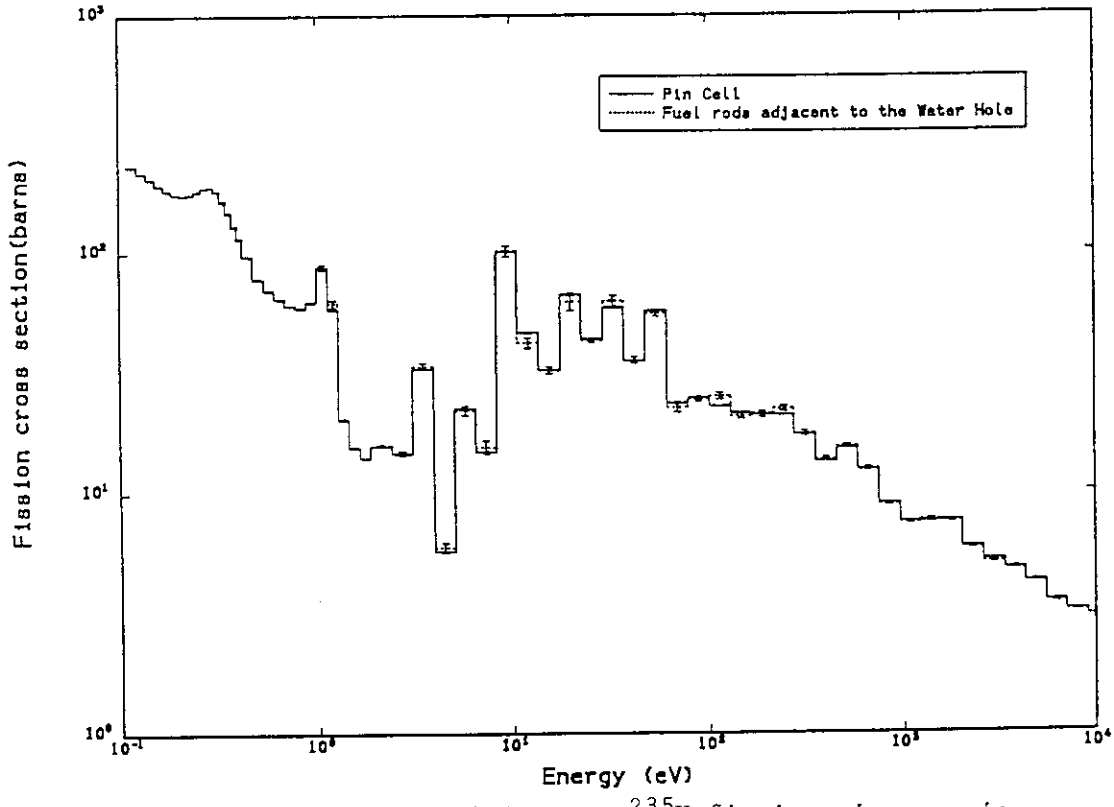

Figure A.14 Comparison of multi-group ^{235}U fission microscopic cross section between the unit pin cell and the fuel rod adjacent to the water hole from the VIM calculation

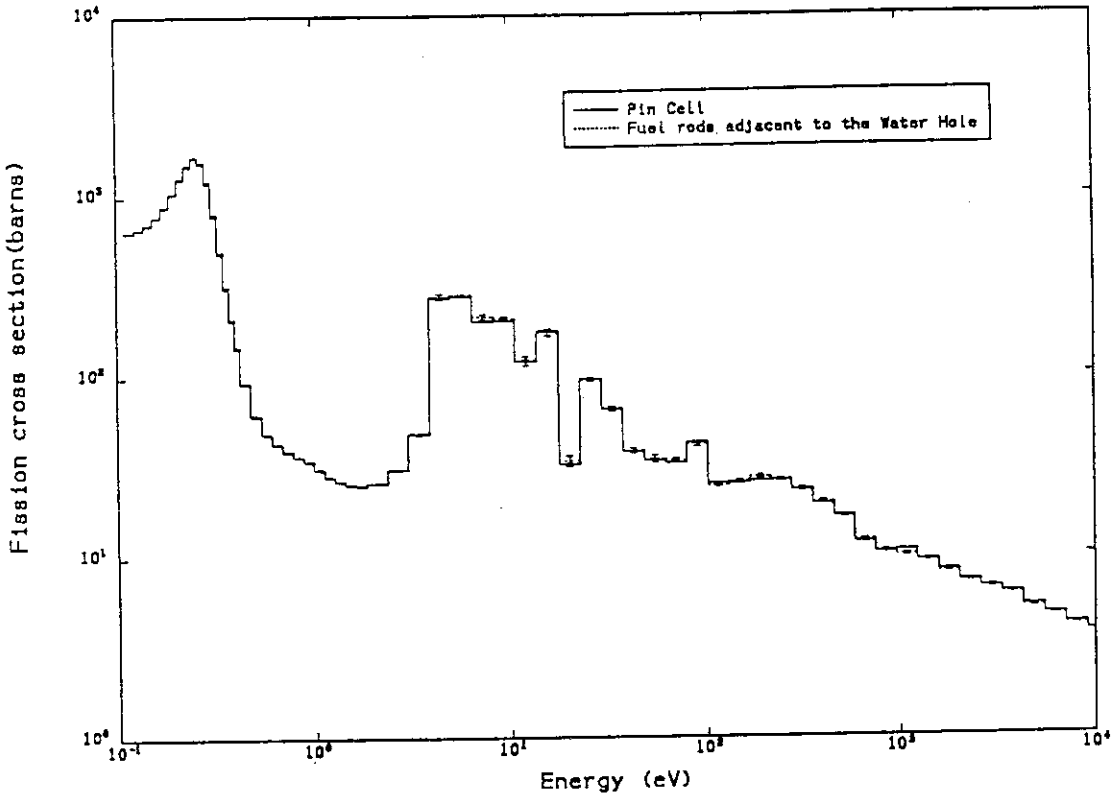

Figure A.15 Comparison of multi-group ^{241}Pu fission microscopic cross section between the unit pin cell and the fuel rods adjacent to the water hole from the VIM calculation

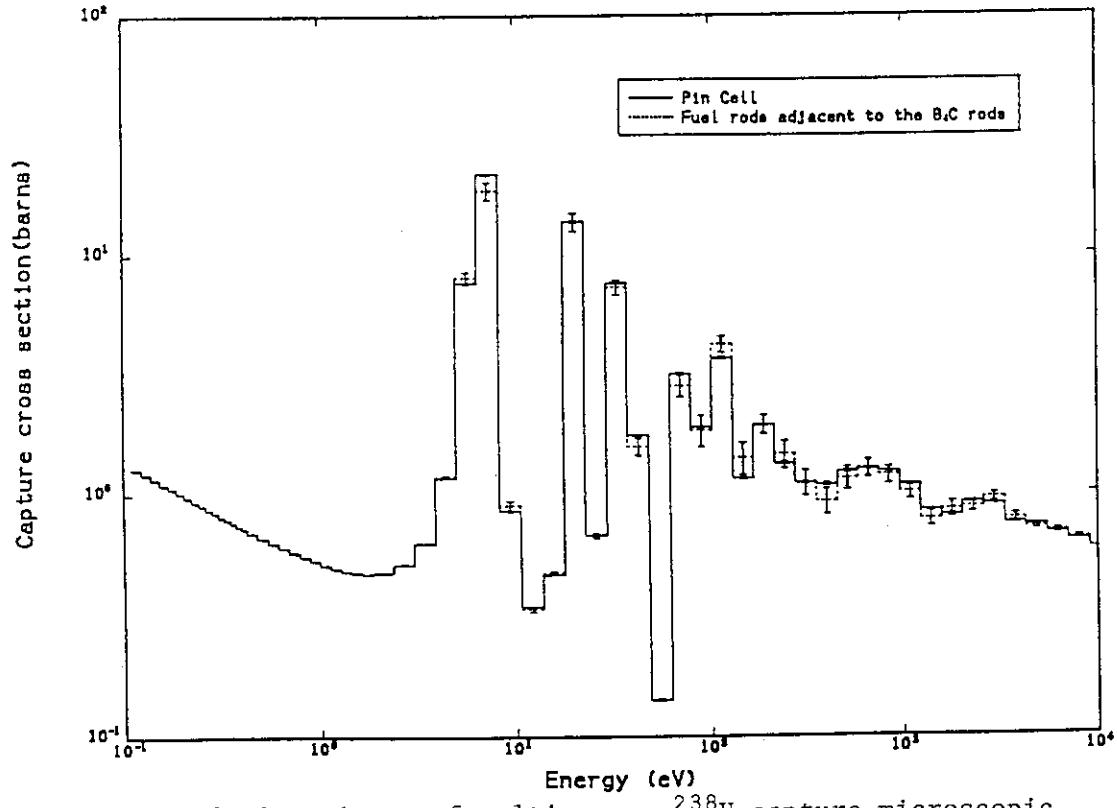

Figure A.16 Compairson of multi-group ^{238}U capture microscopic cross section between the unit pin cell and the fuel rod adjacent to the B_4C rod from the VIM calculation

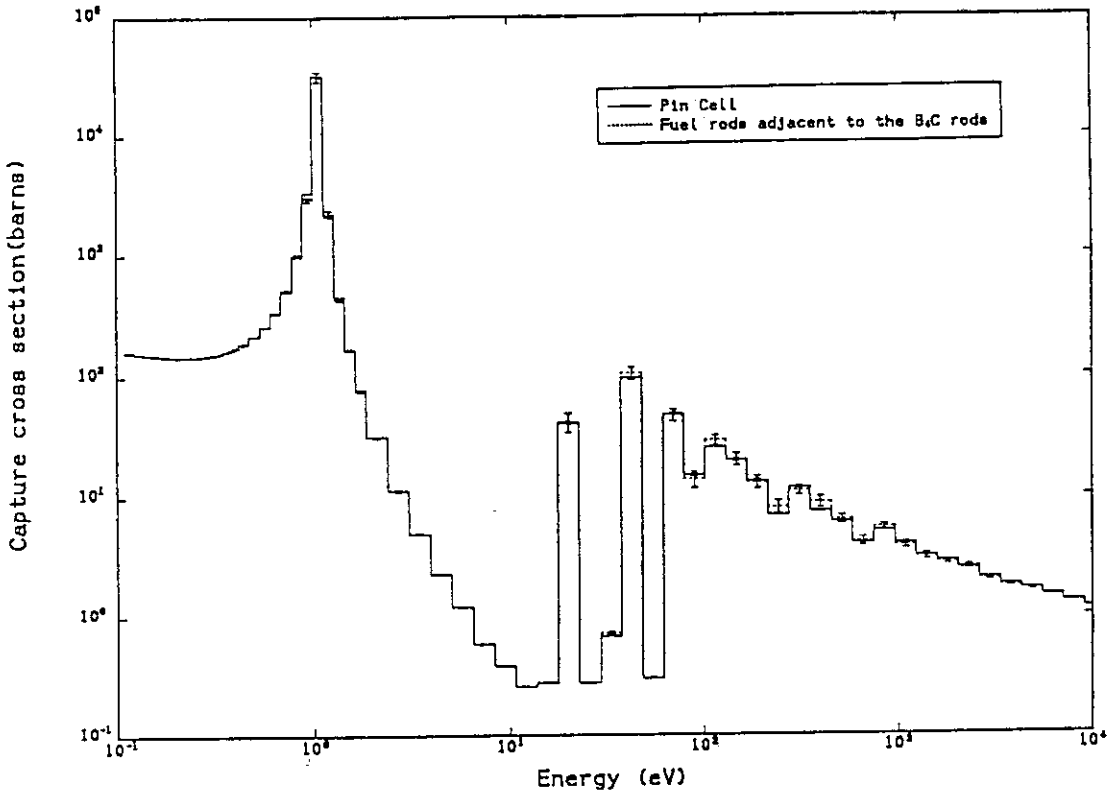

Figure A.17 Comparison of multi-group ^{240}Pu capture microscopic cross section between the unit pin cell and the fuel rods adjacent to the B_4C rod from the VIM calculation

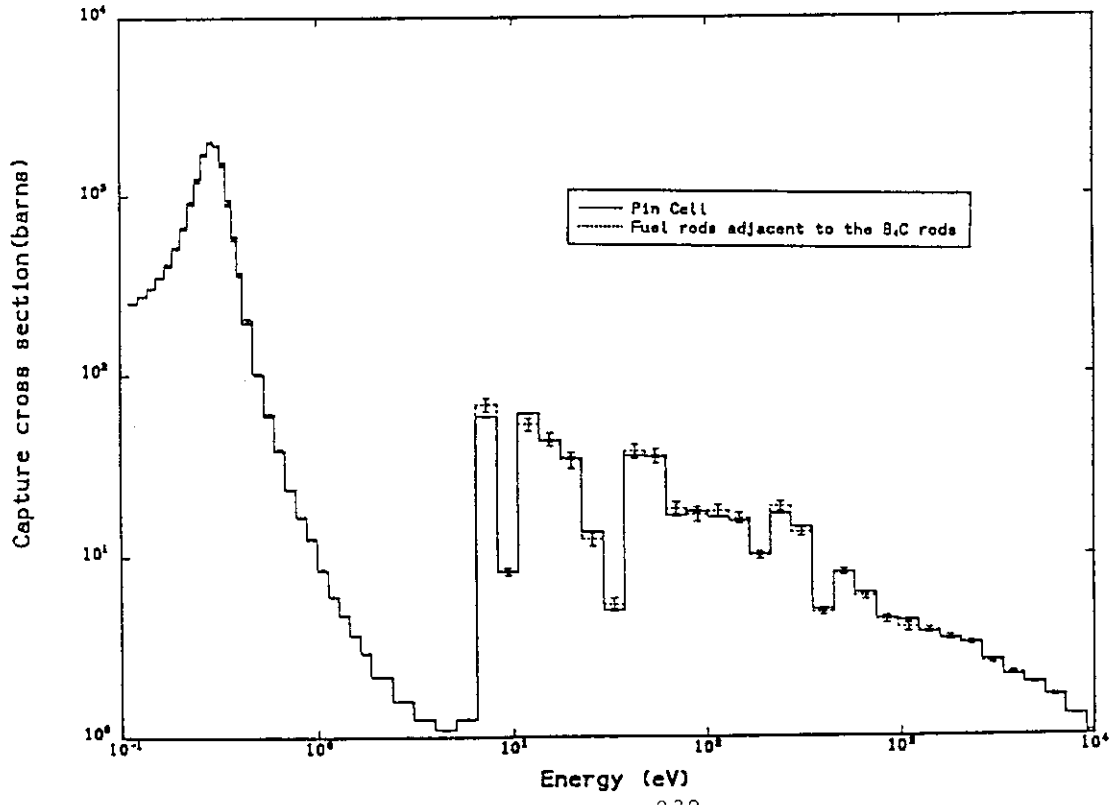

Figure A.18 Comparison of multi-group ^{239}Pu capture microscopic cross section between the unit pin cell and the fuel rods adjacent to the B_4C rod from the VIM calculation

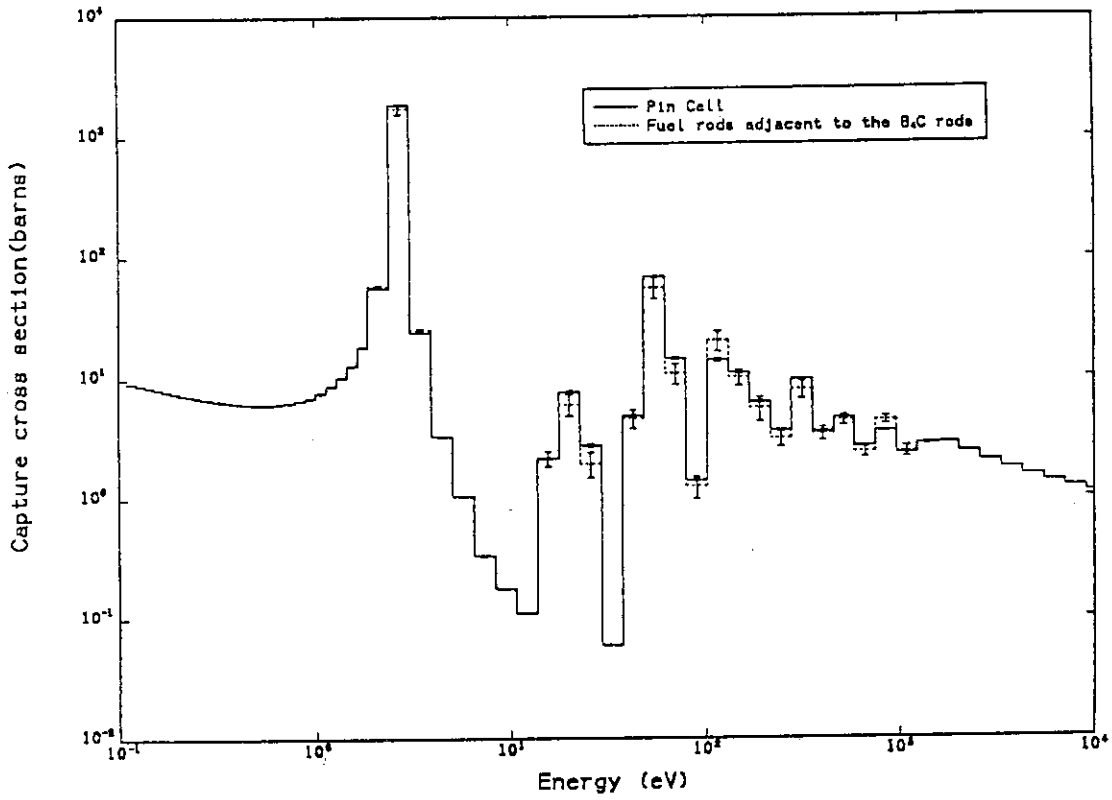

Figure A.19 Comparison of multi-group ^{242}Pu capture microscopic cross section between the unit pin cell and the fuel rods adjacent to the B_4C rod from teh VIM calculation

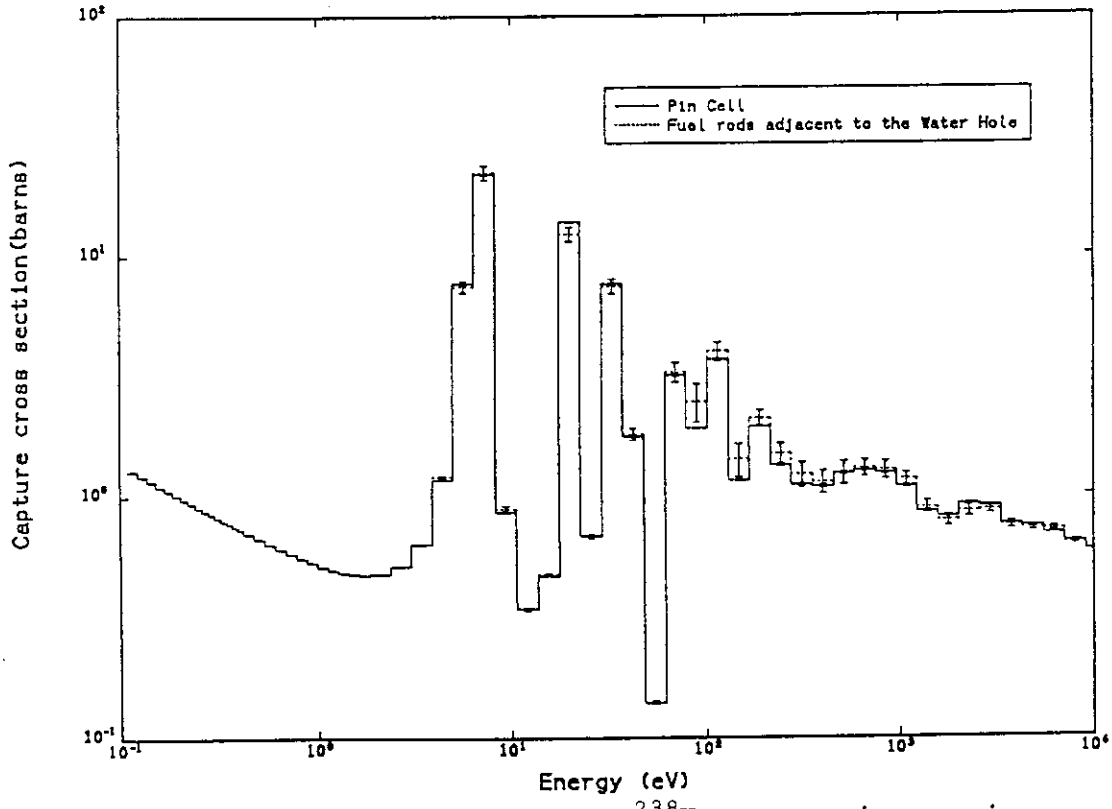

Figure A.20 Comparison of multi-group ^{238}U capture micrsocopic cross section between the unit pin cell and the fuel rods adjacent to the water hole from the VIM calculation

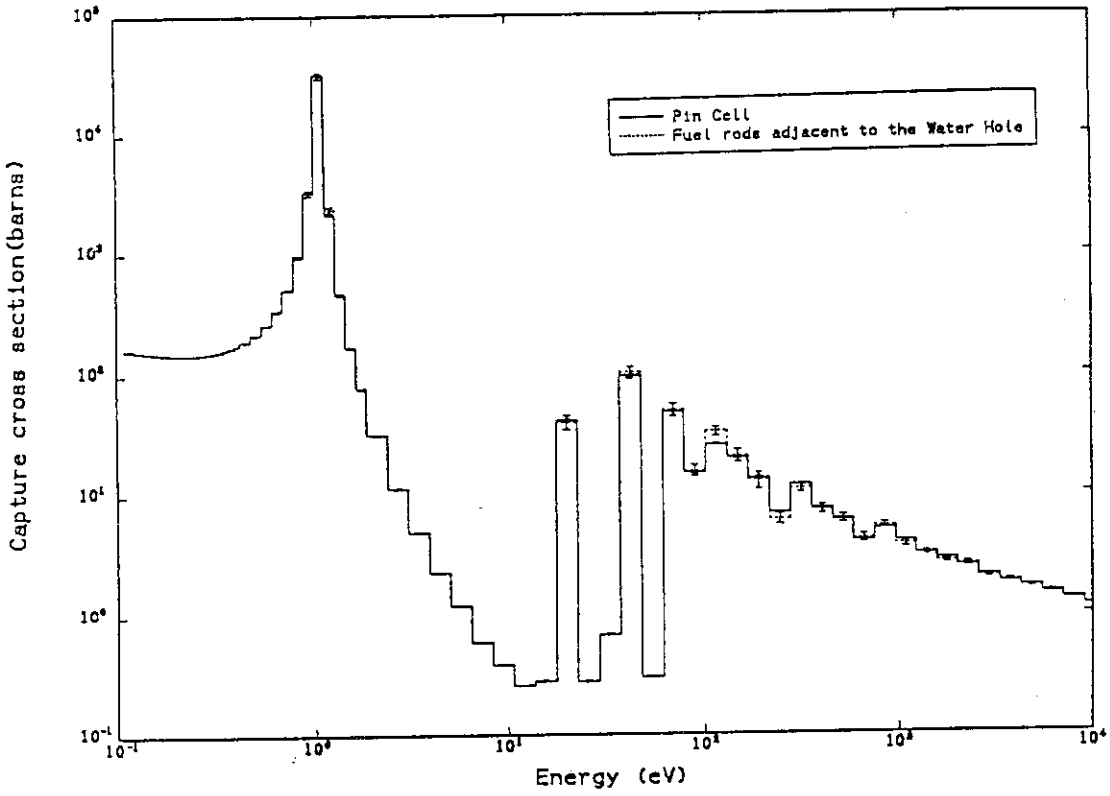

Figure A.21 Comparison of multi-group ^{240}Pu capture microscopic cross section between the unit pin cell and the fuel rods adjacent to the water hole from the VIM calculation

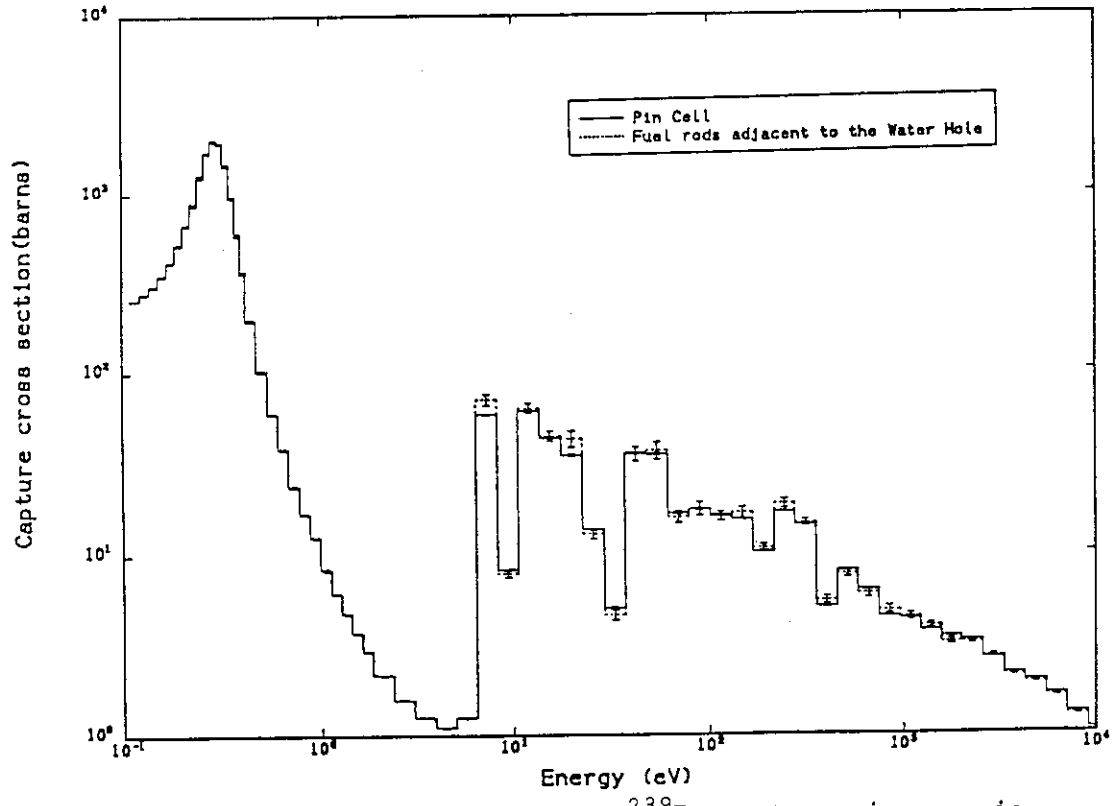

Figure A.22 Comparison of multi-group ^{239}Pu capture microscopic cross section between the unit pin cell and the fuel rods adjacent to the water hole from the VIM calculation

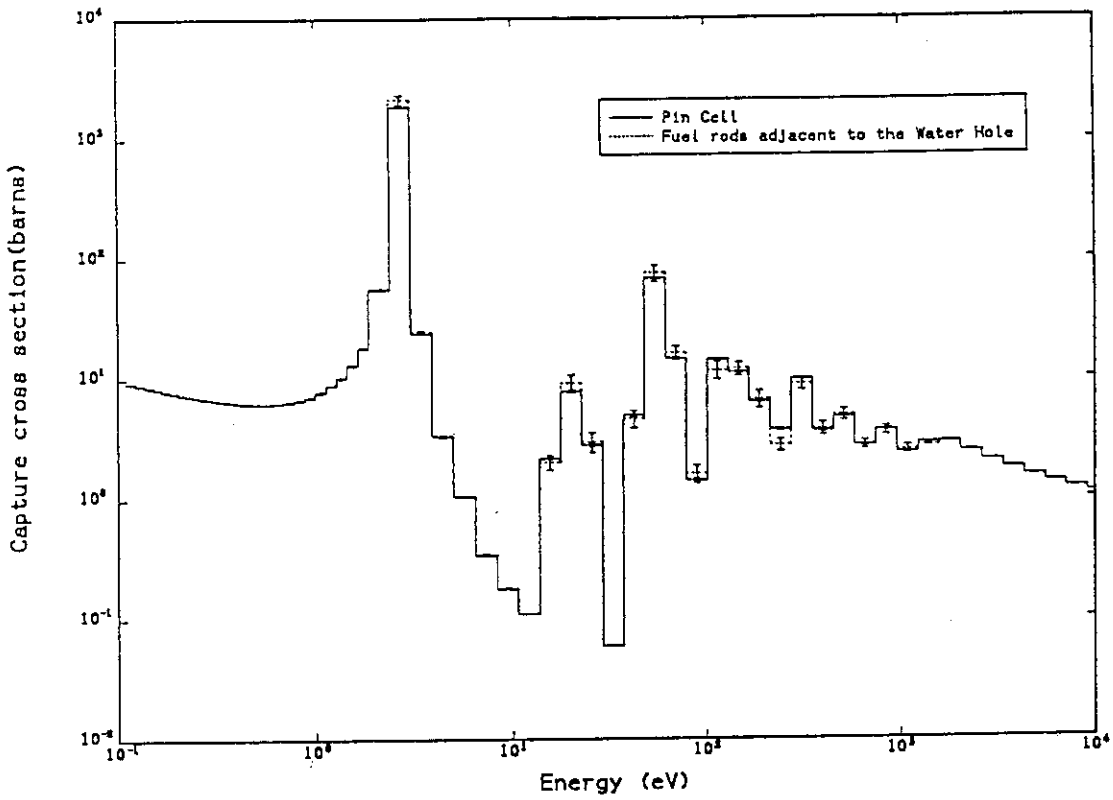

Figure A.23 Comparison of multi-group ^{242}Pu capture microscopic cross section between the unit pin cell and the fuel rods adjacent to the water hole from the VIM calculation